Development of an electrochemical lactate sensor for foetal monitoring during birth

Jessica Kremer

A thesis submitted for the degree of Master of Philosophy

Heriot-Watt University

School of Engineering & Physical Sciences

November 2017

Abstract

Foetal monitoring during birth is essential to determine foetal well-being throughout labour. The current method that complements foetal heart rate monitoring, foetal scalp blood sampling for pH determination, is laborious, prone to errors and invasive. Lactate has been identified as a potential alternative measurand for intrapartum foetal monitoring, due to the ability to distinguish between different types of acidosis. A literature review from the medical and technical perspective and a patent review were conducted to identify the current advancements in the field of lactate sensing with regards to foetal monitoring. It was concluded that a less invasive and a continuous monitoring device is required to fulfil the clinical needs for intrapartum foetal monitoring. Therefore, a novel biosensor, combining microneedle technology and electrochemical lactate sensing, was proposed and developed for this purpose.
A fabrication process using the microneedle array was established using an electron beam evaporator. Commercial screen-printed electrodes were utilised for the development of an immobilisation protocol exploring covalent bonding and cross-linking. Electrochemical impedance spectroscopy, cyclic voltammetry and amperometry experiments were conducted to assess the success.
A complete microneedle three-electrode prototype sensor was fabricated. The initial electrochemical analysis of commercially available, screen-printed electrodes concluded that platinum electrodes, in combination with covalent bonding, have the potential to provide the basis for further development towards a lactate sensor for foetal monitoring during birth.
This work has identified developmental work required for the immobilisation process to be able to determine the compatibility with the microneedle array as an electrode surface.

Dedication

This thesis is dedicated to Abelle and Geka.

Acknowledgement

I would like to thank my supervisor Prof. Marc Desmulliez for sharing with me his considerable expertise and his provision of the training and space required to conduct my research. I would like to thank Dr. Helen Bridle and Dr. Anne Bernassau for their professional support and guidance, which contributed to the completion of this project. I would also like to express my thanks to Dr. Fiona Denison for her instigation of this research and whose medical expertise was so vital to the project. I would like to extend special thanks to Dr. Till Bachmann and Dr. Holger Schulze at the Division of Pathway Medicine at the University of Edinburgh, for providing the experimental apparatus, professional guidance and expertise for the execution of the experiments conducted for this project. Furthermore, I am grateful for the training in fabrication methods, patience, assistance and valued support from Mark Leonard and Neil Ross.

I am deeply grateful to my family and friends for their patience, understanding and emotional support. I would particularly like to thank my parents, Sabine and Luděk, and my sister Isabelle for their unwavering support and encouragement. I would also like to offer my special thanks to my friends Jamie, Philip, Iain, Frank and Severin, whose professional and emotional support was invaluable throughout the course of my project. My last thanks to the swans and cygnets in the University Loch: a quiet and peaceful place to think.

Contents

List of Tables

List of Figures

List of Abbreviations

AlGaAs	Aluminium gallium arsenide
AM	Amperometric
ATP	Adenosin triphosphate
Au	Gold
BGA	Blood gas analyser
BSA	Bovine serum albumin
CCD	Charged-coupled device
CE	Counter electrode
CNT	Carbon nanotubes
CO_2	Carbon dioxide
CS	Caesarean section
CTG	Cardiotocography
CV	Cyclic voltammetry
DIPM	Division of Pathway Medicine
DTT	DL-Dithiothreitol
EC	Electrochemical
ECG	Electrocardiogram
ECL	Electro-chemiluminescence
ECSA	Electrochemical surface area
EIS	Electrochemical impedance spectroscopy
EISF	Eyeball interstitial sclera fluid
FSBS	Foetal Scalp Blood Sampling
FSE	Foetal Scalp Electrode
GC	Glassy carbon

GCNF	Graphitized carbon nanofiber
GSA	geometrical surface area
H+	Hydrogen
H_2O_2	Hydrogen peroxide
HEC	Hydroxyethyl cellulose
HG	Hydrogel
IF	Interstitial fluid
In	Indium
LDH	Lactate dehydrogenase
Lox	Lactate oxidase
MD	Microdialysis
MN	Microneedles
MWCNT	Multi-walled carbon nanotubes
NA	Not available
NAD^+	Nicotinamide adenine dinucleotide
NADH	reduced nicotinamide adenine dinucleotide
NC	Negative control
NP	Nanoparticles
NT	Nanotube
NW	Nanowires
O_2	Oxygen
OF	Optical fibre
OFET	Organic field-effect transistor
ON	Overnight
PBS	Phosphate buffer saline
PCB	Printed circuit board
PMMA	Poly(methyl methacrylate)
Pt	Platinum

PTFE	Polytetrafluoroethylene
QMRI	Queen's Medical Research Institute
RE	Reference Electrode
SEM	Scanning electron microscope
SG	Sol-gel
SPE	Screen-printed electrode
SPEES/PES	Sulphonated polyether–ether sulphone–polyether sulphone
ST	Segments of ECG signal
STAN	ST-wave analysis
TCEP	Tris (2-carboxyethyl) phosphine hydrochloride
TS	Test solution
WE	Working Electrode
ZnO	Zinc oxide

1 Introduction

1.1 Motivation

During labour, foetal oxygen supply and carbon dioxide elimination can be impaired and threaten foetal well-being. Prolonged exposure to decreased gas exchange means the foetus may become hypoxic or develop acidosis, which can lead to irreversible damage to its nervous system. The resulting pathologies include hypoxic ischaemic encephalopathy, cerebral palsy and ultimately foetal death [1]. Currently, foetal well-being is assessed by monitoring the foetal heart rate using cardiotocography (CTG). As the CTG has a low true positive value, leading to unnecessary caesarean sections, non- reassuring heart rate patterns, indicated by the CTG, are verified by foetal scalp blood sampling (FSBS) to determine foetal pH and lactate value [2].

FSBS is an invasive procedure in which a blood sample is obtained from the unborn foetus, which is accessed through the mother's vagina. The sampled blood is analysed using a blood gas analyser. Based on the results of the blood analysis the clinical decision is made as to whether the foetus requires immediate delivery or whether the natural birth process can be continued.

However, FSBS exhibits a number of downsides. Firstly, it can only be performed when the cervix is dilated more than 3 cm. Secondly; the method is invasive and complex to perform, requiring trained staff [3]. Additionally, the procedure is lengthy (12-30 mins) [4] and does therefore not provide real-time or continuous results. The two separate processes of blood sampling and blood analysis are furthermore susceptible to blood clotting, air bubble (in the capillary tube) and contamination by the amniotic fluid [5]. FSBS also does not distinguish between foetuses which suffer from a temporary oxygen shortage

and foetuses that suffer from a more severe oxygen impairment and require immediate delivery [6].

Due to the downsides of the current foetal monitoring procedures outlined above, a more reliable, less invasive and less complex real-time method is researched to enable improved data collection and facilitate the safe delivery of babies.

1.2 Specifications

For the development of a new device for foetal monitoring during birth, expert clinicians dealing regularly with complex labours, Dr. Fiona Denison and Dr. Sarah Stock, from the Queen's Medical Research Institute (QMRI), have provided clinical specifications, which are summarised in this section. Two measurands, pH and lactate concentration in the foetal blood, are utilised in FSBS. In order to obtain useful information from the new device, it has to be able to detect a pH value to two decimal places between 6.50 - 7.50 and to one decimal place in the ranges of 6 - 6.5 and 7.5 -7 .7. A lactate sensor would need to provide reliable measurements between 2.0 - 14 mmol/L to one decimal place. It is required to measure both or either of these measurands over the whole duration of labour, which can take 12 hours or longer for more complex labour processes.
Due to the requirements of continuous monitoring, an *in-situ* sensor that can be applied to the foetal scalp, is considered to fulfil the clinical need.
Additionally, the sensor has to be easy to apply and not cause more trauma than the current foetal scalp electrode. The sensor also has to conform to the dimensions of the environment. It has to be able to be applied from cervical dilation as small as 1 cm and, if a cable is used to transmit the information, it has to overcome the distance between the foetal scalp to outside the vagina which is approximately 15-20 cm.
These specifications form the basis for the development of a foetal monitoring device during birth.

1.3 Aims and Objectives

In addition to the specification above, a medical and a technical literature review, with a focus on foetal monitoring and lactate sensing, was conducted. Based on the specifications and the literature review a label-free detection approach, which has been successfully applied in different application areas has been chosen. Therefore, the aim of this research is to design, manufacture and characterise the performance of an electrochemical based foetal monitoring system.

Specific objectives to achieve this goal include:

1. Identification and selection of the most appropriate measurand(s).
2. Review of existing electrochemistry based biosensors for the chosen measurand to guide selection of sensing approach, i.e. which type of sensor and what sort of recognition element.
3. Design and manufacture of an electrode system capable of foetal scalp integration.
4. Characterisation of immobilisation protocols on different electrode surfaces.
5. Characterisation of the performance of the resulting system.

1.4 Layout of the thesis

The thesis consists of eight chapters, which are summarised in this section.

Chapter 2 - Fundamentals of Electrochemistry In this chapter a broad overview about electrochemical sensing and common electrochemical methods (including cyclic voltammetry and amperometry and basic analyses of the results) are presented.

Chapter 3 - Literature review: Medical Perspective In this chapter

background information about the foetal and maternal physiology and current foetal monitoring procedures are described. Furthermore, potential measurands and biofluids are explored for the development of the foetal monitoring device.

Chapter 4 - Literature Review: Technical Perspective This chapter provides a comprehensive review of biosensor focusing on lactate sensing covering the topics of sampling, recognition, immobilisation, transduction and sensor materials. Additionally, results of a patent review with regards to foetal monitoring and lactate/pH sensing are presented.

Chapter 5 - Methods and Results: Sensor Design and Fabrication In this chapter the design and the fabrication methods and steps are outlined. The materials and the equipment employed are introduced, which are used to validate the fabrication methods, develop a mask for electron beam deposition and to fabricate an adapter.

Chapter 6 - Methods and Results: Immobilisation This chapter provides the protocols for the covalent bonding and cross-linking immobilisations methods. Additionally, the results of the characterisation of the success of the immobilisation are presented.

Chapter 7 - Methods and Results: Amperometric Measurements This chapter provides the methods and results for the amperometric measurements of the previously functionalised electrodes.

Chapter 8 - Conclusions This chapter concludes the work conducted in the previous chapters. Furthermore, suggestions for future work for the continuing development of the foetal monitoring device are given.

2 Fundamentals of Electrochemistry

The aim of this work is to develop an electrochemical lactate sensor. This chapter therefore provides an overview about the basics of electrochemistry. After explaining the setup of an electrochemical cell and the processes occurring upon application of a potential, cyclic voltammetry (CV) and amperometry measurements are then described.

2.1 General Overview

A biosensor is a sensor in which the sensing is based on a biochemical or biological reaction. In general, sensing can be divided into two categories; label-free sensing and labelled sensing; the latter uses an additional reagent to make the analyte more visible [7]. Label-free sensing holds the following advantages over labelled sensing [8]:

- Reduction in assay cost
- Reduction of complexity
- Increased amount of quantitative data
- Higher throughput
- Reduced assay development time
- Increased accuracy

As the aim of this project is to develop a lactate sensor for foetal monitoring during birth, the addition of reagents is to be avoided. For this reason, this chapter focuses on label-free sensing.

The process of biosensing can be divided into (a) recognition of the analyte and (b) transduction of the signal, as illustrated in Figure 2.1. The recognition

element can be based on enzymes, living cells and affinity interactions. The choice of the recognition element depends on the application, environment and the analyte. The signal obtained from the recognition element can be transduced by thermometric, mechanical, capacitive, electrochemical or optical means [7].

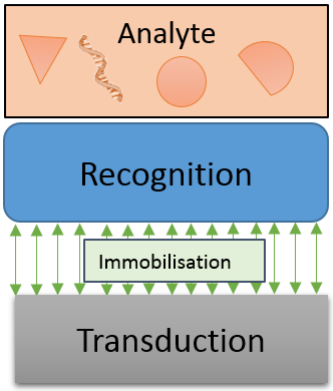

Figure 2.1: *Functionality of biosensors: With the recognition element immobilised onto the transduction surface to detect an analyte.*

The quality of the sensor functionality can be benchmarked by characteristics such as sensitivity, selectivity, response time and limit of detection. The sensitivity of a sensor is defined as the step change of the output value with regard to the input value. The selectivity defines the ability to distinguish between the measurand of interest and another substance. The time for the sensor to detect a signal is the response time [9]. The smallest measurand concentration that is reliably detected is defined as the limit of detection[10].

An electrochemical sensor can have a two-electrode or a three-electrode arrangement (Table 2.1). In a three-electrode system the working electrode (WE) is the electrode at which the electrochemical reaction of interest occurs. If that reaction is an oxidation, the opposite reaction, a reduction, takes place at the counter electrode (CE). The third electrode in a three-electrode system is the reference electrode (RE), which maintains a constant potential. This is necessary as the potential at the WE must be set to a certain potential for the chemical reaction to occur. The reference electrode, as the name suggests, acts as a reference point, which is used to set the potential for the WE. A two-electrode system only has a WE and a CE, which also acts as the RE.

Table 2.1: *Electrodes and their function in an electrochemical cell.*

Electrode	**Function**
Working Electrode (WE)	Chemical reaction of interest
Counter Electrode (CE)	Opposite reaction to WE
Reference Electrode (RE)	Provides stable potential for WE. No current passes through.

As the RE is also the CE, current is passing through the RE, which may alter the supposedly constant potential of the RE, which subsequently may change the potential at the WE by the same value, and could compromise the quality of the results [11].

Figure 2.2 A) presents a schematic drawing of a three-electrode setup connected to a potentiostat [12]. All three electrodes are immersed in the solution of interest and the potential at the WE is set with regard to the RE. The resulting current is measured between the WE and the CE. Electronically, the three-electrode system can be represented by the electrical equivalent circuit in Figure 2.2 B) [13]. The sensitivity of an electrochemical sensor can be improved with a larger electrode surface area, either by increasing the geometrical size of the working electrode or by providing a larger electrochemical specific surface area. The latter can be obtained by engineering a rougher electrode surface resulting in a larger surface area. This is the reason for the wide use of nanomaterials such as nanocubes, nanowires, nano particles and nanotubes (Section 4.6.5) [14, 15]. Additionally, the specificity of the sensor can be increased by additionally immobilizing a recognition element on the surface of the working electrode. The WE will react with the substrate forming species that will oxidise or reduce at the electrode surface, and change the electronic parameters (e.g. current, voltage and resistance) by a quantity that depends on the concentration of the measurand.

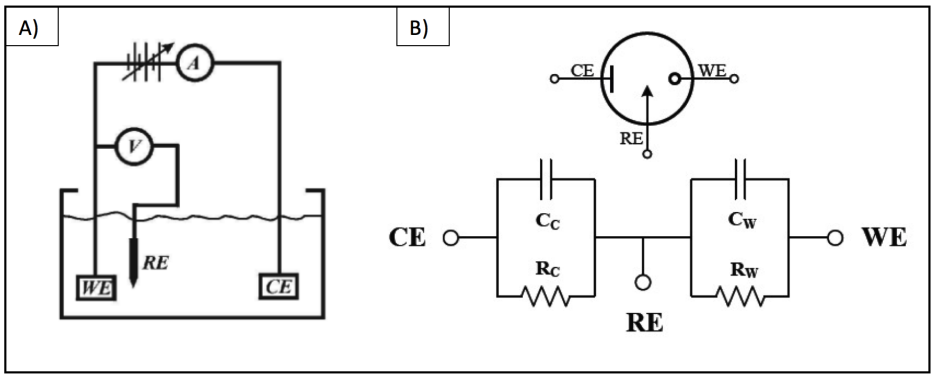

Figure 2.2: *A) Schematic drawing of an electrochemical cell connected to a potentiostat [12]. B) Electrical circuit representing an electrochemical cell [13].*

Usually, experimental electrochemical reactions take place in a solution, which is called the supporting electrolyte. It is required that the supporting electrolyte provides a high concentration of inert electrolyte 100 times higher than the electroactive species of interest. The typical concentration range for a supporting electrolyte is 0.01 M - 1.0 M [16, 17].

When an electrode is immersed in such an electrolyte and a potential is applied with regards to the reference electrode a double layer is formed, which is a film closest to the electrode surface and it behaves like a capacitor. It can be visualised to be comprised of three layers. The two layers closest to the electrode which are called the inner and outer Helmholtz plane include ions that balance out most of the charge. A third layer is the diffusion layer which acts as the connection between the bulk solution and the Helmholtz planes. In general, the concentration of the electroactive species near the electrode decreases with time and increases with the distance from the electrode surface.

A simplified illustration is given in Figure 2.3. The image on the left-hand side shows the concentration of ions near the electrode surface at the beginning of the measurement and the image on the right presents the situation after the system has been exposed to a certain potential for a specific time. The concentration of the ions near the electrode decreases over time.

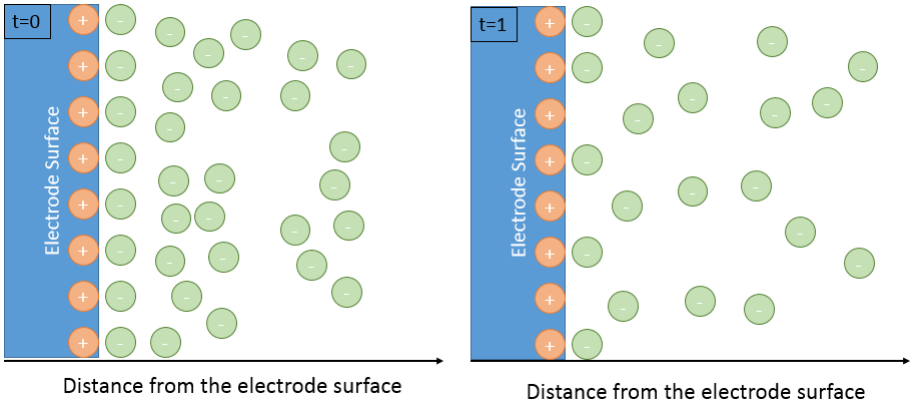

Figure 2.3: *Simplified representation of the double layer and its development over time with regard to the distance to the electrode surface.*

A concentration profile of this development is shown in Figure 2.4.

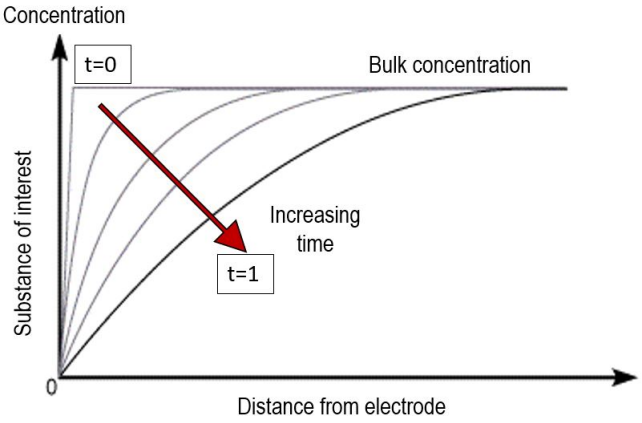

Figure 2.4: *Representation of formation concentration gradient [18].*

The composition of the double layer changes with a change in potential [19]. The exchange of electrons and ions due to the oxidation or reduction reactions facilitates the flow of current. Initially, upon the application of a potential, all electroactive species close to the electrode surface are oxidised or reduced. As there is an exchange of electrons during such reactions, this initial depletion is represented by a current peak in the current vs. time plot. Once the diffusion layer is formed the current is limited by the diffusion of the electroactive species to the electrode surface [11].

The rate of diffusion is represented by Fick's first law[19]:

$$J = -D\frac{\delta C}{\delta X} \tag{2.1}$$

Where J is the flux of the substance of interest, C is the concentration, D the diffusion coefficient and X the distance from the electrode surface. Both, the graph and the equation show that the flux decreases with an increasing distance from the electrode surface [11]. The cell potential is described by the Nernst equation [19]:

$$E = E^{\Theta} - \frac{RT}{nF} \ln Q \tag{2.2}$$

Where E is the cell potential, E^{Θ} the standard potential, R the gas constant (8.314 J/Mol.K), T the temperature in Kelvin, n the number of electrons involved in the chemical redox reaction, F the Faraday constant (96,485 C/mol) and Q the reaction quotient (ratio of concentration of the oxidised species versus the ion concentration of the reduced species). For standard state conditions at a temperature of 25°C, the Nernst equation can be simplified to [11]:

$$E = E^{\Theta} - \frac{0.0592}{n} \ln Q \tag{2.3}$$

2.2 Cyclic Voltammetry (CV)

Cyclic Voltammetry (CV) is a method used in electrochemistry to study the thermodynamics and kinetics of an electrochemical system. It can also provide information about the concentration profile and the potential at which the rate of reaction is the highest, which is important for amperometric measurements of an electroactive species as explained in the next section.

In CV, a potential that is swept at a constant rate is applied to the WE relative to the RE. This results in a current flow due to the oxidation/reduction of the electroactive species as explained in Section 2.1. An example of the applied potential waveform is shown in Figure 2.5 (A)). The resulting current is plotted against the applied potential in a voltammogram (Figure 2.5 B)).

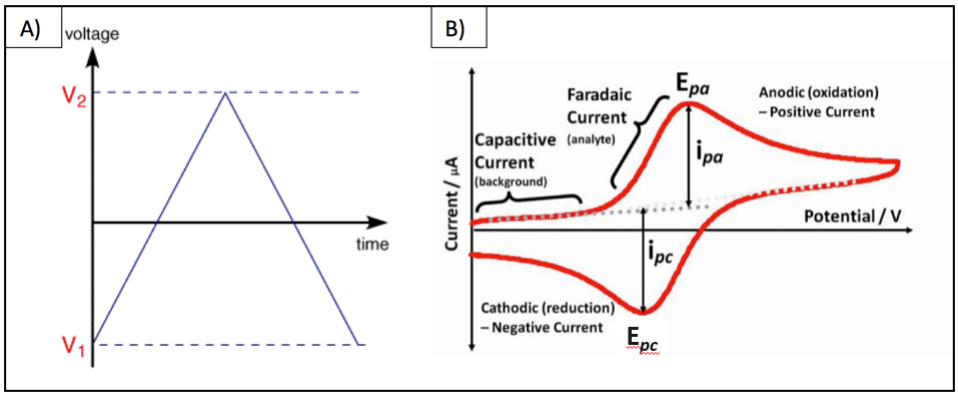

Figure 2.5: *Potential wave applied during cyclic voltammetry (A)) [20]. Typical cyclic voltammogram with current peaks (B)) [21]. E_{pc} = Cathodic peak voltage, E_{pa} = Anodic peak voltage, i_{pc} = Cathodic peak current, i_{pa} = Anodic peak current*

A cyclic voltammogram (Figure 2.5 B)) consists of a positive and a negative current response. The peak of the positive current is the oxidation peak and the peak of the negative current is the reduction peak resulting from the forward and backward potential sweep applied to the cell, respectively.

The measured current can be further divided into different sections. The measurement is started at a potential at which no chemical reaction is expected, after which the potential is gradually swept further towards the potential at which the highest rate of reaction takes place. The initial low current measured is the capacitive current, I_C, which represents the charging of the double layer. The current recorded after the capacitive current is the Faradaic current, I_f, as the potential is increased, which represents the onset of the chemical reaction (oxidation of the analyte). The peaks represent the potential at which the electrolyte oxidises/reduces the most, producing the highest positive or negative currents recorded in the voltammogram. Following the oxidation peak the current decreases despite the increase in potential due to the depletion of the double layer. Therefore, the total current is [11]:

$$I_{total} = I_C + I_f = C_d \frac{dE}{dt} = I_f = \nu C_d = I_f \tag{2.4}$$

The capacitive current (charging of the double layer) acts like a capacitor changing its charge with increasing potential over time (scan rate ($\nu(V/s)$), C_d = capacitance of double layer). A higher scan rate does not allow the

double layer to reach an equilibrium, meaning that the total current increases with an increasing scan rate as shown in Figure 2.6.

When sweeping the potential in the opposite direction at the WE, the current reverses and the species is re-oxidised (re-reduced) until its peak is reached and the current is again limited by the rate at which the species diffuses to the electrode surface [11].

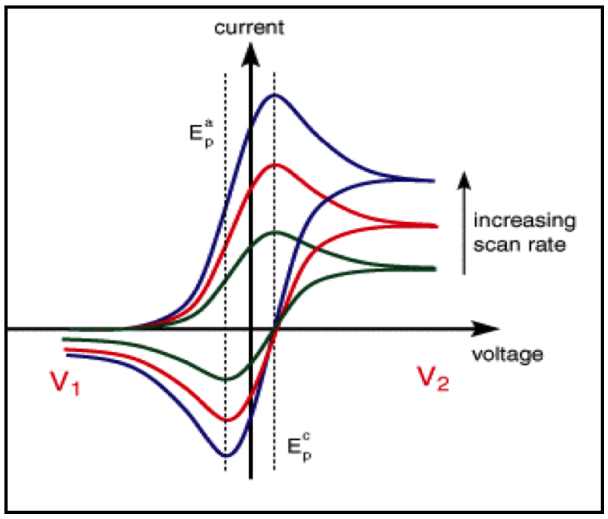

Figure 2.6: *Typical cyclic voltammogram at different scan rates [20].*

During the analysis of a cyclic voltammogram, the potential difference related to the peaks of currents and the ratio of the current peaks are the two main characteristics that provide information about the reversibility of the reaction of the electrochemical cell. The peak currents of a voltammogram can be calculated with utilising the Randle Sevcik equation [22].

$$I = -2.96 \cdot 10^5 n^{3/2} A D^{1/2} C \nu^{1/2} \tag{2.5}$$

Where A (cm^2) is the electrochemical surface area of the WE, D (cm^2/s) the diffusion coefficient of the electroactive species, C ($\mathrm{mol}/\mathrm{cm}^3$) the concentration of the electroactive species, ν (V/s) the scan rate and n the number of electrons.

For a reversible system, the separation between the two peaks is $57/n$ mV (n = number of electrons) Figure 2.5 B) and the peaks are of the same height [11].

$$|E_{p,a} - E_{p,c}| = \frac{57}{n} \text{ mV} \tag{2.6}$$

$$\left|\frac{I_{p,a}}{I_{p,c}}\right| = 1 \tag{2.7}$$

In sensing applications it is common to only receive one peak because the substance is only present in one form (reduced or oxidised) and might be broken down into other substances. This leaves no substances to be re-reduced or re-oxidised at the electrode surface resulting in no opposite peak when scanning the potential the opposite way. For the development of an amperometric biosensor, cyclic voltammetry is used to determine the overpotential at which the amperometric measurements will be performed. The overpotential is the potential at which the highest current is observed.

2.3 Amperometry

Amperometry is an electrochemical method for the analysis of electrochemical cell reactions. A potential step, which ranges from -0.2 V to 0.7 V, is applied to the WE with regard to the RE [23, 24, 25]. A potential electrolysis (reduction or oxidation) takes place which is measured as a current over time. The current response is proportional to the concentration of the analyte being measured/reduced [19] . For planar electrodes it is described by the Cottrell equation [26]:

$$i = \frac{nFAD^{1/2}C}{(\pi t)^{1/2}} \tag{2.8}$$

Where i is the current response (A), n the number of electrons, F the Faraday constant, A the electrochemical surface area (cm^2), D the diffusion coefficient (cm^2/s), C the concentration of the electroactive species (mol/cm^3) and t the time in seconds [11, 18].

A typical resulting current response is shown in Figure 2.7 right. The current response represents the reaction to the first potential step (Figure 2.7 left). The spike represents the instantaneous charging of the diffusion layer upon application of the potential step. After this spike, the current decays due to its dependency on the diffusion of the electroactive species to the electrode surface before plateauing at constant current level [11, 18]. Amperometric lactate sensors measure the current flow generated by electrons which have been produced either through the breakdown of H_2O_2 or NADH. These intermediates originate from Lactate oxidase (Lox) and Lactate dehydrogenase (LDH))(Section 4.3), respectively. The current received upon the application of the overpotential is equivalent to the concentration of the lactate in the solution.

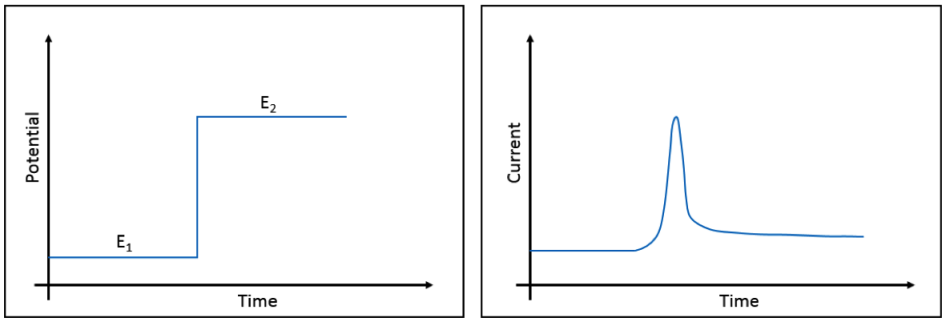

Figure 2.7: *Potential step for amperometry (left) and the current response (right).*

3 Literature Review: Medical Perspective

3.1 Introduction

The rationale, which underpins all intrapartum foetal monitoring, is that timely diagnosis of foetal compromise, may allow treatment by *in utero* resuscitation or delivery before acidaemia, irreversible tissue injury and foetal death occurs. In the following sections, the circumstances surrounding the foetus during birth and the gas exchanges with the mother, are explained. This study informs the technologies explored in this thesis. Furthermore, the past and current foetal monitoring methods and procedures are presented, following a discussion about potential biofluids for a new foetal monitoring system.

3.2 Foetal-maternal Physiology

The placenta replaces the function of the lungs of the foetus to provide sufficient gas exchange *in utero*. The foetal heart pumps deoxygenated blood through the two umbilical arteries to the placenta for the exchange of CO_2 and O_2. Oxygenated blood is pumped back into the foetal system through the single umbilical vein. Gas exchange and therefore oxygen supply are dependent on the normal perfusion of the placenta by maternal and foetal blood. Oxygen provides the basis for energy production from glucose [27]. Uterine contractions can restrict maternal and foetal blood flow within the placenta and therefore impair normal gas exchange. Normal contractions are tolerated well by a healthy foetus via natural compensating mechanisms, due to a general oxygen oversupply. If oxygen supply is further restricted, the foetus has additional methods to preserve perfusion to all vital organs, which include:

- Increased extraction of O_2 from the maternal blood at the placenta.
- Higher proportion of O_2 extracted from the foetal blood by foetal tissue.
- centralisation of blood flow towords vital organs (e.g. brain, heart, adrenal glands) [28].

Oxygen impairment can endanger growth restricted foetuses more than well-grown foetuses, due to their different compensation capabilities [29]. Failure to compensate for placental insufficiency may cause a prolonged restriction of foetal gas exchange followed by an increasing lactate concentration and a decreasing pH value. This process can lead to cell death, threatening foetal health [27].

Different biochemical pathways are followed for energy production when oxygen is present in comparison when it is not, leading to different outcomes, as shown in Figure 3.1.

In the presence of O_2 the human body generates energy in form of adenosine triphosphate (ATP) through glycolysis and the Krebs cycle. However, if the O_2 supply is limited, energy production is made less efficient by the breakdown of pyruvate by lactate dehydrogenase in the presence of the reduced form of nicotinamide adenine dinucleotide (NADH) and a H^+ ion into lactate and nicotinamide adenine dinucleotide (NAD^+). The NAD^+ is vital to maintain a limited energy production through glycolysis (red arrow in Figure 3.1). The lactate is broken down into lactic acid and H^+ ions causing the pH value to decrease [30]. When oxygen becomes available again, the fermentation process is reversed, and lactate dehydrogenase converts lactate back into pyruvate, which is then used for more efficient energy production in the Krebs cycle [30, 31, 32]. Whether the energy in the foetus is produced under aerobic or anaerobic processes depends on the oxygen supplied by the mother.

During the second stage of birth, which is dominated by contractions, the perfusion in the placenta can be restricted, leading to oxygen deficiency [33]. Oxygen deficiency can lead to two different types of acidosis, respiratory and metabolic which differ in the source of their development and their impact on

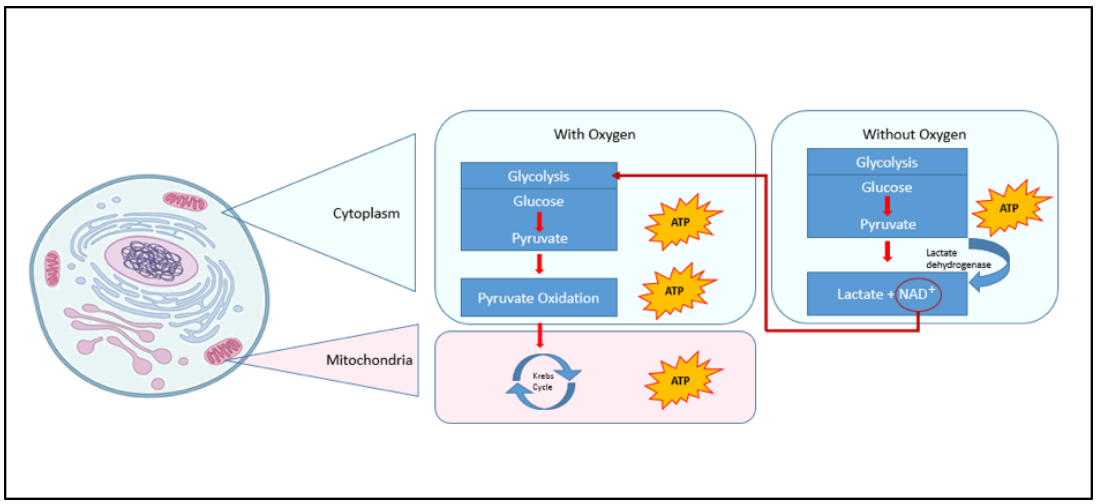

Figure 3.1: *Aerobic and anaerobic metabolisms [32].*

the foetus being delivered. In a respiratory acidosis, the H^+ ion concentration increases due to an accumulation of CO_2, decreasing the pH. Respiratory acidosis is not a source of long-term neurological consequences, and the foetus can withstand it with its compensatory methods [1, 27]. Respiratory acidosis is diagnosed when the pH is lower than 7.36 without the change in base deficit [1](will be explained in Section 3.5.2 in more detail)[28, 34, 35]. Continuing lack of oxygenation can lead to the more dangerous metabolic acidosis associated with long-term damage [27]. Metabolic acidosis is based on the production of lactate and H^+ ions via the anaerobic metabolism, which decreases the pH and increases the lactate concentration [1]. A decrease in pH and elevated base deficit value is indicative of a metabolic acidosis as shown in Table 3.1 [28, 34].

Table 3.1: *Threshold values of pH and base deficit indicative of respiratory and metabolic acidosis [14, 36].*

	pH	**Base Deficit**
Normal	7.36-7.44	-1.0-8.9
Respiratory Acidosis	<7.36	-1.0-8.9
Metabolic Acidosis	<7.36	>8.9

[1]The base deficit represents the number of bases (chem.) that would neutralise the blood to a pH of 7.2-7.4.

An initial respiratory acidosis can lead to a metabolic acidosis if the normal gas exchange cannot be established again. Since a lack of oxygen eventually leads to cell death, a prolonged exposure to this situation can lead to postnatal neurological complications. Hypoxic-ischemic encephalopathy can be a short-term complication following intrapartum metabolic acidosis. The more severe complication, cerebral palsy (2-3 per 1000 live births worldwide [37]) , leads to long-term disabilities such as spastic quadriplegia [38]. Profound intrapartum asphyxia can result in stillbirth (4.4 per 1000 in England and Wales in 2016 [39]) or neonatal death (1.9 per 1000 from 2001-2015 in England and Wales [40])[35].

3.3 Past, Present and Future of Foetal Monitoring

The first report of using the foetal heart rate to screen for intrapartum foetal wellbeing was in 1600s (Figure 3.2). Auscultation[2] was initially undertaken using stethoscopes (e.g. Pinnard) specifically designed for direct auditory auscultation of the foetal heart rate through the maternal abdominal wall. Ultrasound is now used for external non-invasive assessment of foetal heart rate using devices such as hand-held sonic aids and cardiotocography (CTG). CTGs, which measure both heart rate and uterine activity, can be used intermittently or continuously [42, 43].

The latter technique was introduced because it was thought to provide a better insight in foetal well-being (fewer Caesarean sections), which was found not to be the case [44]. If it is not possible to auscultate the foetal heart rate through the maternal abdominal wall, for example due to maternal adiposity or foetal position, then a foetal scalp electrode (FSE) can be applied directly

[2]Auscultation: Listening to the sound oft he heart, lungs or a foetal heartbeat for the purpose of a medical diagnosis or monitoring [41].

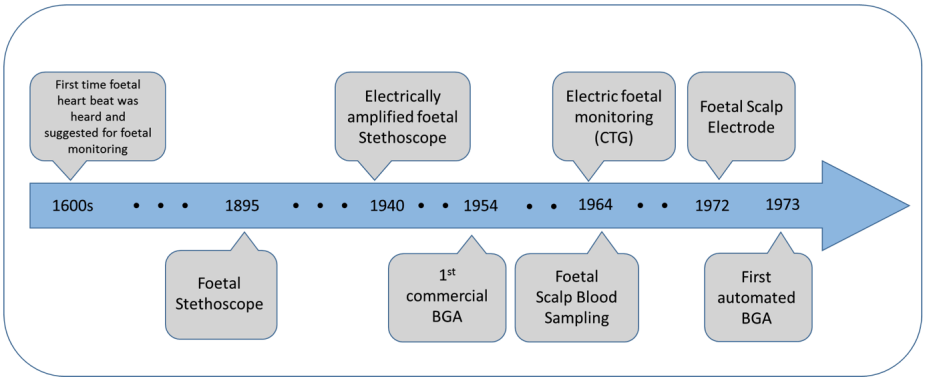

Figure 3.2: *History of the development of foetal monitoring. BGA= Blood Gas Analyser [42].*

to the foetal head to measure heart rate or foetal electrocardiogram (ECG). The FSE, usually provides a more stable foetal heartrate signal, but there is a higher risk of injury and infection [45] due to the device needing to puncture the foetal scalp to obtain a signal. Foetal oxygenation has been proposed as an alternative method of screening for intrapartum well-being. For the direct measurement of foetal oxygenation, Kanayama *et al.* [46] developed an oximeter with the sensor attached to the finger of the clinician. They were able to measure foetal oxygenation in real time and intermittently. The group of Nijland [47] developed a new transmission pulse oximetry device which is embedded into the hook of a FSE. Although they have shown correlation between scalp oxygen and foetal oxygen concentration, modifications are required to develop a more advanced version of an oximeter for future studies due to remaining inaccuracies based on fabrication and calibration variations [47]. Although it was found by Nonnenmacher *et al.* [48] that foetal pulse oximetry reduces the frequency of foetal scalp blood sampling (FSBS) when a non-reassuring heart rate is observed, a systematic review conducted by East *et al.* [49] recommended not to apply oximetry for intrapartum foetal monitoring. In their study, the efficiency and safety of pulse oximetry for foetal monitoring during labour was compared to CTG and ECG. They found that the complementing CTG or ECG with oximetry does not reduce the rate of Caesarean sections (CSs) [49].

Finally, using the foetal ECG, ST-wave analysis (STAN) (where S and T are segments in the ECG signal) was developed through an algorithm that analyses the change in the ST-wave of the foetal ECG. Although initial studies, conducted by Amer-Wahlin *et al.* [50], found that STAN correlated with foetal hypoxia during labour [50], the additional use of STAN has shown to reduce the need for FSBS and the number of CSs performed for foetal distress not however, foetal outcome [50, 51, 52]. Although STAN provides additional information, reduces the need for FSBS and commercial products based on the technique are available, professionals still doubt if STAN can fully replace foetal scalp blood sampling [53, 54].

3.4 Current Foetal Monitoring Process

Currently, during birth the maternal and foetal physiological parameters are monitored by observing the foetal heart rate and the maternal contraction using cardiotocography (CTG). An example CTG signal is shown in Figure 3.4 (A)). As mentioned above, it can be troublesome to obtain a reliable signal externally due to the position of the foetus, maternal obesity or in the case of twin pregnancy.

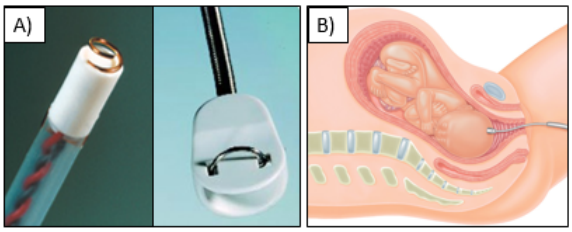

Figure 3.3: *Two foetal scalp electrodes. Attached with a screw and with a hook [47, 55] (A)). Attachment of foetal scalp electrode [56](B)).*

In these cases the application of a foetal scalp electrode can overcome these problems and is attached to the foetal scalp by a small screw or a hook to monitor the foetal heart rate [38, 55, 56]. However, monitoring the foetal heart rate (using CTG or FSE) holds a high risk for unnecessary caesarean sections and hypoxic babies due to a positive predictive value of 30% [44] and

a negative predictive value to 86 % [57]. This means that although the heart rate pattern presented is indicative of hypoxia and suggest intervention, the foetus is well, which would lead to an unnecessary CS.

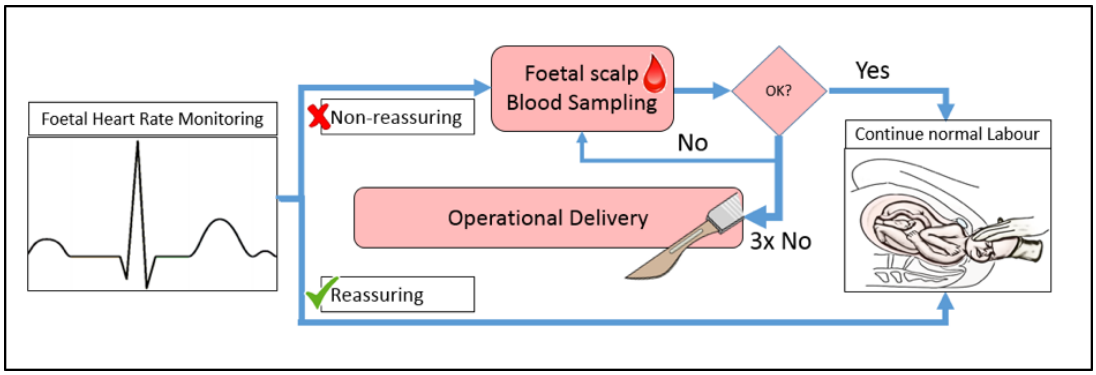

Figure 3.4: *Process of foetal monitoring.*

On the other hand, the heart rate pattern may not be indicative of any abnormalities or foetal compromise although the foetus might be suffering from hypoxia. Therefore, FSBS is performed to obtain additional information about the foetal well-being by measuring foetal blood pH and base deficit, which helps to distinguish between respiratory and metabolic acidosis. FSBS is repeated up to three times. If the pH values are not within the thresholds, the foetus is delivered through a caesarean section or an operational vaginal delivery. In cases where the pH value is within the normal range the normal labour process is continued. Foetal scalp blood sampling is recommended if the contraindications, listed in Table 3.2, can be excluded [2, 28, 58]:

Foetal scalp blood sampling is usually performed using a sampling kit, as illustrated in Figure 3.5 [59]. For the procedure, the mother is in the lithotomy[3] position to allow better access to the foetal scalp.

After preparing the sampling wand, by placing the capillary tube in its holder, the amnioscope[4] is inserted into the vagina. To prevent contamination from the surrounding environment, the amnioscope is placed against the foetal scalp

[3]Lithotomy position: A supine position of the body with the legs separated, flexed, and supported in raised stirrups.

[4]Amnioscope: An endoscope that, is introduced into the cervical canal.

Table 3.2: *Contraindications for Foetal Scalp Blood Sampling [2].*

Contraindications for foetal scalp blood sampling
Clinical picture demands early delivery
Cervix 3 cm dilated or thick meconium with scanty fluid
Pathological heart rate prompts immediate delivery
Changes are due to oxytocic overstimulation
Clotting disorders in the foetus are suspected
Mother infected with blood-borne infection such as HIV, hepatitis B/C
If spontaneous vaginal delivery is imminent
Easy instrumental vaginal delivery is possible
During or soon after, prolonged bradycardia

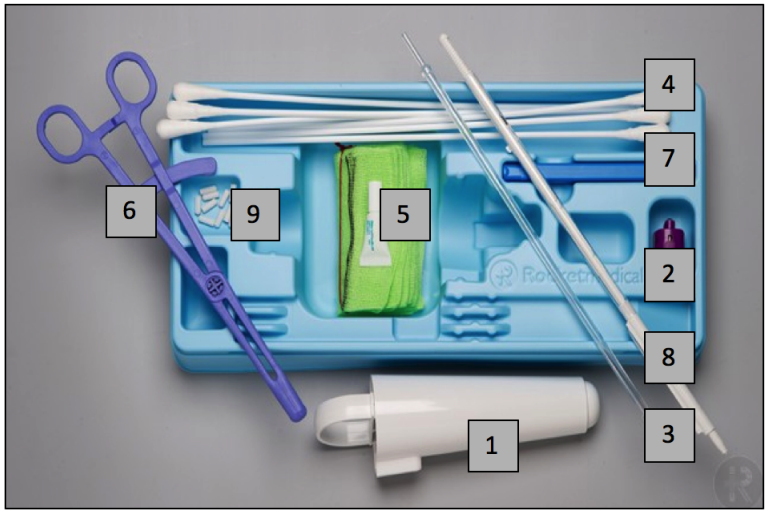

Figure 3.5: *Foetal Scalp Blood Sampling Kit [59]:1.Amnioscope+Obturator,2. Light source, 3. Sampling wand, 4. Swabs, 5.Petrolium Jelly, 6. Sponge-holding forceps, 7 High heparine capillary tubes, 8 Tube holder, 9 Tube covers.*

skin. To obtain a pure sample, the foetal skin is cleaned with cotton swabs, which can also be used to move hair, if necessary. The scalp is numbed, and perfusion is promoted by applying ethyle chloride and petroleum jelly respectively [60].

The incision is made by a small scalpel, which is located at the distal end of the sampling wand. After a sufficient blood drop has formed, it is collected with the heparinised capillary tube mounted on the sampling wand. The sampling system is retracted to retrieve the capillary tube, which is then closed with tube

caps on both ends. Additionally, to prevent clotting and bubble formation, a mixing wire can be added to the tube if a delayed insertion of the sample into the blood gas analyser (BGA) is expected. The amnioscope is removed from the vagina, whereby the blood sample is then inserted into the BGA for analysis [60]. This procedure may vary depending on the kit used and the guidelines in the respective hospital.

FBS is laborious, prone to errors (20% error rate [61]), invasive and it has also been criticised for not having been proven to be beneficial for foetal health and the associated complexities [62, 63, 64]. Furthermore, it does not provide continuous and real-time information about the well-being of the foetus. Therefore, alternative measurands representing foetal health status with the ability to distinguish between respiratory and metabolic acidosis, are being researched [6].

3.5 Diagnostic Parameters

The following measurands can be utilised in foetal blood sampled during FSBS, with the results obtained being used to diagnose foetal acidosis and determine clinical management. The advantages and disadvantages of each measurand, and clinical implications of abnormal results are summarised below.

3.5.1 pH

By definition, the pH value is the negative logarithm to the base 10 of the hydrogen ion (H^+) concentration in a solution. The pH value (Equation (3.1)) is expressed in mol/L [31]. This measurand plays an important role fluctuating between 7.2 and 7.4 to maintain normal metabolic processes.

$$\mathrm{pH} = -\log_{10}(\mathrm{H}^+) \tag{3.1}$$

The lower the pH, the more acidic a solution is. When the hydrogen ion concentration equals the hydroxyl ion (OH^-) concentration, the pH is 7.4

and represents a neutral solution like water. The pH value in the human body is influenced by hydrogen ion concentration and the partial pressure of carbon dioxide (pCO_2) [34]. Therefore, the pH value in the body can be regulated by the depth and frequency of breathing (which regulates pCO_2) and by the kidneys (which regulate H^+). In the foetus, the pH value is mainly regulated by gas exchange at the placenta, which makes it more susceptible to any disturbance in foetal-maternal respiration [65]. The pH can be acquired for foetal monitoring. When the oxygenation of the foetus is insufficient, more H^+ ions are produced, which leads to a lower pH value as described above. Currently the pH value is a common measurand for foetal monitoring using the thresholds given in Table 3.3.

Table 3.3: *pH thresholds for foetal monitoring [35].*

Interpretation	**pH**	**Clinical Decision**
Normal	≥7.25	Repeated sampling within an hour if indicated by CTG trace
Borderline	7.21-7.24	Repeated sampling within 30 minutes is indicated by CTG trace
Abnormal	≤7.20	Delivery of baby

3.5.2 Base Deficit

The base deficit (BD) represents the number of bases (*chem.*) that would neutralise the blood to a pH of 7.2 - 7.4. It is representative of the foetal reserves and enables to differentiate between a respiratory and metabolic acidosis, which is an important parameter in clinical decision making during birth [66]. The carbonic acid (H_2CO_3)-bicarbonate (HCO_3^-) buffer is represented by the following equation (Equation (3.2))[67]:

$$H^+ + HCO_3^- \leftrightarrow H_2CO_3 \leftrightarrow CO_2 + H_2O \tag{3.2}$$

The produced carbon dioxide (CO_2) is eliminated through the gas exchange

at the placenta [68]. The base deficit is calculated from pCO_2 and HCO_3^- by using a derived algorithm (Equation (3.3)) of the Siggard-Andersen chart [27].

$$BD = -0.9149 \cdot (0.12 \cdot \mathrm{pCO_2} \cdot \mathrm{CO_2} \cdot 10^{pH-6.1} - 24 + 16.21 \cdot [pH - 7.4]) \quad (3.3)$$

The normal range for base deficit is -1.0-8.9 mmol/L [28]. A value of 12 mmol/L is associated with severe newborn complications and is, therefore, the threshold for foetal metabolic acidosis [69]. The base deficit has the capability to distinguish between respiratory and metabolic acidosis, and therefore it has been used as an additional measurand for foetal well-being not only as retrospective but also as an intrapartum monitoring analysis in addition to pH analysis. However, the base deficit is not a measured but an artificially calculated parameter. Different equations are used to calculate the base deficit and it has been found that different blood gas analysers use different algorithms for the determination of the base deficit [67]. A correlation between foetal vitality and base deficit has only been found in severely affected new-borns. Additionally, the base deficit does not only represent a change in the acid-bicarbonate system but is a measurand for all buffering systems in the body. Therefore, the base deficit is not suggested to be used as a parameter for the determination of foetal well-being and lactate measurements should be used instead [68].

3.5.3 Lactate

As explained in Section 3.2 lactate is the end product of anaerobic metabolism, due to the lack of oxygen (O_2). Whether the energy in the foetus is produced under aerobic or anaerobic circumstances depends on the oxygen supplied by the mother. During the second stage of birth, which is dominated by contractions, the perfusion in the placenta can be restricted, leading to oxygen deficiency [33]. For an easier comparison of the three different parameters have been summarised in Table 3.4 [35]. The lactate values have been added for an approximate comparison. It has been shown that the thresholds for lactate

values differ depending on the device and need to be determined separately [70].

Table 3.4: *Respiratory and metabolic acidosis value of pH, base deficit and lactate. R.A = Respiratory Acidosis, M.A. = Metabolic Acidosis[28, 35, 69].*

	pH	**BD**	**Lactate [mmol/L]**	**Interpretation**
Normal	7.36-7.44	-1.0-8.9	≤ 4.1	Normal
R.A.	$<$7.36	-1.0-8.9	4.2-4.8	Borderline
M.A.	$<$7.36	$>$8.9	≥ 4.9	Abnormal

Lactate is more specific and more sensitive to predict foetal outcome and is therefore a potential alternative for pH [71, 72]. Hospitals in Sweden and Australia are replacing pH measurement with lactate measurements for FSBS [73, 74]. However, since pH has been used for clinical decision-making during birth it has been found that clinicians find it easier to base their decisions on pH values rather than lactate values. Rørbye *et al.* [75] have found, that if they based their decisions on lactate, it would have increased the operational delivery rate by as much as 30% [75]. It has also been suggested to measure lactate only during the first stage of labour, due to the lactate values generally being higher during the second stage, which could lead to unnecessary operational deliveries [45]. Therefore, the combined measurement of pH and lactate was considered as an alternative to pH measurements only. However, Wiberg-Itzel *et al.* [76] have found that when lactate and pH is used side by side to determine foetal well-being, it may increase the operation delivery rate without decreasing the rate of metabolic acidosis. On one hand, Liljeström *et al.* [73] findings correlate with these results. They concluded that pH and lactate differ in 55% of the cases, but on the other hand they have also shown that it reduces the number of operational deliveries from 95% to 66% compared to measuring pH values only [72].

3.6 Biofluids

The complex circumstances during labour only allow access to either foetal blood or interstitial fluid. Blood has many different functions in the human body. One of the main functions is to transport O_2 and nutrients to the organs and tissues while collecting waste products and CO_2 for disposal [77]. Regarding lactate, blood is used as a transport system to distribute and eliminate lactate. Interstitial fluid (IF) is the fluid that surrounds all cells in the human body. It holds different electrolytes and is a component of the extracellular fluid, which also includes blood plasma and lymph. The IF can be considered as a transport system between the cells and the blood vessels and has a similar composition to blood, with a lower concentration of proteins [78]. Currently blood is sampled for foetal monitoring. Due to its less invasive access IF has gained more attention in research for lactate detection. However, there is an on-going discussion about whether blood or IF serves as a better sample for lactate detection [79, 80, 81, 82]. There are only a few groups that have studied the correlation between lactate values in blood and interstitial fluid. One consistent conclusion is that there is a time delay between the lactate values in blood compared to the lactate value in IF [79, 80, 81, 82]. In these studies ranging from the year 1994 to 2012, lactate levels were either measured in humans during exercise [79, 81], after overnight fasting [80] and in critically ill patients [82]. Although different biofluids were used for lactate measurements, they were all compared to blood lactate values. Most of the papers report a delay of 6-10 minutes between blood lactate and IF lactate concentrations [79, 80, 81]. However, if foetal lactate concentrations are observed continuously, the trend of the concentration measured may provide enough information for clinical decision-making. A study comparing blood and tissue lactate in critically ill patients utilising microdialysis, has found that the correlation between blood and tissue lactate increases with time [82]. Another finding of this study conducted by Kopterides *et al.* [82] was that blood lactate is generally lower than tissue lactate, contrary to other findings in which the blood lactate is always higher than the tissue lactate [81]. One explanation could be that,

in this study by Kopterides *et al.* [82], the lactate was measured in patients experiencing shock. They only found higher tissue lactate level (compared to blood lactate levels) in patients with shock (compared to patients who were not in shock). It has to be taken into consideration that those measurements were not taken from foetuses but from adults whose physiology is different. In conclusion, it can be said that lactate concentration always rises first in blood and then in the tissue. Although professionals agree on the time delay between the lactate concentrations in blood and in interstitial fluid, there is no agreement about the way those two concentrations correlate.

3.7 Conclusions

Although foetal monitoring has improved over the past two centuries, there is a common agreement amongst professionals that foetal monitoring during birth requires improvements with regard to its non-invasiveness, its sensitivity, specificity and reliability. Current methods are laborious, prone to errors and invasive [62, 63, 64]. Lactate has been identified as potential alternative measurand for intrapartum foetal monitoring, due to its ability to distinguish between different types of acidosis. Therefore, lactate has been chosen as a measurand for the development of new monitoring device for foetuses during birth. It is important to fully understand the foetal physiology and to take the stages of labour into consideration, when using lactate as the key parameter for clinical decision-making [6]. Once confidence in the technique has been gained, measurements of lactate concentration may be used in the future for intrapartum foetal monitoring.

4 Literature Review: Technical Perspective

4.1 Introduction

In the previous chapter, the clinical need for an improvement of foetal monitoring during birth was pointed out and lactate was identified as a potential alternative to the current pH detection based on foetal scalp blood sampling. This chapter presents a coherent technical literature review on potential solutions to achieve this. In order to measure lactate, a biofluid needs to be excessed first for subsequent measurements. Potential sampling methods are explored in that effect. Secondly, the chapter explores the means of how lactate is recognised in biosensing and how these recognition elements can be attached to a biosensor surface. Subsequently, the key transduction methods for lactate detection and materials for biosensors are introduced. The outcome of a patent review regarding lactate sensing and foetal monitoring is also provided to complete the overview about the technologies in the field. Lastly, the experimental way forward based on the literature review is outlined in the conclusions section.

4.2 Sampling Biofluids

In section Section 3.6 blood and interstitial fluid have been introduced as potential biofluids to be sampled for foetal monitoring during birth. The following literature review on sampling biofluids presents microdialysis and the use of microneedles as the two potential sampling methods. The sections will also include the description of their functionality and current advances.

4.2.1 Microdialysis

Microdialysis follows the same mechanism as normal dialysis but on a smaller scale. A microdialysis probe consists of an inside tube, the inlet, and a second tube surrounding the first one, the outlet as shown in Figure 4.1. The outer surface area is made of a semipermeable membrane of a particular pore size depending on the substance to be sampled [83]. After inserting the probe into the tissue, a perfusate is pumped into the probe through the inlet flowing back through the outlet. The substance to be analysed (e.g. the lactate) experiences a concentration gradient between the perfusate and the surrounding fluid. As a consequence, this substance diffuses down the concentration gradient into the perfusate. The perfusate containing the sampled substance is called dialysate [84]. The dialysate is then transported to the sensing element at the distal end of the microdialysis catheter.

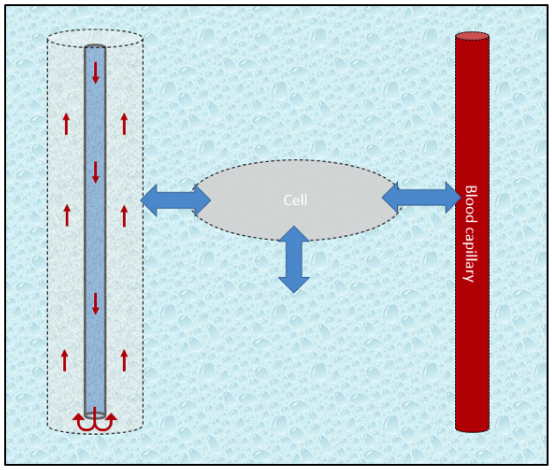

Figure 4.1: *Sketch of microdialysis probe (left) in interaction with cells and blood capillaries in the human body.*

Microdialysis has been primarily used in research to sample analytes. It is used in combination with electrochemical sensors for the measurement of the concentration of lactate [79, 85], glucose [85, 86], potassium [87].

Using microdialysis for sampling in a sensing device improves the selectivity due to the semi-permeable membrane only allowing substances of a certain target size to diffuse [85]. Furthermore, the membrane works as a physical barrier

between the sensing element and the body fluid, reducing bio-fouling and protecting the body from possible reactions towards materials and reagents used for the sensing electrode. Microdialysis probes are as small as about 240-500 μm in diameter [88] and therefore it is a useful sampling method for point of care applications. However, due to the time the analyte requires to diffuse into the perfusate, this approach only provides a limited time resolution, which makes it less attractive for the intended application. Time resolutions between 1-30 minutes for glucose and lactate have been reported for microdialysis sampling [84, 85, 89, 90]. When using microdialysis there is also the risk of small substances diffusing into the interstitial space (space between the cells and the blood capillaries). The depletion of the analyte at the area surrounding the probe, may lead to false results.

4.2.2 Microneedles

Microneedles are small needles(25 -2000 μm in height) [91] (usually arranged in an array) used to either access blood or interstitial fluid or to deliver a drug. Depending on the application different types of microneedles are used. They are divided into hollow [92], solid [93] and biodegradable [94, 95] microneedles (Figure 4.2). The delivery of drugs [93] and glucose monitoring [96, 97] have played a major role in the development of microneedles. The fabrication methods for microneedles vary depending on the material and application. The most common fabrication techniques are photolithography/photoetching, laser cutting, metal electroplating/electropolishing and micromoulding [17, 98, 99, 100, 101, 102, 103, 104, 105, 106].

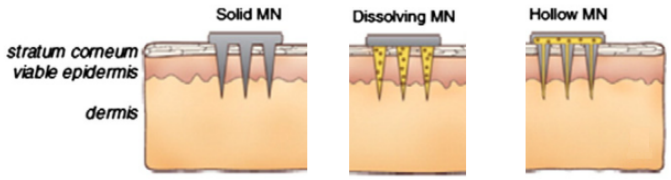

Figure 4.2: *Different types of microneedles applied to the skin. Solid microneedles (left), Dissolving microneedles (middle) and hollow microneedles (right) [96].*

Solid microneedles are fabricated from silicon [107], metal [108], and polymers [109]. They are used for sensing and drug delivery. An electrochemical sensor for lactate and glucose based on solid microneedles was developed by Vasylieva *et al.* (Figure 4.3) [109]. The microneedles were fabricated from SU8 polymer onto which three-electrode system was deposited. *In vitro* and *in vivo* tests have been executed successfully. For delivering drugs with solid microneedles they are coated with the specific drug. That layer will then dissolve upon application into the skin. Gill *et al.* [93] have developed a controllable process utilising micro-dipping to coat solid microneedles with enzymes amongst other substances [93].

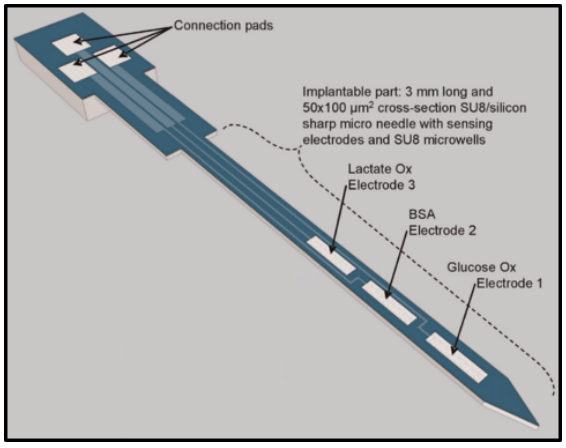

Figure 4.3: *Silicon/SU8 microneedle multi-electrode sensor on a 3 mm microneedle [109].*

Hollow microneedles are made from silicon and polymers and are used for biosensing and for the delivery of drugs. A hollow microneedle lactate biosensor has been developed and investigated by Windmiller *et al.* [110]. An array of pyramidical microneedles has been manufactured by a UV rapid prototyping technology and filled with metallised carbon paste (Figure 4.4). A response time of 15 seconds was achieved with a negligible rate of interference which is indicative of a good selectivity shown by recording the current of lactate and lactate with different potential interfering substances (ascorbic acid, uric acid, and acetaminophen). All solutions exhibited the same current values, which can also be clearly distinguished from a the negative control [110].

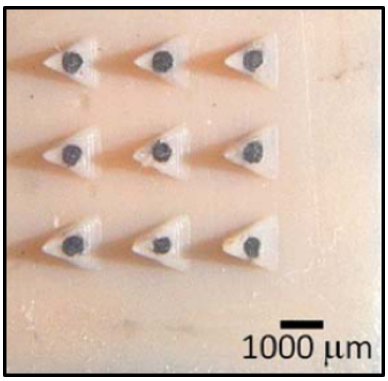

Figure 4.4: *Microneedles filled with metallised carbon paste [110].*

Biodegradable microneedles are made from biodegradable polymers and sugars for the delivery of drugs, which dissolve after applied to the skin [111]. The drug is encapsulated in the polymer/sugar during the fabrication process. The common fabrication process is micromolding. Sullivan *et al.* have developed a biodegradable microneedle patch (Figure 4.5) for influenza vaccination [112]. They have shown that the microneedles safely dissolve into pork skin within minutes.

Figure 4.5: *Example of biodegradable microneedles [112].*

The dimensions and geometry of microneedles determine and influence their mechanical strength and pain sensation. This has been tested computationally and experimentally [113, 114, 115]. Microneedles have to be long enough (100 - 2000 μm) to reach interstitial fluid or blood vessels and requires a thin sharp tip to minimise potential nerve contact. The longer a needle is, the more likely it is to reach the nerve endings in the dermis (approx. 200 - 2000 μm from the skin surface) [116] (Figure 4.6), such as in the case of a hypodermic needle. Davis *et al.* [115] have assessed different microneedle geometries regarding their insertion force and the maximum force before structural failure. The mi-

croneedles were fabricated from polyethylene terephthalate (PET) coated with a layer of titanium and copper. The insertion force has been found to be in the range of 0.1 - 3 N, low enough for manual insertion. The force required to break the needles was found to be around 3.8 N for most sizes and geometries, which is beyond the manual insertion force [115].

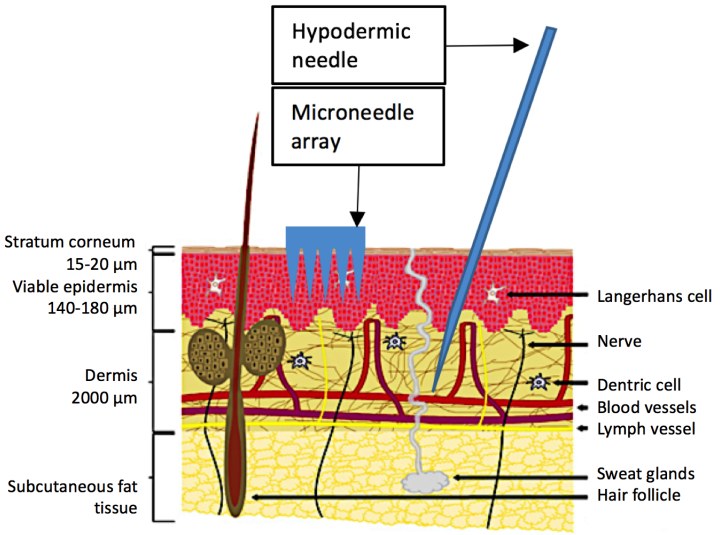

Figure 4.6: *Representation of the skin microanatomy [117].*

More practical studies have looked at the pain sensation and the skin irritation induced by the microneedles. It was proven that an increasing number of microneedles in an array and the microneedle length both increase the pain sensation [113]. The irritation of the skin after the application is dependant on the shape and dimension of the microneedles. The degree of irritation is compared to "tape stripping" [114], returning to a no-irritation state two hours after the application. The skin irritation experienced from the application from microneedles can, therefore, be classified as minimal [114]. This would be an improvement to the current method of foetal scalp blood sampling using a scalpel. A patent for a microneedle lactate sensing device has been registered as "Lactate measuring device and method for training adjustment in sports" by Jun-Tang Huang. The device describes a microneedle patch for the continuous measurement of lactate during exercise. The microneedle size is 10 - 1,000 μm in height and 150 - 450 μm base width [17, 98, 99, 100, 101, 102, 103, 104, 105, 106].

Due to their size and shape, microneedles have several advantages compared to normal hypodermic needle applications. Both the advantages and disadvantages are listed in Table 4.1 [111].

Table 4.1: *Advantages and disadvantages of microneedles [111].*

Advantages	**Disadvantages**
Reduced pain and wounds	Still invasive
Combinational possibilities	Skin irritation
Minimally invasive	Stability
Can sample interstitial fluid and blood	Difficult application
Lowered risk of infection	
Enables continuous sampling/monitoring	

4.2.3 Conclusions

Microdialysis and microneedles have been found to be the current means of sampling in research for biosensing and therefore also for lactate sensing. Although microdialysis has several advantages over microneedles including its higher selectivity due to the semi-permeable membrane, microdialysis requires the addition of equipment and fluids such as a pump and perfusate. Different microneedles have been developed successfully. Solid and hollow microneedles can be used potentially for the application of foetal monitoring during birth. The sizes and mechanical strength found in the literature are compatible with the aim of this project. Based on these characteristics microdialysis is not suitable for the aim of this project and microneedles will be explored further for the purpose of developing a foetal monitoring device (Section 5.3).

4.3 Recognition

The recognition element for lactate detection is enzymes. There are two different enzymes that are used to recognise lactate. Lactate oxidase (Lox) [118]

and lactate dehydrogenase (LDH) [119]. These enzymes will be described in the following sub-sections.

4.3.1 Lactate oxidase

Lactate oxidase (Lox), also referred to as lactate mono-oxygenase, is a globular flavoprotein[1] that promotes the oxidation of lactate to pyruvate in the presence of oxygen forming hydrogen peroxide (H_2O_2) [120]. H_2O_2 can then be reduced or oxidised to determine the lactate concentration [121]. The reaction (Equation (4.1a) and Equation (4.1b)) with lactate oxidase does not require a co-factor [122, 123].

$$\text{Lactate} + O_2 \xrightarrow{\text{Lox}} \text{Pyruvate} + H_2O_2 \tag{4.1a}$$

$$H_2O_2 \rightarrow O_2 + 2\,H^+ + 2\,e^- \tag{4.1b}$$

H_2O_2 requires a high potential to oxidise, which reduces the sensor specificity, due to increases in interference from other substances, such as ascorbic acid, uric acid, and acetaminophen, in the sample [123, 124, 125]. It has been shown that interference can be eliminated or reduced by covering the sensing surface with a Nafion™[2] [126] or electropolymerised thin films [25], which improve the selectivity of a sensor. From the chemical equations (Equations (4.1a) and (4.1b), the reaction between lactate and lactate oxidase is dependent on oxygen and thus susceptible to oxygen fluctuations in the sample. This oxygen dependency affects the detection limit, manufacturing cost and miniaturisation negatively [123]. However, as long as pO_2 is not lower than 8 mmHg, the chemical reaction is not affected [127].

[1] A protein contains flavin. It is involved in oxidation processes in cells.

[2] Nafion™is a polymer, which is used as a membrane or coating

The majority of the research being conducted on lactate sensors use Lox (Table 4.2), of which most of these have the fastest response times (1-5 seconds). An example of this research is given by Wei *et al.* [45], who have developed a lactate sensor based on chitosan and have achieved a detection limit of 50 nM. The two lactate sensors with the fastest response also have the lowest detection limits (3 pM and 50 nM) [128, 129], which is essential for a sensitive biosensor.

Table 4.2: *The six fastest lactate sensors based on Lox listed regarding response time. AlGaAs=Aluminium gallium arsenide, Pt=Platinum, GC=Glassy Carbon, In=Indium, ZnO=Zinc oxide, NW=Nanowires, CNT=Carbon Nanotubes, HG=Hydrogel, NP=Nanoparticles MWCNT=Multi-walled carbon nanotubes, AM=Amperometric.*

Substrate	Enzyme	Material	Transduction	Application	Resp. Time [s]	LoD [nM]	Ref.
AlGaAs	LOx	In-doped ZnO NW	AM	Test solution	1	0.003	[129]
Pt	LOx	Chitosan	AM	Test solution	1	50	[128]
GC	LOx	CNT	AM	Test solution	2	4.10	[130]
Pt	LDH	Teflon, sulfonate HG	AM	Test solution, beverage	2	4.10	[125]
GC	LOx	Pt NPs, MWCNT	AM	Test solution	5	250	[131]
GC	LOx	MWCNTs	AM	Whole blood	5	300	[132]

4.3.2 Lactate dehydrogenase

Lactate dehydrogenase (LDH) is a protein of great importance for the human body. It is released to break down lactate in damaged tissue or muscles. LDH also promotes the oxidation of lactate to pyruvate but instead of oxygen, it requires the oxidised form of nicotinamide adenine dinucleotide (NAD^+) for the reaction to occur. NADH is the outcome of this reaction (Equation (4.2a) and Equation (4.2b)) which can then be oxidised [123].

$$\text{Lactate} + \text{NAD}^+ \xrightarrow{\text{LDH}} \text{Pyruvate} + \text{NADH} + \text{H}^+ \tag{4.2a}$$

$$\text{NADH} \rightarrow \text{NAD}^+ + \text{H}^+ + 2\,\text{e}^- \tag{4.2b}$$

Lactate dehydrogenase (LDH) is more selective than lactate oxidase (Lox) due to its oxygen independence [14, 119]. Furthermore, sensing with lactate dehydrogenase, qualifies for optical sensing, due to the fluorescent characteristic of the co-factor NADH [133]. Besides these advantages, sensing with LDH holds, however, a few disadvantages. LDH is an unstable protein and requires high overpotential for the oxidation of NADH, which again is the cause of interference from other substances, such as ascorbic acid, uric acid, and acetaminophen, reducing the specificity of the sensor [119, 134, 135]. Furthermore, the substance produced during the chemical reaction can cause fouling of the electrode thus impairing operational stability [134].

Less data on sensor characteristics, such as detection limit and response time, is given in the publications of lactate sensors based on LDH (Table 4.3). Researchers make use of the fluorescent characteristic of NADH and have developed electrochemiluminescence (ECL) lactate sensors [136, 138]. To achieve more sensitive lactate sensors based on LDH, additional reagents such as luminol are added [136]. However, luminol is not biocompatible because it causes skin irritation and also has a negative impact on the digestive and the respiratory system and is therefore not suitable for *in vivo* applications [139]. Both

Table 4.3: *Lactate sensors based on LDH listed from lowest to highest detection limit. Pt=Platinum, GC=Glassy carbon, NT=Nanotube, OF=Optical fibre, LDH=Lactate dehydrogenase, CNT=Carbon nanotubes, Au=Gold, NP=Nanoparticles, MWCNT=Multiwalled carbon nanotubes, ECL=Electrochemiluminescence, AM=Amperometric, NA=Not available*

Substrate	**Enzyme**	**Material**	**Transduction**	**Application**	**Resp. Time [s]**	**LoD [nM]**	**Ref.**
Pt	LDH	CNTs	ECL	Test Solution, sweat	NA	0.001	[136]
Graphene	LDH	Au NPs	AM	Artificial serum	8	130	[119]
GC	LDH	NPs/MWCNT	AM	Serum	NA	300	[15]
NT paste	LDH	MWCNT	AM	Blood	NA	5,000	[137]
OF	LDH	N/A	ECL	Test Solution, single cell	1	7,500	[138]

advantages and disadvantages of lactate oxidase and lactate dehydrogenase are summarised in Table 4.4.

Table 4.4: *Summary of the advantages and disadvantages of lactate oxidase and lactate dehydrogenase.*

Enzyme	**Advantages**	**Disadvantages**
Lactate oxidase	No co-factor required	Oxygen dependency trace
Lactate dehydrogenase	Fluorescent characteristic of the cofactor NADH Independent of oxygen	Electro fouling is more likely

Despite being a disadvantage for LDH, there is a wide range of overpotentials used for both enzymes. For both enzymes, high and low overpotentials have been identified and are summarised in Table 4.5.

Table 4.5: *Overpotentials of lactate sensors based on Lox and LDH. GC=Glassy carbon Pt=Platinum, AlGaAs=Aluminium gallium arsenide, LDH=Lactate dehydrogenase, Lox=Lactate oxidase, AM=Amperometric.*

Substrate	Enzyme	Transduction	Working Potential [V]	Ref.
Graphene	LDH	AM	0.48	[119]
GC	LDH	AM	0	[15]
Graphite	LDH	AM	0.35	[140]
Pt	LOx	AM	0.4	[128]
Carbon	LOx	AM	-0.1	[141]
Pt	LOx	AM	0.65	[142]
Pt	LOx	AM	0.65	[143]
Glass	LOx	AM	-0.05	[144]
GC	LOx	AM	0.5	[132]
AlGaAs	LOx	AM	0.5	[129]
Carbon	LOx	AM	0.3	[145]
GC	LOx	AM	0.1	[146]
Pt	LOx	AM	0.7	[127]
Pt	Lox	AM	0.7	[25]
Pt	LOx	AM	0	[147]
Pt	LOx	AM	0.65	[148]

4.4 Immobilisation

Immobilisation is the attachment of recognition elements (e.g. enzymes) to a substrate or within a support material [7]. There are different ways of immobilising enzymes, which are shown in Table 4.6.

4.4.1 Adsorption

Physical adsorption is the attachment of enzymes through forces such as Van der Waal forces, hydrogen bonding and hydrophobic interactions [150]. This way of immobilisation is simple because neither enzymes nor the support need

Table 4.6: *Immobilisation methods [7, 149].*

Support based	**Not support-based**
Adsorption	Cross-linking
- Physical	
- Ionic	
- Covalent	
Entrapment/Encapsulation	

to be charged. Another advantage of using physical adsorption is that the support does not require much preparation. Activity is also maintained due to the little deformation applied to the enzyme [150].

Ionic adsorption makes use of the electrostatic interaction between ions. The connection between negatively and positively charged ions is dependent on the surrounding pH, temperature, and ionic strength and forms the foundation for the ion bonding. As it is a weak bonding, the enzymes do not experience much deformation and the immobilisation is easily reversed. However, this can also cause leaching making the sensor less effective and stable [151].

Covalent adsorption is based on covalent bonding, in which two atoms share electrons. Although this immobilisation method is a time-consuming process, this attachment method forms a strong connection between the enzyme and the support material, which makes it more stable and less prone to leaching. However, this immobilisation method can lead to reduced enzyme activity due to enzyme deformation, restricted enzyme movement, and blocking of active sites [7, 149].

Table 4.7 summarises the list of lactate sensors using adsorption as the immobilisation method. More than half of the listed lactate sensors meet the required detection limit of 0.001 mM [15, 24, 124, 129, 137]. Most of those employ amperometry in combination with Lox [124, 132]. The sensors with the lowest detection limit share the property that they both apply nanoparticles to their substrate for the enhancement of the surface area [15, 129]. From this table, the optical-electro-chemiluminescence (ECL) sensor achieved the lowest

detection limit [15]. Immobilisation through adsorption seems to work well with LDH as good detection limits and response times were obtained, achieving the fastest response times (of 1 second) in combination with optical ECL sensors [138].

Table 4.7: *Lactate sensors based on adsorption as an immobilisation method. Pt= Platinum, AlGaAs=Aluminium gallium arsenide, GC=Glassy Carbon, Au=Gold, OF=Optical fibre, SPE= Screen-printed electrode, Lox=Lactate Oxidase, LDH=Lactate dehydrogenase, CNT=Carbon Nanotubes In=Indium, ZnO=Zinc oxide, NW=Nanowires, NP=Nanoparticles, MWCNT=Multi-walled carbon nanotubes, GCNF=Graphitized carbon nanofiber, SPCE=Screen-printed carbon electrodes, ECL=Electro-chemiluminescence, AM=Amperometric, CCD=Charged-coupled device, NA=Not available*

Substrate	Enzyme	Material	Transduction	Application	Resp. Time [s]	LoD [nM]	Ref.
Pt	LDH	CNTs	ECL	Test Solution, sweat	NA	0.000001	[151]
AlGaAs	LOx	In-doped ZnO NW	AM	Test Solution	1	0.000003	[144]
Plastic	LOx	Pt NPs	AM	Test Solution, sweat,blood	NA	0.11	[140]
GC	LOx	Pt NP, MWCNTs	AM	Whole blood	5	0.3	[152]
GC	LDH	NPs/MWCNT	AM	Serum	NA	0.3	[24]
GC	LOx	Carbon	ECL,CCD	Human serum	NA	2	[153]
GC	LOx	CNT	AM	Test Solution	2	4.1	[145]
Carbon	LOx	Pt-NPs/GCNF-SPCEs	AM	Food Samples	NA	6.9	[154]
Au	Lox	NPs	AM	Test Solution	NA	15	[155]
OF	LDH	NA	ECL	Test Solution, single cell	1	20	[138]
GC	LOx	Co-polymer	AM	Test Solution	NA	20	[156]
SPE	Lox	MWCNT	AM	Cell culture	30	28	[157]

4.4.2 Entrapment/Encapsulation

Immobilisation of enzymes by entrapment or encapsulation consists in the formation of a lattice or matrix around the enzymes without forming a connection. Due to the minimal modification of the enzyme, activity is maintained and the stability is increased. Furthermore, since there is no connection between the enzyme and the support, the active sites do not get blocked [158]. However, mass transfer can be impaired due to the dependency on the porous network surrounding the enzymes. Common materials used for entrapment and encapsulation are sol-gel and hydrogel [159]. Sol-gel requires a non-biocompatible precursor and forms alcohol-causing gel-shrinkage during the manufacturing process [7, 149].

Table 4.8 provides a list of the sensors using entrapment/encapsulation to immobilise the lactate sensing enzymes onto the substrate. Both sol-gel and hydrogel seem to have the potential to detect lactate concentration as low as 130 nM [41] and 6.4 nM [157], respectively. Immobilisation through entrapment/encapsulation is mostly used in combination with amperometric transduction. Although good response times (2-7 seconds) have been achieved [125, 132, 160], such sensors tend to have a slower response time such as 2:24 minutes and 15:12 minutes [85, 118]. This slow response may be due to the diffusion barrier created through the gel around the enzyme, which is also a protective barrier against the surrounding environment.

4.4.3 Cross-linking

Cross-linking uses a two-step process, which adds different reagents to provide sufficient immobilisation. Although this method forms a stable immobilisation of the enzyme and does not require additional support such as gels or membranes, it may cause a conformational change, which reduces enzyme performance. This method can be improved by using a support material such as chitosan [7, 149].

Table 4.9 summarises the list of lactate sensors with cross-linked enzymes on

the substrate. More than half of the listed sensors utilising cross-linking offer a sufficient detection limit needed for foetal monitoring [24, 25, 110, 122, 140, 147, 153, 154, 155, 156, 157, 161]. The response time ranging from 5 s to 180 s for the electrochemical sensors may not be entirely due to the immobilisation method but be the result of different protective layers employed, not allowing fast diffusion. However, cross-linking is a common method for immobilising enzymes and protocols are readily available [124, 142, 145, 162, 163].

Table 4.8: *Lactate sensors based on entrapment/encapsulation as an immobilisation method. GC=Glassy Carbon, Au=Gold, Pt=Platinum, Lox=Lactate oxidase, LDH=Lactate dehydrogenase, NP=Nanoparticle, , MWCNT=Multi-walled carbon nanotubes, CNT=Carbon Nanotubes, HG=Hydrogel, PCB= Printed circuit board, SG=sol-gel, AM=amperometric, ECL=electro-chemi-luminescence, TS=Test solution, NA=Not available*

Substrate	**Enzyme**	**Material**	**Transduction**	**Application**	**Resp. Time [s]**	**LoD [μM]**	**Immobilisation**	**Ref.**
Glass	Lox	NA	AM	Test Solution	20	0.0064	HG	[164]
Graphene	LDH	Au NPs	AM	Artificial serum	8	0.13	SG	[119]
GC	Lox	Pt NP, MWCNTs	AM	Whole blood	5	0.3	SG	[132]
Au	Lox	CNT	AM	TS	7	5	Entrapment	[160]
Graphite	Lox	Chitosan/CNT	AM	TS, cell culture	NA	22.6	Entrapment	[23]
GC	Lox	Polymer	AM	NA	NA	50	SG	[153]
Polymer	Lox	Carbon paste	AM	TS	NA	420	entrapment	[110]
NA	Lox	HG	Optical	TS	912	NA	HG	[118]
Polyimide	Lox	Pt	AM	NA	30	NA	HG	[156]
Plastic	Lox	PCB	AM	TS, dialysate	144	NA	HG	[85]
Graphite	LDH	sol-gel	AM	TS	NA	NA	SG	[140]
Pt	Lox	Sol-gele	AM	TS	NA	NA	SG	[147]
Glass	LDH	sol-gel	ECL	TS	NA	NA	SG	[133]

Table 4.9: *Lactate sensors based on cross-linking as an immobilisation method. Pt=Platinum, PVC=Polyvinyl chloride, NA=Not available, Lox=Lactate oxidase, Au=Gold, ZnO=Zinc oxide, NR=Nanorods, HG=Hydrogel, NC=Nanocubes, SPEES/PES=Sulphonated polyether ether sulphone–polyether sulphone , AM=amperometric, OFET=Organic field-effect transistor, CV=Cyclic voltammetry EISF=eyeball interstitial sclera fluid.*

Substrate	**Enzyme**	**Material**	**Transduction**	**Application**	**Resp. Time [s]**	**LoD [μM]**	**Ref.**
Glass ceramic	Lox	Au thin film	AM	Test Solution, wine	15	0.005	[139]
Glass	Lox	Al Au	OFET	Test Solution	NA	0.066	[23]
Glass	Lox	Au, ZnO NR	PM	Test Solution	10	0.1	[165]
Pt	Lox	HG mucin/albumin	AM	Blood	50	0.8	[142]
Pt	Lox	Pt	AM	Blood and EISF	120	2.22	[166]
Glass	Lox	Carbon film	AM	Test Solution/rat brain	NA	2.3	[167]
Pt	Lox	monomer	AM	Food Samples	60	8	[168]
PVC	Lox	PB nanocubes	CV	Test Solution	5	10	[169]
silicon	Lox	Pt	AM	Biological samples	15	45	[165]
Polymer	Lox	Pt	AM	Test Solution	35	50	[170]
NA	Lox	HG	Optical	Test Solution	912	NA	[15]
Pt	Lox	SPEES/PES	AM	Rats	180	NA	[148]

4.4.4 Conclusion

As the sensor will be in direct contact with human tissue, an immobilisation method is required, which provides a strong bond between the enzyme and the electrode surface, and prevents leaching. Covalent bonding and cross-linking are most likely to provide a strong immobilisation of the enzyme. Therefore these methods will be explored further for the development of the lactate sensor for foetal monitoring during birth (Chapter 6).

4.5 Transduction

Transduction is defined as the translation of the signal generated by the recognition element into a measurable signal. This can be achieved by multiple means such as electrochemical, optical and thermometric transduction. The transduction method is dependent on the measurand, the signal obtained from the recognition element and the output signal required [7]. The main transduction methods used for lactate detection are optical [118, 136] and electrochemical [122, 132] transduction . The basic underlying principle of these techniques is explained in the following paragraphs.

4.5.1 Optical sensors

Optical sensors transform an optical signal, obtained at the recognition site, into an electrical signal. In optical sensing, the system consists of the light source and the light detector with the light source being an external light source or light emitted by the analyte. The transmitted light is then received by the light detector. There are different types of optical detectors (Table 4.12), which provide different output signals.

Electro-chemiluminescence (ECL) and colorimetry have been utilised for lactate sensing [133, 138, 172]. ECL is based on a (bio-) electrochemical reaction resulting in a luminescence compound [7]. Colorimetry is used in combination

Table 4.10: *Types of optical detectors [171].*

Type	Function
Photoresistor	When light is applied to a photoresistor, its resistance changes.
Photodiodes	Change in electric current upon light application.
Phototransistors	A phototransistor is a combination of a photodiode and a transistor. The light intensity regulates the current flow through the transistor [87].

with a dye that changes colour in relation to the lactate concentration [172].

In lactate sensing, co-enzyme-based optical transduction plays an important role. NAD^+ is a co-enzyme for lactate dehydrogenase and display exhibits characteristic absorption (350 nm) and fluorescence (450 nm), enabling optical detection[7].

Although optical sensing holds several advantages over electrochemical sensing as defined in Table 4.11, comparatively few researchers have explored optical detection (Table 4.12) as an alternative method for the determination of lactate concentration.

Table 4.11: *Advantages of optical sensing [173].*

Easy to miniaturise
Selectivity
Inexpensive
No reference signal required
Self-contained
Immunity to electro-magnetic interference
No electrical risk for patient

Li *et al.* [133] have encapsulated lactate dehydrogenase and NAD+ in silica powder and films. Due to the mild manufacturing method, sufficient enzyme

activity has been obtained for further development of a lactate sensor. However, their experimental design experienced enzyme leaching problems from the sol-gel employed [133]. A more successful approach was achieved by Cai *et al.* [136], who developed an optical biosensor for the detection of lactate in sweat. Lactate oxidase was used for optical detection in combination with the luminescent material, luminol, which provided a lactate sensor with a detection limit of $8.9{\cdot}10^{-10}$ mol/L [136]. Luminol is a luminophore with a signal intensity enhanced by the by-product of the reaction between lactate oxidase and lactate H_2O_2 [166, 167]. However, due to associated toxicity, luminol cannot be used *in vivo* [139].

To develop a lactate sensor for cancer research, Zheng *et al.* [138] have studied an optical sensor based on lactate dehydrogenase immobilised on the tip of a nanoprobe, achieving a response time of 1 second. However, only concentrations as low as 0.02 mM have been reported [138]. A few sensors based on colour change related to the concentration of lactate have been studied, which however require a microfluidic chip, adding to the complexity of the sensor [168].

Although optical detection has a great potential for lactate sensing for intrapartum foetal monitoring, due to the advantages stated in Table 4.11, little proof has been identified for the suitability of this method for the intended purpose.

Table 4.12: *Lactate sensors based on optical detection. Pt=Platinum, GC=glassy carbon, OF=Optical fibre, LDH= Lactate dehydrogenase, Lox=Lactate oxidase, CNTs=Carbon nanotubes, Al=Aluminium, PDMS= Polydimethylsiloxan, HG=Hydrogel, SG=Sol-gel, ECL=Electrochemiluminescene, CCD=Charged-coupled device, NA=Not available*

Substrate	**Enzyme**	**Material**	**Transduction**	**Application**	**Resp. Time [s]**	**LoD [μM]**	**Ref.**
Pt	LDH	CNTs	ECL	Test Solution, sweat	NA	0.000001	[136]
GC	LOx	Carbon	ECL,CCD	Human serum	NA	2	[167]
OF	LDH	Al coating	ECL	Test Solution, single cell	1	20	[138]
OF	LOx	PDMS	Colorimetric	Test solution	130	520	[168]
None	LOx	HG	phosphorescent	Test Solution	912	NA	[118]
Glass	LDH	SG	Fluorescence, ECL	Test Solution	NA	NA	[133]

4.5.2 Amperometric sensors

An amperometric sensor measures the resulting current upon an applied potential. This current is equivalent to the measurand concentration. The physical principle is outlined in in more detail in Section 6.3.2. Through an extensive review of lactate sensors, it has become evident that the majority of the lactate sensors utilise amperometry. These sensors are summarised in Table 4.13. All the sensors listed achieve a detection limit of 0.003 nM - 600 nM [129, 161]. However, only two of those react within 1-6 seconds [129, 155]. The working electrodes have been modified by different means such as multiwalled carbon nanotube (MWCNT) [15, 131, 132, 174], chitosan [128], nanowires [129] and nanoparticles [119, 124]. Therefore, the functionalisation before the enzyme immobilisation seems to be one of the important fabrication steps of a lactate sensor. The sensors with a prompt reaction deploy a form of nanomaterial, generating a large electrochemical surface area for the attachment of the enzyme and ultimately for the recognition of lactate. Wei *et al.* [128] have developed an amperometric lactate sensor based on a platinum-chitosan electrode functionalised with lactate oxidase achieving a detection limit of 50 nM within 1 second over a period of 24 hours. Chitosan is made from the chitin shell of shrimps and is biocompatible and non-toxic. Windmiller *et al.* [110] have used carbon paste in microneedles in combination with amperometric transduction. Their research found negligible interference of other substances, however, their operational stability was only tested for two hours. As an operational stability of up to 24 hours is required for the foetal monitoring device, this is an important parameter. Ma *et al.* [129] have developed a lactate sensor using a high electron mobility transistor (HEMT) and zinc oxide (ZnO) nanowires. In this HEMT based sensor, the drain current represents the lactate concentration in the sample. Furthermore, the presented sensor does not require a reference electrode, making it possible to minimise the required size of the gate. The gate is made from aluminum gallium arsenide (AlGaAs), due to its high chemical stability and good electron transport properties. However, toxic effects have been reported for AlGaAs, making it unsuitable for medical application

with potential direct contact with the patient [157].

Table 4.13: *Electrochemical lactate sensors. AlGaAs=Aluminium gallium arsenide, Pt=Platinum, GC=glassy carbon, Lox=Lactate oxidase, LDH=Lactate dehydrogenase, ZnO=Zinc oxide, NW=Nanowires, MWCNT=Multi-walled carbon nanotubes, Al=Aluminium, Au=Gold, NR=Nanorods, NP=Nanoparticles, CNT=Carbon nanotubes, AM=Amperometric, OFET=Organic field-effect transistor, NA=Not available*

Substrate	**Enzyme**	**Material**	**Transduction**	**Application**	**Resp. Time [s]**	**LoD [μM]**	**Ref.**
AlGaAs	Lox	ZnO NW	AM	Test Solution	1	0.003	[129]
Pt	Lox	Pt	AM	Rat	6	0.1	[155]
Carbon	Lox	MWCNT	AM	Food samples	20	0.56	[141]
Glass-ceramic	Lox	Au thin film	AM	Test Solution, wine	15	5	[122]
Glass	Lox	NA	AM	Test Solution	20	6.4	[164]
Pt	Lox	Chitosan	AM	Test Solution	1	50	[128]
Glass	Lox	Al Au	OFET	Test Solution	NA	66	[169]
Glass	Lox	Au, ZnO NRs	PM	Test Solution	10	100	[165]
Plastic	Lox	Pt NPs	AM	Test Solution, sweat,blood	NA	110	[119]
Graphene	LDH	Au NPs	AM	Artificial serum	8	130	[124]
GC	Lox	Pt NPs, MWCNT	AM	Test Solution	5	250	[131]
GC	Lox	Pt NP,MWCNTs	AM	Whole blood	5	300	[175]
GC	LDH	NPs/MWCNT	AM	Human serum	NA	300	[15]
Zinc	Lox	Au NPs, ZnO NRs	AM	Test Solution	NA	600	[161]

4.6 Materials

Two categories of materials are of main interest for biosensors, namely substrate and surface-enhancing materials such as nanoparticles.

Depending on the transduction method, different materials are used. For optical detection, glass and optical fibres are the preferred materials, enabling the transportation of the light towards the light detector [133, 138]. For the enhancement of the surface, materials such as carbon nanotubes, hydrogel, and sol-gel have been applied [118, 133, 136].

For electrochemical lactate sensing the substrate is preferably fabricated from gold [134], carbon [130], platinum [155] or glass [165]. The material is required to be biocompatible , corrosion resistant and conductive to serve as a working electrode for electrochemical sensing for medical applications.

4.6.1 Gold

Table 4.14 summarises lactate sensor based on gold electrodes. Lactate sensors based on gold substrate react to lactate in a solution within 10 - 70 seconds. The detection limits achieved based on gold electrodes was found to be between 1-15 μM [134, 170]. Lower detection limits have been found in lactate sensors using platinum and carbon electrodes (0.1 nM and 0.5 nM) as presented in Table 4.14. Although gold is a popular material for electronic fabrication and is biocompatible, it is an expensive raw material. However, screen-printed gold electrodes are commercially available [176] and gold is furthermore compatible with the fabrication techniques available to this project.

4.6.2 Platinum

Table 4.15 lactate sensors using platinum as a substrate are listed. Platinum has been used for electrochemical sensing because of its high electrocatalytic activity [145], providing a good basis for immobilisation. Platinum is con-

ductive, corrosion resistant and biocompatible. Platinum has been used more frequently for lactate biosensors. Sardesai *et al.* [155] have tested a platinum-based lactate sensor in rat tissue and obtained results within 6 seconds and have detected lactate concentrations as low as 0.1 nM. The remaining Pt-based lactate sensors listed in Table 4.15 require more time (50 - 180 seconds) and cannot detect lactate concentrations as low as the sensor presented by Sardesai *et al.* [155]. Additionally, screen-printed platinum electrodes are available to purchase for research purposes [177]. Furthermore, platinum is also an eligible material for the micro-fabrication processes.

4.6.3 Carbon

Lactate sensors based on carbon are provided in Table 4.16, showing both low detection limits and fast response times. Carbon is another popular material used as electrode material. It is very versatile and is used in different formations. It is used as glassy carbon, which is corrosion resistant, conductive and chemically inert. Carbon is also used in the form of graphene; a one-atom-thick layer of carbon, which is very strong, conductive and provides a large surface area ideal for surface functionalisation. Graphite sheets are flexible, enabling flexible sensors for direct application onto skin. Perez and Fabregas [141] have developed an amperometric lactate sensor based on carbon detecting lactate concentration as low as 0.56 nM within 20 seconds. A faster response time of 2 seconds was achieved by Goran *et al.* [130] with carbon-based lactate sensor. The detection limit, however, was significantly higher (4.1 μM) than the previously described carbon lactate sensor [141]. Carbon shows good potential to serve as a substrate for lactate sensors. Despite the advantage of the use of carbon for electrochemical sensor and their commercial availability [178], carbon is not compatible with the fabrication process available to this project.

4.6.4 Glass

Lactate sensor, based on glass substrates, are frequently used and are listed in Table 4.16. However, because a conductive surface is required for electrochemical sensors, the glass substrate has been modified with layers of metal or carbon such as ZnO [165] and nitrogen-doped carbon [130]. Ibupoto *et al.* [165] have developed a lactate sensor using glass and ZnO nanorods achieving a detection limit of 0.1 μM to be detected within 10 seconds. Faster lactate sensors, which react within 2 seconds to a change of lactate concentration, have been developed creating a substrate from glassy carbon in combination with nitrogen-doped carbon nanotubes [130]. As microneedles are proposed as the basis for the development of the lactate sensor, glass is not the ideal choice as a substrate for the sensor because microneedles are mainly fabricated primarily from polymers [179] or metal [172].

4.6.5 Nanomaterials

Nanoparticles are frequently incorporated in lactate sensors to enlarge the surface area, providing possibilities for the enzymes to attach. Nanoparticles, such as multi-walled carbon nanotubes (single or multi-walled carbon nanotubes [15, 141]) and carbon nanocubes serve as a bridge between the working electrode and the site of the chemical reaction. They have advantageous characteristics for biosensor applications because they create a large surface area, have a high surface reaction energy, high sensitivity, and high catalytic efficiency. They also improve the response time and the ability to adsorb the enzyme [123]. Nanoparticles can be applied to various materials such as gold, glass, carbon and glassy carbon [15, 134, 141, 165]. However, nanomaterials are potentially toxic [180] and as the sensor will be in direct contact with human tissue, they are not compatible with the development of the proposed sensor.

Table 4.14: *Sensors based on gold substrates. Au=Gold, Lox=Lactate Oxidase, LDH=Lactate dehydrogenase, NP=Nanoparticles, CNT=carbon nanotubes, HG=Hydrogel, AM=Amperometric, NA=Not available*

Substrate	**Enzyme**	**Material**	**Transduction**	**Application**	**Resp. Time [s]**	**LoD [μM]**	**Ref.**
Au	Lox	NPs	AM	Test Solution	NA	15	[170]
Au	LDH	CNT	AM	Test Solution, milk, serum	10	1	[134]
Au on glass	LOx	HG	AM	Test Solution	70	NA	[181]

Table 4.15: *Sensors based on platinum substrate. Pt=Platinum, Lox=Lactate oxidase, HG=Hydrogel, PPD= Phenylenediamine, PPY=Polypyrrole, SPEES/PES= Sulphonated polyether ether sul- phone/Polyether sulphone, AM=Amperometric, EISF=Eyeball interstitial sclera fluid, IF=Interstitial Fluid, NA=Not available*

Substrate	Enzyme	Material	Transduction	Application	Resp. Time [s]	LoD [μM]	Ref.
Pt	Lox	Pt	AM	Rat tissue	6	0.0001	[155]
Pt	Lox	Chitosan	AM	Test Solution	1	0.05	[128]
Pt	Lox	HG mucin/albumin	AM	Blood	50	0.8	[142]
Pt	Lox	Pt	AM	Blood and EISF	120	2.22	[143]
Pt	Lox	Monomer	AM	Food Samples	60	8	[182]
Pt	Lox	HG mucin/albumin	AM	Test Solution	90	0.7	[152]
Pt	Lox	PPD	AM	Test Solution	60	NA	[127]
Pt	Lox	PPY film	AM	IF	NA	NA	[25]
Pt	Lox	SPEES/PES	AM	Rat	180	NA	[148]
Pt	Lox	Nylon net	AM	Subcutaneous	NA	NA	[183]
Pt	Lox	Sol-gel	AM	Test Solution	NA	0.1	[147]

Table 4.16: *Sensors based on carbon, glass, and glassy carbon. GC=Glassy carbon, Au=Gold, Lox=Lactate oxidase, LDH=lactate dehydrogenase, MWCNT=Multi-walled carbon nanotubes, Al=Aluminium, ZnO=Zinc oxide, NR=Nanorods, NP=Nanoparticles, CNT=Carbon nanotubes, GCNF=Graphitized carbon nanofiber, HG=Hydrogel, AM=Amperometric, OFET= Organic field-effect transistor, NA=Not available*

Substrate	**Enzyme**	**Material**	**Transduction**	**Application**	**Resp. Time [s]**	**LoD [μM]**	**Ref.**
Carbon	Lox	MWCNT	AM	Food samples	20	0.00056	[141]
Glass-ceramic	Lox	Au thin film	AM	Test Solution, wine	15	0.005	[122]
Glass	Lox	Al Au	OFET	Test Solution	NA	0.066	[169]
Glass	Lox	Au, ZnO NR	PM	Test Solution	10	0.1	[165]
Graphene	LDH	Au NPs		AM Artificial serum	8	0.13	[119]
GC	Lox	Pt NPs, MWCNT	AM	Test Solution	5	0.25	[131]
GC	Lox	Pt NP,MWCNTs	AM	Whole blood	5	0.3	[132]
GC	LDH	NPs/MWCNT	AM	Human serum	NA	0.3	[15]
Carbon	Lox, LDH	CNTs	AM	Test Solution	NA	0.37	[141]
GC	Lox	Carbon	Optical	Serum	NA	2	[167]
Glass	Lox	Carbon film	AM	Test Solution/rat brain	NA	2.3	[89]
GC	Lox	CNT	AM	Test Solution	2	4.1	[130]
Carbon	Lox	Pt NPs/GCNF	AM	Food	NA	6.9	[145]
Graphite	Lox	chitosan/CNT	AM	Cell culture	NA	22.6	[23]
GC	Lox	Polymer	AM	NA	10	50	[153]
GC	Lox	Polymer	AM	Test Solution	NA	200	[146]
Au on glass	Lox	HG	AM	Test Solution	70	NA	[181]
GC	Lox	Pt	AM	Blood	30	NA	[184]

4.6.6 Conclusions

For the development of an electrochemical lactate sensor, the electrode needs to be biocompatible, corrosion resistant and conductive. Furthermore, for the initial development phase and for the second stage, involving the fabrication of a sensor, it is necessary that the material can be processed using the electron beam evaporator. For the above reasons, gold and platinum are the most suitable for the sensor for foetal monitoring during birth.

4.7 Patent Review

In addition to the literature review, an extensive patent review has been conducted regarding lactate sensing and foetal monitoring, utilising the database Espacenet [185]. The patents have been categorised according to their detection method, namely, electrochemical, optical, electrical and other. In total 60 patent were reviewed. The reviewed patents were analysed and filtered according to the chart presented in Figure 4.7. Not relevant patents, such as patents that do not cover pH, lactate and foetal monitoring and patents that are not available in the English language, have been excluded. The patents have then been further ranked regarding the key measurand (lactate, pH and other). Following that, the five most relevant patents to foetal monitoring have been identified [186, 187, 188, 189, 190] (Table 4.17).

Through the patent review, it has become evident that several approaches have been made to simplify the process of FSBS by automating steps and developing a more contained device. However, most devices still have an invasive approach and do not provide continuous real-time results. However, illustrated in Table 4.17, there is a distinct tendency towards less invasive sampling for lactate sensing, either through the application of microdialysis or microneedles [188, 189, 190]. Although there are several advances within the field of lactate sensing and foetal monitoring, no patent has been found, fulfilling the requirements laid out for foetal monitoring in Chapter 1

Table 4.17: *Results from patent review: Most relevant patents according to the filters applied which are represented. MD=Microdialysis, MN=Microneedles, EC=Electrochemical, NA=Not available.*

No.	Title	Sampling	Detection	Ref.
1.	Device for determining foetal reserves during childbirth (2002)	Blood, IF	EC	[186]
2.	Implantable multi-parameter sensing system and method (2005)	Implanted	EC/optical	[187]
3.	Device for detecting oxygen depletion in foetuses during childbirth (2009)	MD.	NA	[188]
4.	Integrated electrode for sampling of lactate and other analytes (2015)	MD	Enzymatic	[189]
5.	Lactate measuring device and method for training adjustment in sports (2015)	MN.	EC	[190]

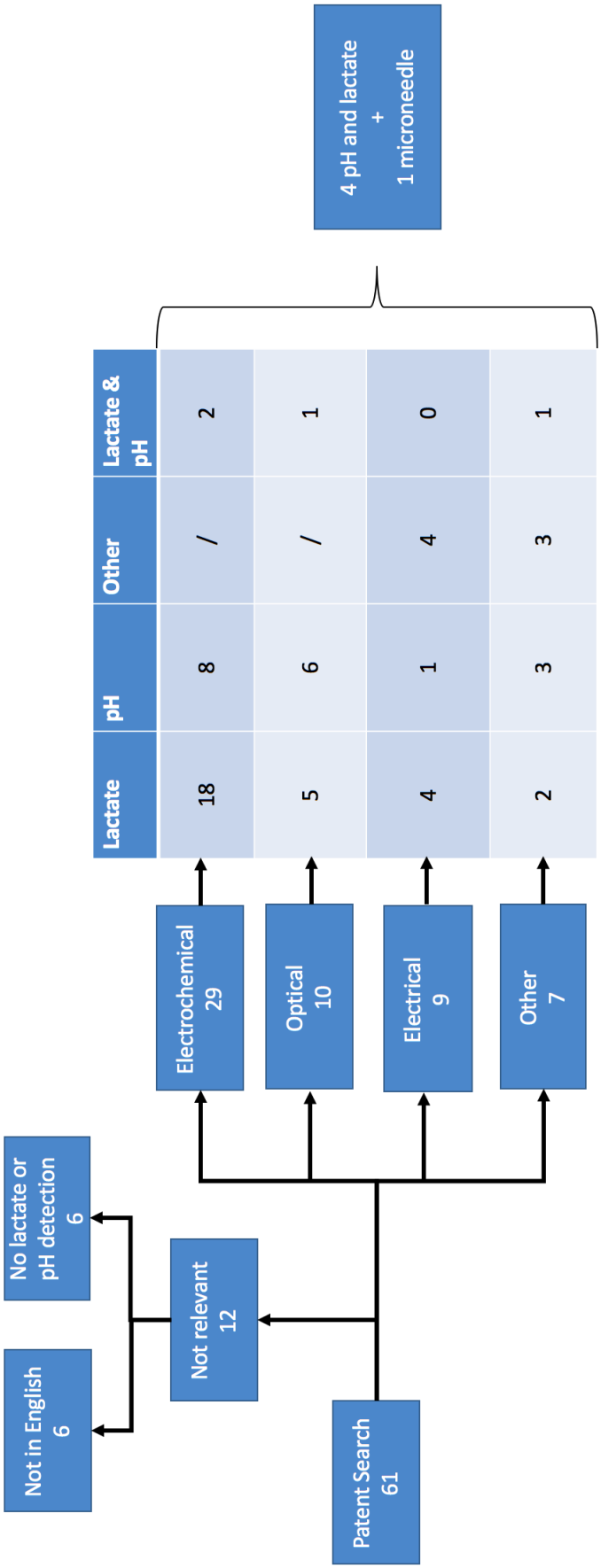

Figure 4.7: *Chart representing the filters applied for the patent analysis chart.*

4.8 Conclusion

Following a literature and patent review, a clear direction for the development of a lactate sensor for foetal monitoring has been identified. For accessing either interstitial fluid or blood, microdialysis and microneedles are the options for means of sampling. However, microdialysis is a complex process and therefore less suitable for the application of intrapartum foetal monitoring. For this reason, microneedles can be considered a more appropriate sampling method due to reduced complexity than the microdialysis method, providing access to the biofluid and with the advantage of being minimally invasive.

For a greater specificity of lactate sensors, either lactate oxidase or lactate dehydrogenase are immobilised onto the working electrode. Both enzymes have been shown to successfully provide a basis for lactate sensing, although, a significant proportion of published research focuses on the use of lactate oxidase. As lactate dehydrogenase is a less stable protein and requires a larger overpotential, lactate oxidase will be used for the development of the intrapartum foetal monitoring in this work. Covalent bonding and cross-linking have been identified as the most suitable means of immobilising the enzymes to the electrode surface. This is due to the observed tendency to prevent leaching of the enzyme, which is important when in contact with human tissue. Encapsulation requires an additional gel that is not compatible with the use of microneedles and, consequently, covalent binding and crosslinking are investigated for application in this research.

Study of the available literature has shown that amperometry is the most common transduction method for lactate methods, only requiring a potentiostat. The measured current is proportional to the lactate concentration in the sample. Other means of transduction have been researched, but are not as advanced in their development. Thus, amperometric transduction will be utilised for the development of the lactate sensor. The materials used for the working electrode of lactate sensors include gold, platinum, carbon, and glass, which can be further modified with nanomaterials. However, as nanomaterials can

potentially leach and are toxic, they cannot be utilised for the development of a foetal sensor. As gold and platinum electrodes are commercially available, and both raw materials are compatible with the electron beam evaporator for the fabrication of the sensor, gold and platinum will be explored experimentally. This will provide further insight about the suitability for lactate sensing for foetal monitoring.

The patent review conducted underlines the proposed direction for the development of an intrapartum foetal monitoring sensor. There is a clear trend of less invasive application to monitor babies during birth, for which microneedles and microdialysis have been utilised.

In conclusion, the work in this thesis will be focused towards the development of a prototype sensor in which lactate oxidase is employed as a recognition element, which is immobilised onto microneedles using covalent binding and crosslinking and the resulting signal is transduced through amperometry. Gold and platinum are to be investigated as materials for the working electrode.

5 Methods and Results: Sensor Fabrication

This chapter provides information about the materials and methods used for the fabrication of the sensor prototype. Firstly, commercial electrodes are introduced from which the sensor design will be adapted for the developmental phase. This design is presented and explained in Section 5.2 after which the fabrication process and characterisation methods are introduced. Lastly, the results of the characterisation of the commercial electrodes and the prototype are presented.

5.1 DropSens Electrodes

For the development of the lactate sensor, commercial screen-printed electrodes were purchased from DropSens. These electrodes are intended for single use measurements and can be modified with regard to the immobilisation of enzymes for example. For the purpose of this project, gold [176] and platinum [177] electrodes were acquired, a specimen of which is are represented in Figure 5.1. These electrodes are based on a ceramic substrate with a length of 33 mm, a width of 10 mm and height of 1 mm. Both electrodes have 4 mm diameter working electrode and a silver reference electrode. All electrochemical measurements were performed on these DropSens electrodes.

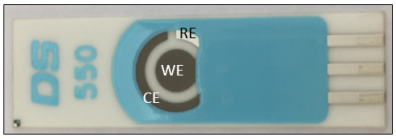

Figure 5.1: *Example of DropSens unmodified screen-printed electrodes. WE = Working Electrode, CE = Counter Electrode, RE = Reference Electrode.*

A connector, provided by DropSens, was purchased in order to connect the

electrodes to a potentiostat. The electrode is plugged into the slot as indicated in Figure 5.2(B).

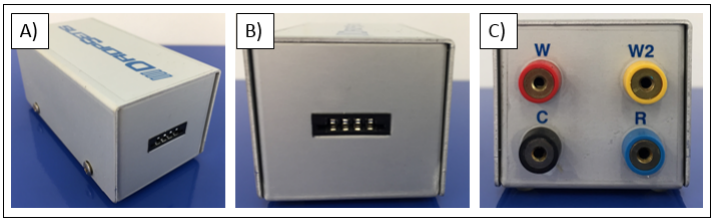

Figure 5.2: *DropSens connector. A) Side view. B) Front view: Slot for electrode. C) Back view: Connection for potentiostat.*

5.2 Aim

The aim of this chapter is the development and the fabrication of a prototype electrochemical sensor. The electrode will be based on a three-electrode system as described in Section 2.1. The pattern for this three-electrode system will be adapted from the DropSens electrodes introduced in Section 5.1. As the aim is to apply the sensor to the foetal scalp during birth, the three-electrode system will be applied to a microneedle array for access to the biofluid and electrochemical measurement. This is done to improve the laborious and erroneous method currently applied (Section 3.4) in size, duration and invasiveness. A schematic drawing of the sensor prototype is given in Figure 5.3. The sensor prototype will consist of two parts. Firstly, the microneedle array with the electrode pattern. Secondly, a printed circuit board to connect the microneedle array with the potentiostat.

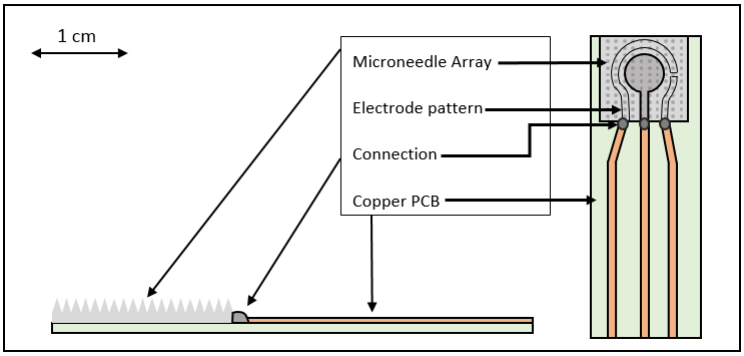

Figure 5.3: *Schematic drawing of the composition of the electrochemical sensor for the development phase.*

Figure 5.4 shows how the sensor is connected to the potentiostat using the DropSens connector for measurements. The sensor in Figure 5.4 is represented by the blue chip above the DropSens connector in the right-hand box. In order for the fabricated microneedle sensor to fit into the connector, an adapter, which is labeled "Copper PCB" in Figure 5.3, is required.

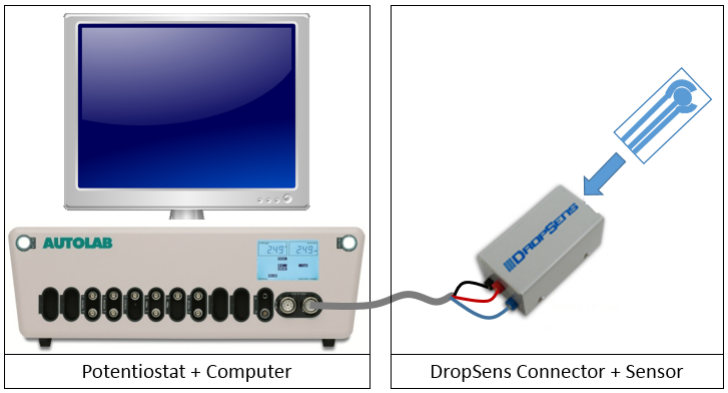

Figure 5.4: *Connection between the sensor and the potentiostat using the DropSens connector.*

5.3 Microneedles

For the development of the electrochemical lactate sensor for foetal monitoring during birth, the microneedle array must not be larger than 1x1 cm to provide monitoring from an early stage of labour. Furthermore, the microneedles must be made from a non-conductive material to create a three-electrode system from deposited metal on top of the microneedle arrays. For the final device, the microneedle arrays need to be biocompatible as it will be in direct contact with human tissue. A search for commercially available microneedles was undertaken. Two companies, namely MicroPoint [191] and Innoture [192], were identified to fulfill the criteria outlined above. Samples from both companies were acquired for inspection with regard to the following fabrication processes. Firstly, the microneedles by MicroPoint are introduced. Secondly, the microneedles samples supplied by Innoture are presented in this section.

5.3.1 MicroPoint Microneedles

A sample of the microneedle arrays purchased from MicroPoint is shown in Figure 5.5. The image was acquired using a Dino-Lite camera. The microneedle arrays are made from Poly(methyl methacrylate) (PMMA) and each has 15x15 microneedles on a square of the size of approximately 8x8 mm. Each microneedle is 500 μm in height and a base thickness of 200 μm. The distance between each microneedle (pitch) measured from centre to centre, is 500 μm. These characteristics are summarised in Table 5.1.

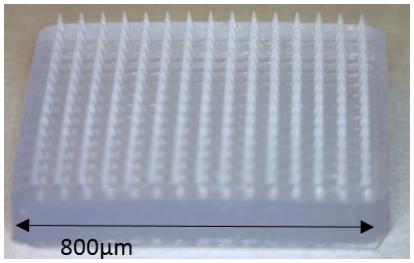

Figure 5.5: *PMMA Microneedle Array with 15x15 microneedles.*

Table 5.1: *Characteristics of MicroPoint microneedle array.*

Property	**Value**
Material	Poly(methyl methacrylate) (PMMA)
Height	500 μm
Base width	200 μm
Pitch	500 μm
Size	15x15 microneedles
Dimensions	$\approx$ 8x8 mm

5.3.2 Innoture Microneedles

In addition to the microneedles, sourced via MicroPoint, Innoture provided microneedle array samples (Figure 5.6). The sample sheet contained microneedle arrays of different pitches; 600μm, 800μm and 1000μm. All parameters are summarised in Table 5.2. Figure 5.6 shows the three different arrays with

a magnified image of the needles below, which were taken using a Dino-Lite camera.

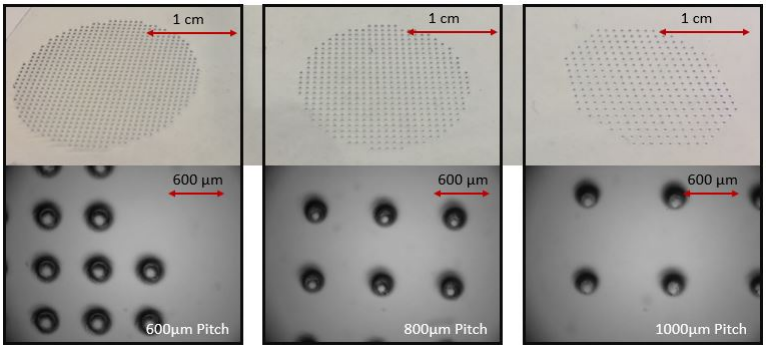

Figure 5.6: *Innoture microneedle arrays and respective close-up images using the Dino-Lite camera.*

The microneedles are constructed from a thin flexible laminate and are therefore not suitable for the fabrication process, due to heat development .

Table 5.2: *Characteristics of Innoture microneedle array.*

Property	**Value**
Material	Laminate (flexible)
Height	600 μm
Base width	200 μm
Pitch	Variable (600, 800, 1000 μm)
Diameter of array	approx. 1.5 cm

The initial inspection of the microneedle samples provides by MicroPoint and Innoture, concluded that the microneedle arrays supplied by MicroPoint, fit the requirements for the microneedle sensor prototype. Therefore, the fabrication process was tested with the MicroPoint microneedle arrays. However, a confidentiality agreement between Heriot-Watt and Innoture has been established for future collaboration.

5.4 Fabrication

5.4.1 Patterning using Tape

In this section, the development of the fabrication process is presented. Different options for the deposition of the metal three-electrode system were considered including electroplating which was rejected since it requires two conducting electrodes (one of which would be the microneedle array), which the PMMA microneedle arrays is not. In addition to that, sputtering was considered but was also rejected as it is more likely to damage to surface from impacting atoms. Electron beam evaporation was chosen as the means to deposit metal onto the microneedle arrays because it provides a conformal deposition of the metal due to its higher vacuum. The compatibility of the electron beam evaporation with the microneedle arrays was investigated. The microneedle arrays were exposed to the deposition process and the result was examined for damage on the microneedles. For the initial test, the microneedle array was masked, using an adhesive-free tape (Polytetrafluoroethylene (PTFE) tape) to avoid microneedle contamination. The PTFE tape was purchased from Sigma-Aldrich. The microneedle array was masked manually using the PTFE tape by carefully wrapping it around the rows of the microneedle array that will not be exposed to the deposition. An example of the masked microneedle array is shown in Figure 5.7(left).

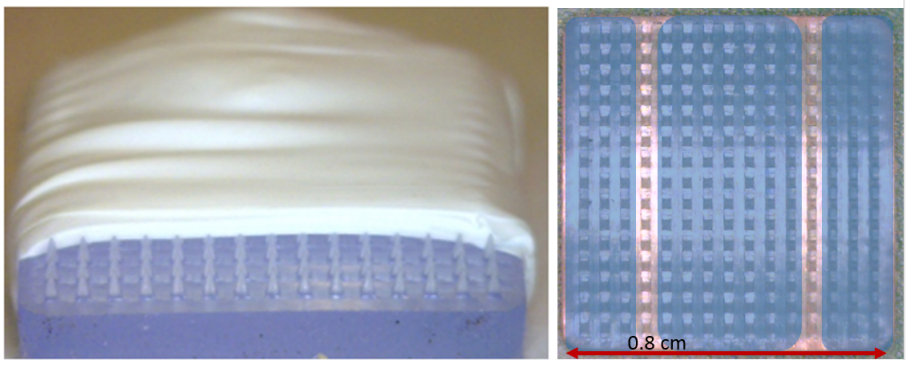

Figure 5.7: *Microneedle array masked with PTFE tape (left). Schematic drawing of were metal will be deposited. The blue areas will be deposited with silver (right).*

In that way, the pattern shown schematically in Figure 5.7 (right) was de-

posited onto microneedle array (blue= metal deposition) by following the three masking steps presented in Figure 5.8 in which the grey areas represent the PTFE tape and the visible microneedles were exposed to the metal deposition. The metal deposition was carried out by the student using a electronn/beam evaporator, after appropriate training.

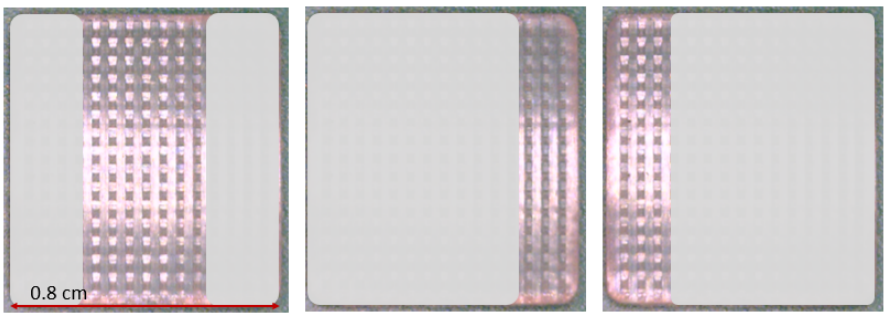

Figure 5.8: *Schematic drawing of the three different masking steps in order to achieve three stripes of silver deposition as presented in Figure 5.7 (right). The grey areas represent the masked microneedle rows.*

The appropriately masked microneedle array (placed on a silicon wafer) and the crucible containing the metal was placed into the electron beam evaporator. The metal used at this stage was silver because it is more economical for a test run than gold or platinum. After the chamber was evacuated to a high vacuum of $2 \cdot 10^{-5}$ mbar, silver was deposited by heating the silver in the crucible by an electron beam created by a high current passing through a tungsten filament. This causes the metal to melt and due to the vacuum, the metal vapour evaporated onto all the exposed surfaces in the chamber, depositing a uniform and measurable layer of atomic thickness of 300 nm. This was controlled by a crystal piezo sensor inside the chamber. Silver was deposited in three steps indicated in Figure 5.8. These were conducted three times to achieve the pattern introduced in Figure 5.7 (right). The time required for one cycle of deposition is listed in Table 5.3. The durations listed cannot be improved using this device. However, the number of arrays added into one deposition step can be increased to make this process more efficient.

Table 5.3: *Electron-beam evaporation steps and durations.*

Step	Duration
Warming up pumps	30 minutes
Roughing (atmospheric pressure to $1 \cdot 10^{-1}$ mbar)	30 minutes
Backing ($1 \cdot 10^{-1} - 2 \cdot 10^{-5}$ mbar)	1.5-2 hours
Evaporation	5 minutes
Cooling down	30-60 minutes
Shutting down system	20 minutes
Total	**≈4.5 hours**

5.4.2 Patterning using PMMA Mask

As the masking method applied in the testing deposition is time-consuming, not repeatable and is challenging to form complex geometries, a new masking method was developed. A masking jig, as shown in Figure 5.9, was designed using AutoCAD (Autodesk) based on the electrode pattern used on the DropSens electrodes. The middle cut-out will create the working electrode, the left cut-out will create the counter electrode and the right cut-out will create the reference electrode (Figure 5.9 B). The masking jig consists of a bottom patterned substrate (Figure 5.9A) and a top mask (Figure 5.9B) which were both fabricated from PMMA sheet utilising an Epilog laser cutter. The bottom jig was fabricated from 2 mm thick PMMA and the mask from 0.5 mm thick PMMA.

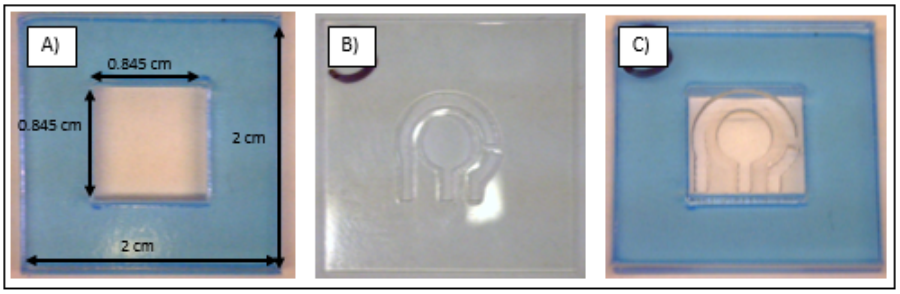

Figure 5.9: *Improved masking jig (A) and mask (B) made from PMMA using a laser cutter. Image (C) shows how the mask is placed on the jig.*

The settings used for the laser cutter are listed in Table 5.4. To test the func-

tionality of the new mask, a plain 1 mm thick PMMA sheet was used instead of the microneedle array to ensure an optimal fabrication process before applying to the microneedle arrays. The PMMA sheet representing the microneedle array was also cut using the Epilog laser cutter. The settings are also listed in Table 5.4. Using this masking method reduces the deposition time by 30% as only two deposition cycles are required.

Table 5.4: *Epilog laser cutter setting to cut different thicknesses of PMMA.*

Thickness	Speed	Power
0.5 mm	30%	20%
1.0 mm	30%	80%
2.0 mm	25%	90%

The bottom jig was placed onto a silicon wafer to fit into the holder in the electron beam evaporator and fixated with double-sided tape. The dummy substrate was placed into the bottom jig (Figure 5.9 A). The mask is securely placed on top using double-sided tape. In this test deposition, gold was used for the working and counter electrode and silver for the reference electrode. To achieve that, the cut-out for reference electrode or the cut-outs for the working and counter electrodes are taped using Tesa Orange Masking Tape (RS Components) as indicated in Figure 5.10 A) and Figure 5.10 B) respectively.

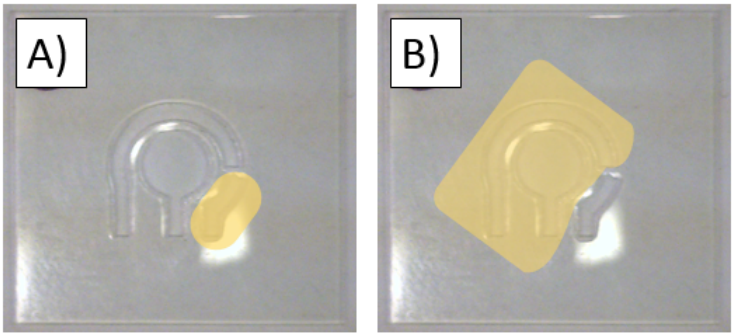

Figure 5.10: *Representation of how to tape off the areas not to be exposed to metal deposition.*

The silicon wafer with the masking jig including the dummy substrate was then placed in the electron beam evaporator and silver and gold were deposited subsequently.

5.5 Adapter

As explained in Section 5.2, the sensor has to be connected to the potentiostat. An adapter was fabricated to connect the sensor to the DropSens connector that is attached to the potentiostat as shown in Figure 5.4. For this purpose, a standard one-sided FR4 copper substrate (Elite Material Co., Ltd) was used. The design was purely based on ensuring to connecting the end-point of the working counter and reference electrode to the electrical connection in the connector as indicated by the colour coding in Figure 5.11.

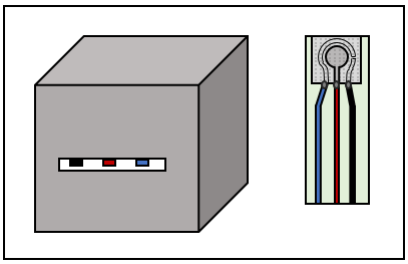

Figure 5.11: *Schematic drawing of the DropSens connector (left). Each colour-coded connection of the sensor (right) connect to the colour-coded connection in the DropSens connector.*

Prior to the fabrication, a precise drawing was prepared using AutoCAD (Autodesk) (Figure 5.12 A), which was then transferred into the drawing software InkScape to produce a mask (Figure 5.12 B) to be printed onto transparent sheets. The in-house electrical workshop fabricated the PCB, using the provided mask. The printed-circuit boards (PCBs) (Figure 5.12 C) can potentially be reused after having conducted measurements with them.

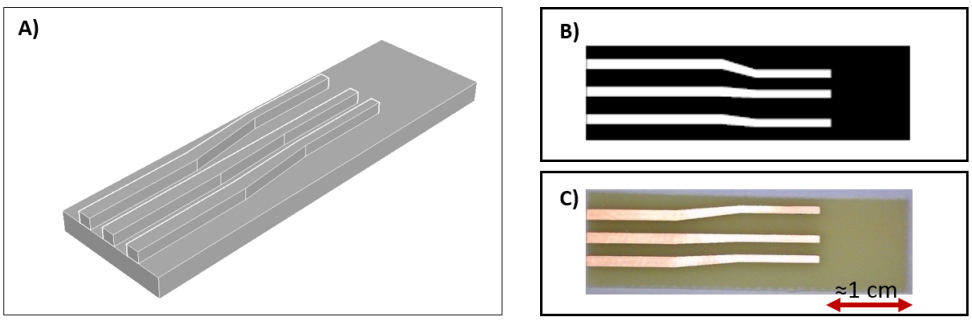

Figure 5.12: *AutoCAD drawing of the adaptor. B) InkScape mask. C) Fabricated adaptor fabricated from standard FR4 copper substrate.*

5.6 Characterisation Methods

In order to characterise the commercial and the fabricated electrodes, different imaging and measurement techniques were utilised. For the measurement of surface height and roughness, a stylus profilometer and white light interferometer were used. In addition to that, the surface was imaged using a scanning electron microscope. Furthermore, the electrochemical surface area of the commercial electrodes was determined electrochemically.

5.6.1 Optical and Mechanical

For the characterisation of the microneedles, commercial and fabricated electrodes a white light interferometer and a stylus profilometer have been utilised. In a white light interferometer, a beam of a white light source is split into a reference beam to be reflected by a mirror and a measurement beam to be reflected by the sample. The system is adjusted so both beams travel the same distances, so that an intensity interference fringing is generated, which is utilised to create a profile of the sample surface. The stylus profilometer is also used to measure profile heights and surface roughness of a sample. However, this profilometer is a contact based method. A stylus is used to move across the sample surface to recreate a two-dimensional map of the sample surface. To have a more visual picture of the electrode surface a scanning electron microscope was used. In a scanning electron microscope, an electron beam is aimed at the sample inside a vacuum chamber. The receiving signal reflecting from the electrically conductive surface of the sample provides information about the topography of the sample surface. In cases in which the surface of a non-conductive material is observed with an SEM, the method is destructive because it is necessary to deposit a conductive metal for the measurement. As the substrates (microneedles and the PMMA sheet) are already coated with conductive metal, the method is non-destructive.

5.6.2 Electrochemical

The DropSens electrodes were analysed electrochemically by determining the electrochemical surface area of the working electrode (WE) [22]. This is an important step to ensure constant quality of the electrode surface. Therefore, an electrochemical process has been established. It utilises cyclic voltammetry (CV) and chronocoulometry for the determination of the electrochemical surface area. The electrochemical surface area is the area of an electrode at which the electron exchange takes place. Therefore, the electrochemical surface area is larger than the geometrical surface area due to the roughness of the surface. If the diffusion coefficient is known or if it can be estimated, only CV is required and the electrochemical surface area, A, can be calculated from rearranging the Randle Sevcik equation (Equation (5.1))[193]:

$$A = \frac{\text{slope}}{268600 \cdot n^{2/3} \cdot D^{1/2} \cdot C} \tag{5.1}$$

Where the slope is the $\sqrt{scanrate}$ expressed in $(\sqrt{V/s})$, n the number of electrons, C the concentration of the analyte in mol/cm^3 and D the diffusion coefficient of the analyte ($6.7 \cdot 10^{-6}$ cm^2/s) [22, 193].

If the diffusion needs to be determined prior to the calculation of the electrochemical surface area, chronocoulometry is performed additionally to the CV. From the chronocoulometry the Anson plot is created by plotting the charge against the square root of time from which the slope is calculated. The slope is used to calculate the diffusion coefficient:

$$D = \frac{\text{slope}^2}{(268600 \cdot C)^2} \tag{5.2}$$

Where C is the concentration in (mol/cm^3). The diffusion coefficient is then used to calculate the electrochemical surface area by rearranging the Anson equation [5]:

$$A = \frac{a}{2nFC \cdot D^{1/2}\pi^{1/2}} \tag{5.3}$$

Where a is the slope of the Anson plot (charge over $\sqrt{time}$), n the number of electrons, F the Faraday constant, C the concentration in mol/cm^3 and D the diffusion coefficient (cm^2/s) [22, 26]. With the calculated value for the electrochemical surface area the roughness factor ρ can be calculated [22]:

$$\rho = \frac{A_{EC}}{A_G} \tag{5.4}$$

Where A_{EC} is the electrochemical surface area and A_G the geometrical surface area [22]. The characterisation procedure follows the following steps:

1. Chlorination of the reference electrode, to create a silver/silver-chloride (Ag/AgCl) electrode from the plain silver electrode
2. Cleaning of the electrode system.
3. Preparation of the electrolyte solution.
4. Cyclic Voltammetry.

In this work, the electrochemical surface area is calculated using an estimated value from the literature for the diffusion coefficient ($6.7 \cdot 10^{-6}$ cm^2/s) [22, 193]. Before the CV can be performed the RE is created by applying a 50 mM Iron (III) Chloride Hexahydrate [$FeCl_3$] onto the RE for 20 seconds before it is rinsed with deionised water and dried with argon gas. Subsequently, the electrode is cleaned by the deposition of a drop of sulphuric acid (0.1 M), followed by cyclic cleaning. This is done to clean the electrodes from dust and roughen the surface. The electrodes were then rinsing with deionised water and dried with argon gas. The cyclic cleaning is conducted by the deposition of 0.1 M of sulphuric acid, followed by cyclic voltammetry. The cyclic voltammetry was run for 3 cycles. The parameters set in the potentiostat are summarised in Table 5.5. The electrodes are then rinsed with deionised water and dried with argon gas.

For the cyclic voltammetry, a 10 mM electrolyte solution of Potassium Ferrocyanide ($K_4(Fe(CN)_6)$) and Potassium Ferricyanide ($K_3(Fe(CN)_6)$ was prepared as a electron transfer agent. Firstly, a 100 mM solution of each com-

Table 5.5: *Parameters for cyclic cleaning for gold and platinum electrodes.*

Parameter	**1^{st} 3 cycles**	**2^{nd} 3 cycles**
Start potential [V]	0.0	0.0
Upper vortex [V]	1.6	1.3
Lower vortex [V]	0.0	0.0
Stop potential [V]	0.0	0.0
Number of scans	3	3
Scan rate [V/s]	0.1	0.1

ponent was made, of which 1 ml of each was added to 8ml Phosphate Buffer Saline (PBS). A drop of 100 μl was deposited onto the cleaned electrodes prior to CV at scan rates of 10, 25 and 50 mV/s [22].

5.7 Results

This section provides the results for this chapter. Firstly, the electrochemical analysis is presented followed by the determination of the electrochemical surface area. Secondly, the results of the characterisation of the microneedles and the fabricated electrode are shown. Lastly, the assembled sensor prototype is presented.

5.7.1 DropSens Electrodes: Electrochemical Analysis

Initially, a basic characterisation of the electrode/electrolyte system was conducted which also aided in the familiarisation with the electrochemical techniques. The DropSens electrodes were analysed regarding their reversibility, peak separation and peak current ratio (Chapter 2). The peaks and their positions were acquired from a voltammogram such as shown Figure 5.13. The cyclic voltammogram was obtained from a cyclic voltammetry experiment in 10 mM ferro-/ferricyanite solution at three different scan rates (0.01 V/s, 0.025 V/s and 0.05 V/s). This solution is only used for the intial electrochemical

analysis of the DropSens electrodes. The ferro-/ferricyanite solution is used as a electron transfer agent.

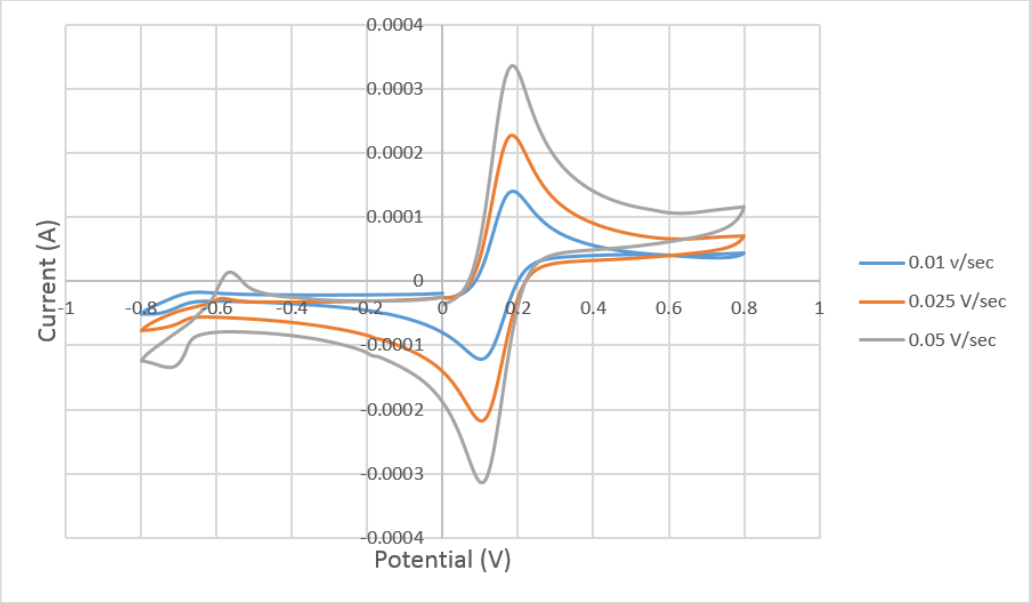

Figure 5.13: *Representative cyclic voltammogram at three different scan rates using 10 mM ferro-/ferricyanite solution.*

The results of the peak separation and the peak current ratio are listed in Table 5.6. The cyclic voltammograms at the different scan rates are shown in Figure 5.13. It can be seen that, although the voltammograms follow the same shape, they differ however in their magnitude. The higher scan rate, the higher the current observed, which is in agreement with the literature [22]. The average peak current ratio is 0.98 which indicates a reversible system as the ideal value is 1 when receiving the same current (opposite algebraic signs) for oxidation and reduction. The results for the peak separation give an average value of 78.74 mV where the ideal value is 57 mV (Chapter 2). The oxidation and reduction process is slightly lower than in an ideally reversible system, however, a reason for this could be that the experiments were conducted at a temperature between 19 - 21°C and not at a temperature of 25°C, for which the ideal values are calculated. With peak current ratio suggesting a reversible system and peak separation values that do not vary much from the ideal value, it can be said that the system using the electrolyte solution is reversible. In Figure 5.14 the CVs of gold (Au) electrodes and platinum (Pt) electrodes in electrolyte solutions (10 mM ferro-/ferricyanite solution) at three different scan

rates (0.01, 0.025, 0.05 V/s) are compared. Each colour represents two cycles at a specific scan rate using a different electrodes for each scan rate. Higher currents were detected for the Pt electrodes which are most likely due to the larger geometrical surface area. The geometrical surface area of the Pt electrode is 12.57 mm^2 and the Au electrode 2.01 mm^2. The current also increases with increasing scan rate as expected. The peak currents of the Au and Pt electrodes at different scan rates are summarised in Table 5.7 and visualised in Figure 5.16. The signal obtained from the blank solution (PBS) is compared to the solution containing the electroactive species. It can be seen that a higher current (20 times greater) was generated in the electrochemical cell with the electroactive species present than in the blank solution (Figure 5.15).

Table 5.6: *Scan rates, Peak separation and peak-current ratio for gold and platinum electrodes10 mM ferro-/ferricyanide.*

Electrode	**Scan Rate (V/s)**	**Peak Sep. (mV)**	**Peak current ratio**
Au 1	0.01	75.68	1
	0.025	83.01	1
	0.05	87.89	1
Au 2	0.01	75.7	1
	0.025	83	1
	0.05	90.34	1
Average Au		**82.60**	**1.00**
Pt 3	0.01	73.25	1.1
	0.025	80.57	1.1
	0.05	78.13	0.9
Pt 4	0.01	68.36	0.9
	0.025	73.24	0.9
	0.05	75.68	0.9
Average Pt		**74.87**	**0.97**

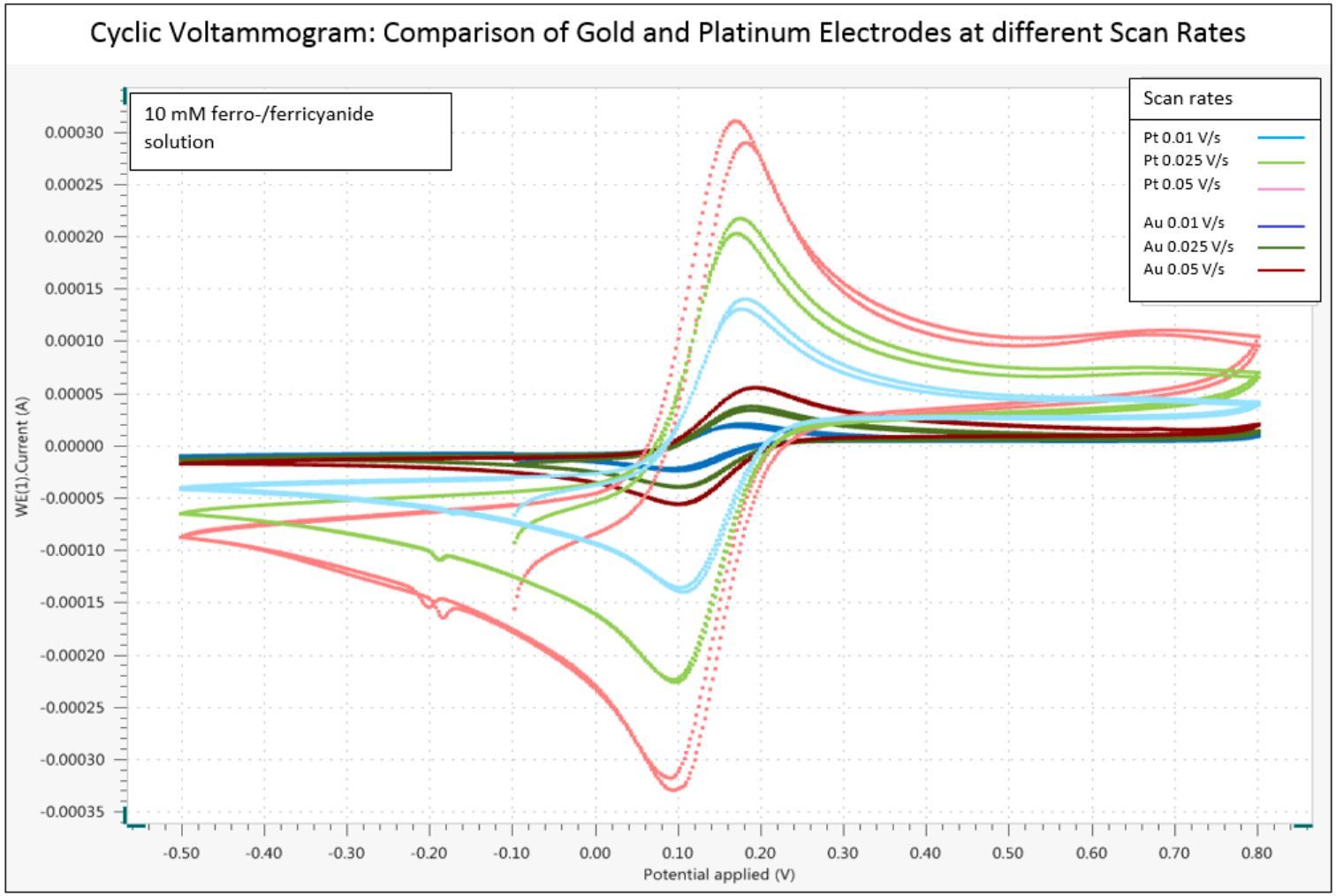

!h

Figure 5.14: *Cyclic voltammograms of gold electrode (dark colours) and platinum electrodes (bright colours) and three different scan rates (10, 25, 50 mV/S) in ferro-/ferricyanide solution.*

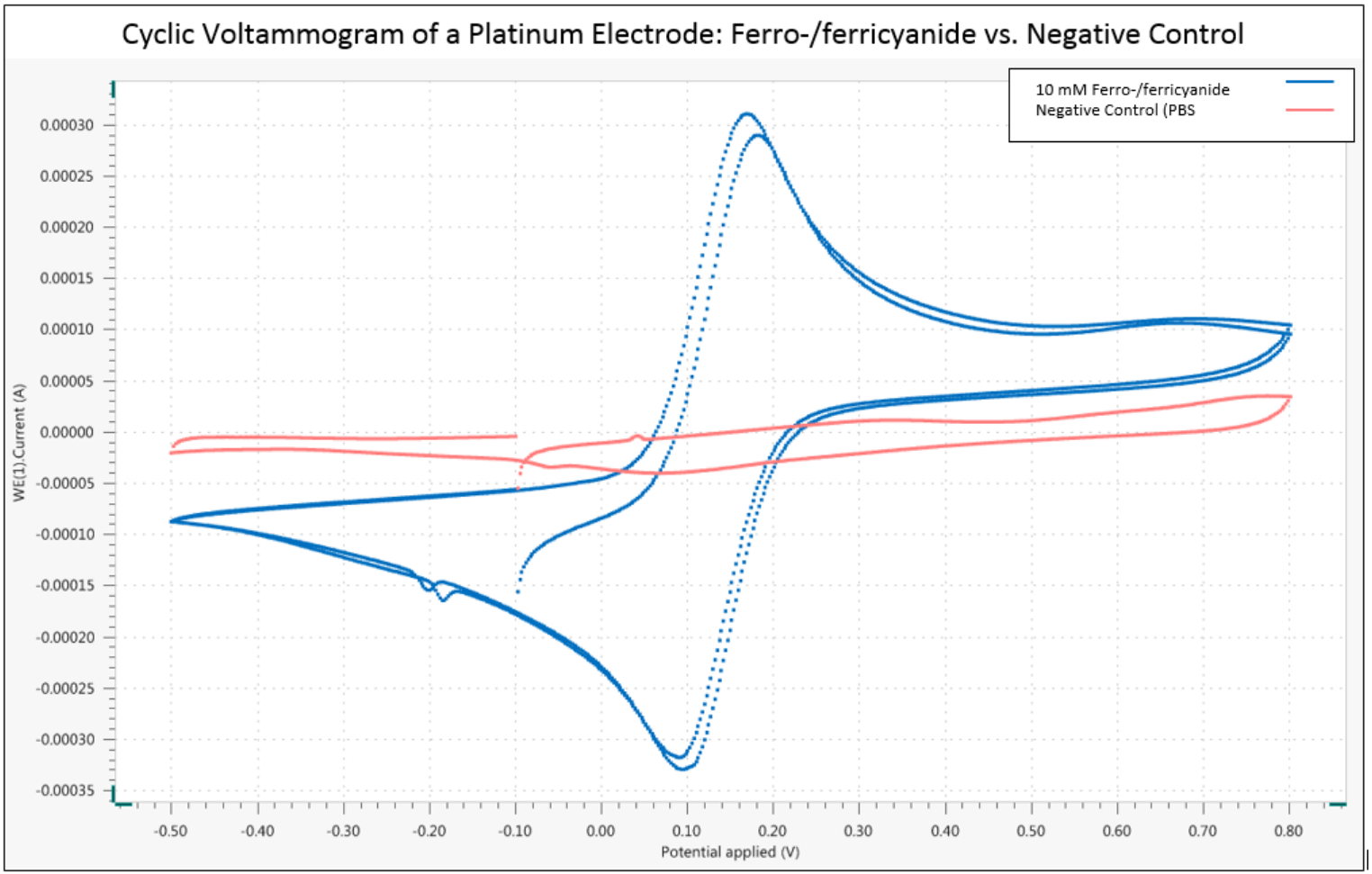

Figure 5.15: *Comparison of cyclic voltammograms of PBS and ferro/ferricyanide solution on a platinum electrode at a scan rate of 0.01 V/s.*

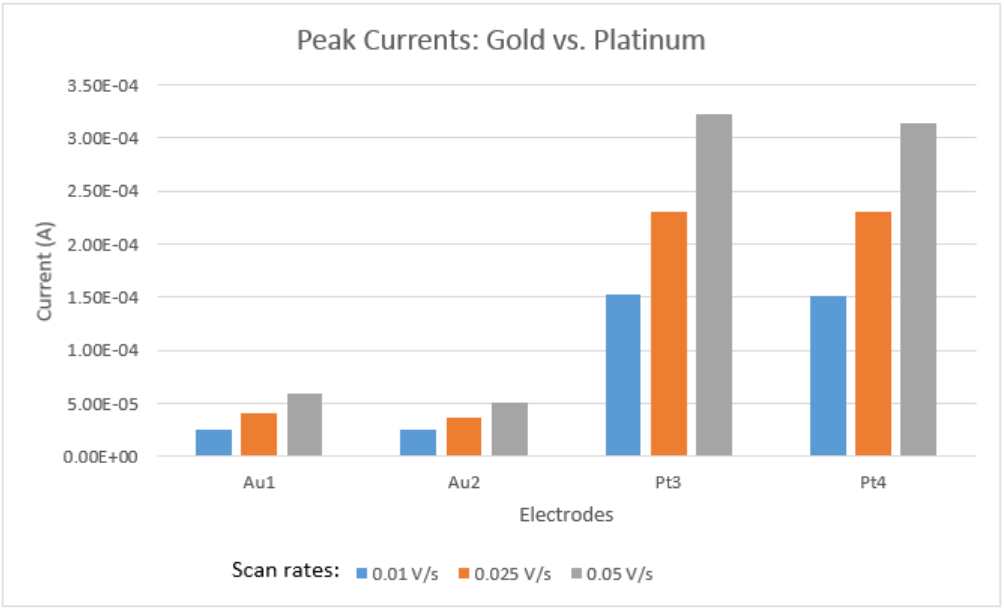

Figure 5.16: *Comparison of peak currents at different scan rates (0.01, 0.025, 0.05 V/s) for gold and platinum electrodes.*

Table 5.7: *Peak currents of two gold and two platinum electrodes at different scan rates.*

Electrode	**Peak Current (μA)**		
Scan Rate (V/s)	**0.01**	**0.025**	**0.05**
Au1	25.2	41.3	58.8
Au2	25.3	37.1	50.1
Pt3	153	231	322
Pt4	151	230	313

5.7.2 Electrochemical Surface Area

The electrochemical surface area was determined electrochemically by the method described in Section 5.6.2 using cyclic voltammetry (CV). An example of voltammograms taken at three different scan rates is shown in Figure 5.13 in Section 5.7.1, from which the peak currents are determined. These are plotted against the square root of the scan rate, (Figure 5.17), providing the slope required for the calculation of the electrochemical surface area. These graphs were created for each measurement.

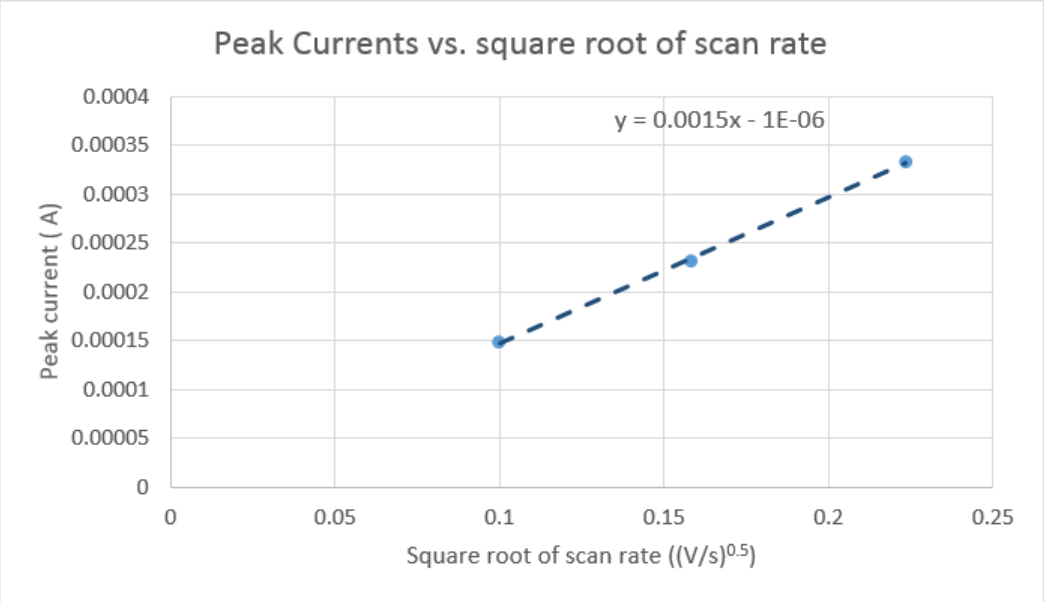

Figure 5.17: *Peak current against the square root of the scan rate for the determination of the slope.*

The Randle Sevcik equation was rearranged to calculate the electrochemical surface area and the roughness factor, giving

$$A = \frac{\text{slope}}{268600 \cdot n^{2/3} \cdot D^{1/2} \cdot C} \tag{5.5}$$

Where the slope is determined from the peak current vs. square root of scan rate plot ($i_p/\sqrt{V/s}$) for each three scan rates, n is the number of electrodes which is 1 for the electrolyte solution used, D the diffusion coefficient (cm^2/s) obtained from the literature $6.3 \cdot 10^{-6}$ cm^2/s and C the concentration of the electrolyte solution (mol/cm^3). The results of the measurements are shown in

Table 5.8.

Table 5.8: *Results of the electrochemical surface area of uncleaned platinum electrodes. ECSA = electrochemical surface area, GSA = geometrical surface area.*

Electrode	CV Slope	ECSA (mm^2)	GSA (mm^2)	Roughness Factor
Pt1	0.0009	13.3	12.57	1.062
Pt2	0.0011	16.3	12.57	1.298
Pt3	0.001	14.8	12.57	1.180
Pt4	0.0011	16.3	12.57	1.298
Pt5	0.0012	17.8	12.57	1.416
Pt6	0.0012	17.8	12.57	1.416

Table 5.9: *Results of the electrochemical surface area of cleaned platinum and gold electrodes. ECSA = electrochemical surface area, GSA = geometrical surface are.*

Electrode	CV Slope	ECSA(mm^2)	GSA (mm^2)	Roughness Factor
Pt1	0.0015	22.25	12.57	1.770
Pt2	0.0014	20.77	12.57	1.652
Pt3	0.0015	22.25	12.57	1.770
Pt4	0.0015	22.25	12.57	1.770
Pt5	0.0015	22.25	12.57	1.770
Pt6	0.0015	22.25	12.57	1.770
Pt7	0.0014	20.77	12.57	1.652
Pt8	0.0013	19.28	12.57	1.534
Au1	0.0003	4.45	2.01	2.214
Au2	0.0002	2.97	2.01	1.476

Table 5.8 shows the results for the electrochemical surface area for electrodes that have not been treated with cyclic cleaning before the measurements. Both tables (Table 5.8 and Table 5.9), give the result of the slope obtained from the CV, the electrochemical surface area (ECSA) calculated from the rearranged Randle Sevcik equation, the geometrical surface area (GSA) and the roughness factor which was calculated by dividing the ECSA by the GSA.

Table 5.9 lists the results of cleaned electrodes. The electrochemical surface area of the uncleaned electrodes is almost equal to the geometrical surface

area of 12.57 mm^2. The electrochemical surface area of cleaned Pt electrodes is almost twice as large. It is apparent that cleaned electrodes exhibit a greater electrochemical surface area than untreated equivalents. These results support the effectiveness of the cleaning process, making the surface clean and rougher and therefore enhancing the electrochemical surface area. The determination the electrochemical surface area of commercial Au electrodes exhibits the same trends. The electrochemical surface area of cleaned Au electrodes is larger than its geometrical surface area. Similar results have been obtained by Fragkou *et al.* [22] who have determined the electrochemical surface area of screen-printed electrodes and found it to be three times as large as the geometrical surface area [22].

5.7.3 Microneedles and PMMA electrodes

For the purpose of an initial quality control of the purchased microneedle arrays and for retrospective analysis to gauge the success of the fabrication process, optical microscope images were taken before the modification of the microneedle array introduced in Section 5.3.1. A representative image is shown in Figure 5.18 (A)). From the image with "high" magnification (Figure 5.18 (B)) a closer portion of the area is shown. As the focus of the image is on the surface and not on the microneedle, the microneedle itself is not visible (black square). In these images, the microneedles appear to be cuboid-shaped. However, the tips of the microneedles are not accurately represented in these images.

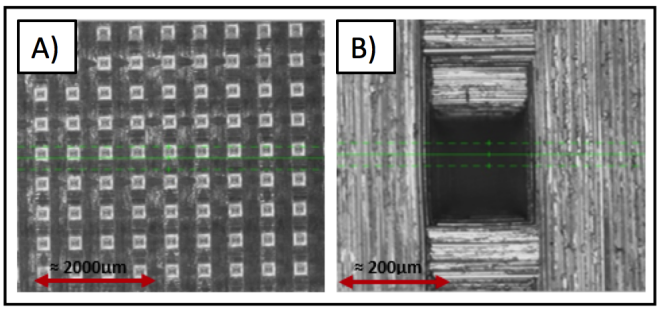

Figure 5.18: *MicroPoint microneedle images using the dice wafer cutter imaging capabilities at a "Low" (A)) and "High" (B)) magnification.*

However, the Dino-Lite images taken suggest that the microneedles have the shape of a square-based pyramids. Therefore, a scanning electron microscope image was taken. The image is presented in Figure 5.19 C) clearly shows a pyramidal shape. The characterisation also confirmed the dimensions of the microneedle arrays (Table 5.1).

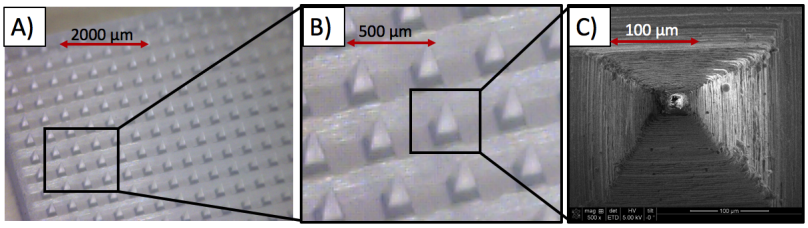

Figure 5.19: *Dino-Lite images of microneedle array (A) and B)) and scanning electron microscopy image of one microneedle (C)).*

The result of the silver deposition (manual tape masking) onto the microneedle array is shown in Figure 5.20. The pictures were taken using a Dino-Lite camera. From these pictures, no notable differences in the silver surface at different locations in the array were observed.

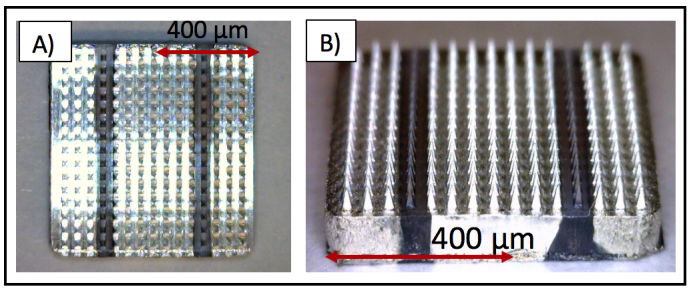

Figure 5.20: *Deposition of silver onto the microneedle array. A) Top view. B) Front view.*

A clear distinction between the deposited and un-deposited rows of needles is observed. However, as the maneuvering of the PTFE tape over the microneedle was challenging, the edges do not show a clear straight distinction between the coated and uncoated area. Furthermore, it becomes apparent that the upper row of the left-hand silver deposition in Figure 5.20 is smaller than the lower row. These inaccuracies can be attributed to the problematic masking method using the PTFE tape. In addition to the observation of the silver deposition with the Dino-Lite camera, the results were also examined using a scanning electron microscope (SEM). Figure 5.21 A) and B) show the

image of the microneedle array at the position indicated by the red circle in Figure 5.21 C) at 50 x magnification. The brighter area on the left-hand side represents the silver deposition and the darker area, on the right-hand side, is the microneedles without silver deposition. From these images, a distinction can be made between the metal and non-metal area on the microneedle array.

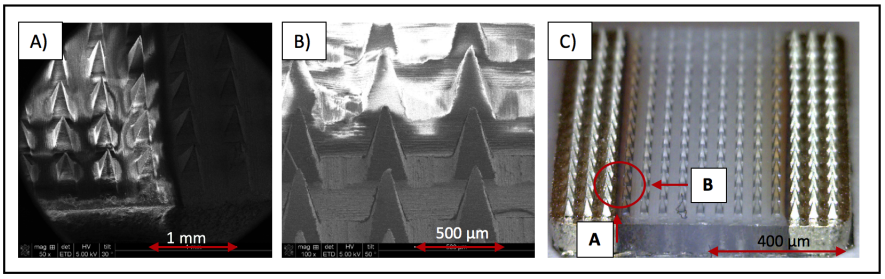

Figure 5.21: *Scanning electron microscope image of the microneedle array at the position indicated by the red circle from the view indicated by the arrow.*

By increasing the magnification further, it becomes apparent that the tips of the microneedles are slightly bent in a range of 30 μm Figure 5.22. Although not all tips were bent, both coated and uncoated microneedles exhibited the same bending. This could be caused by either the heat the microneedle array was exposed to in the chamber of the electron beam evaporator or by the metal tweezers with which they were handled during the characterization procedure. Plastic tweezers were then used to reduce the risk of bending. To reduce the influence of the heat in the vacuum chamber a heat sink can be applied to reduce the heat radiation for the microneedles.

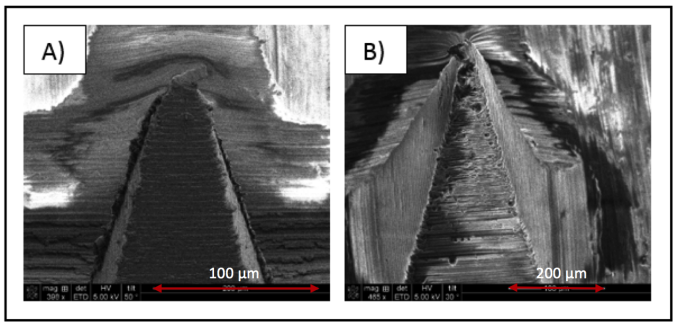

Figure 5.22: *Scanning electron microscope images of two single coated (Ag) microneedles of the microneedle arrays at a A) 398x magnification and B) 465 x magnification.*

Overall, the electron beam deposition technique can be seen as compatible with the deposition of metals onto PMMA microneedle array. However, the

masking technique utilising the manual application of PTFE tape was proven not only to be time-consuming but also problematic, as some microneedles showed bending of the tips. Therefore, the masking technique using the PMMA masks should be used. Additionally, the microneedle should be handled with plastic tweezers instead of metal tweezers to prevent damage.

To prevent deformation due to heat impact in the electron beam evaporator, a heat sink within the vacuum chamber can be installed.

5.7.4 Dummy electrode on PMMA

Following the time-consuming masking method with PTFE tape, a PMMA sheet (dummy substrate) was utilised as described in Section 5.4. In this section, the results of the metal deposition are presented. Figure 5.23 shows the resulting electrode, using a Dino-Lite camera. The pictures show a three-electrode system deposited onto the PMMA sheet. For the working (middle) and counter electrodes (left), gold was deposited and silver for the reference electrode (right)(Figure 5.23).

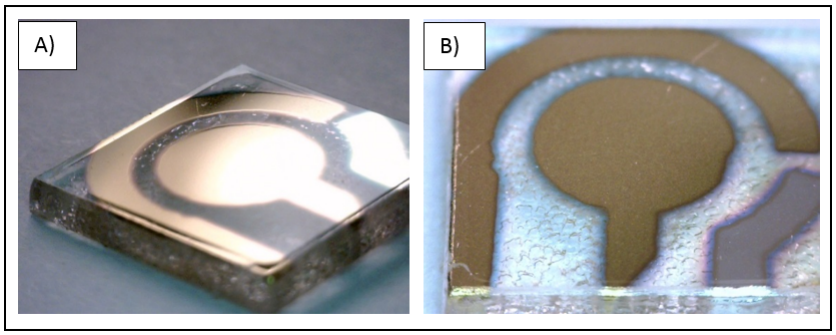

Figure 5.23: *Images of deposited three-electrode cell onto PMMA using the electron beam evaporator. Working electrode and counter electrode: gold, reference electrode: silver. A) Side view B) Front-top view.*

This new masking method has the advantage of providing some protection against heat and a more precise application of the pattern onto the substrate.

From the Dino-Lite images in Figure 5.23, the distinction between the metal and the PMMA is clearly delineated. Dino-Lite images at higher magnification were taken, as shown in Figure 5.24. The area that they were taken from is

indicated by the colours. There is a clear separation between the three different electrodes ensuring that there is no unwanted electrical short circuit.

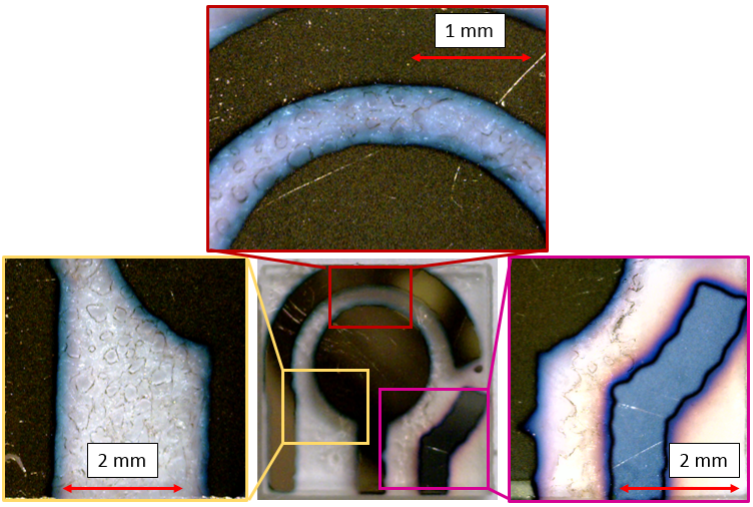

Figure 5.24: *Close-up Dino-Lite images of the edges of the metal deposition.*

An SEM image of the separation between the electrodes was also taken. A representative image is shown in Figure 5.25. The image shows a 299-times magnification of the indicated area of the electrode. From the SEM, a clear separation is difficult to see.

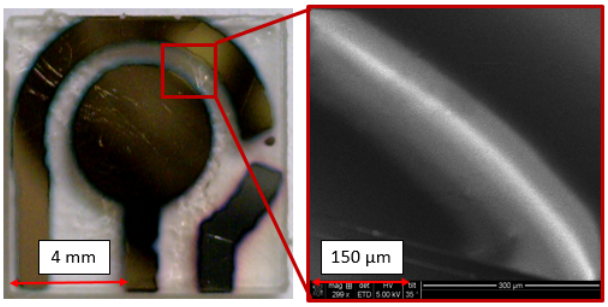

Figure 5.25: *Scanning electron microscopy image of the electrode edges.*

This is most likely due to the problem of "edge effect" found in SEM imaging [194]. As the outside edges of a deposited surface are slightly greater in height than the rest of the surface as shown in the schematic drawing in Figure 5.26. Edges and points generate more electrons when hit with the electron beam in an SEM. Therefore, the gap between the metal deposition and the unexposed PMMA seems smaller than it actually is, due to a larger number of electrons emitted from the surface.

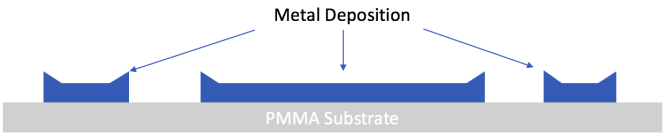

Figure 5.26: *Cross-section of the PMMA sheet with the metal deposition.*

In addition to the Dino-Lite images, the roughness of the PMMA electrodes was analysed and compared to the roughness of the commercial DropSens electrodes. As explained in Section 5.6.2, a rougher surface provides more sites for the enzyme to attach to when immobilised onto the electrode surface. For these measurements, a Zygo white light phase shifting interferometer was utilised, as outlined in Section 5.6.1. The roughness was measured over a length of 1 mm and 3 mm. The roughness of the PMMA electrode was found to be 735.84 Å compared to 10,300 Å for a DropSens electrode. These results show that the fabricated electrode has a very smooth surface compared to the DropSens electrode, which has a rougher surface. This was expected as the substrate used (PMMA sheet) is transparent and has a plain surface. These results are summarised in Table 5.10. Each value represents one measurement.

Table 5.10: *Results for electrode roughness using a Zygo white light interferometer.*

Electrode	Roughness	
Scan range	1 mm	3 mm
DropSens electrode	10,300	11,000
PMMA electrode	297.74	735.84

The increase in roughness of the fabricated electrode when measuring over a larger length is due to the irregularities, such as dust enclosed by the metal deposition. These are represented by the red peaks in the images of the surface produced by the white light interferometer. The representation of the DropSens electrode generated by the white light interferometer is shown in Figure 5.27.

For a clearer imaging of the electrode surfaces, the electrodes were examined under a scanning electron microscope as shown in Figure 5.28. On the left-hand side of Figure 5.28, an image of the fabricated PMMA electrode (uncleaned)

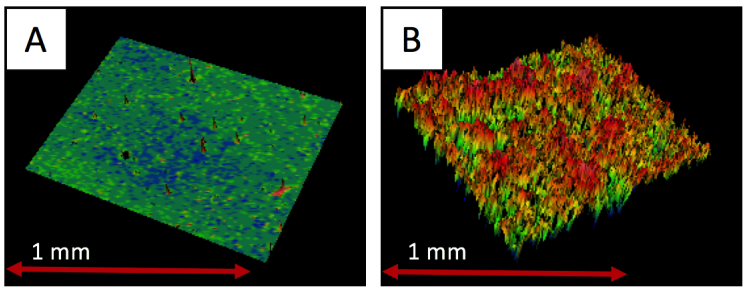

Figure 5.27: *Topographic map of A) PMMA working electrode and B) DropSens electrode.*

in comparison to the DropSens electrode (Figure 5.28 (right))is shown at a magnification of 5000-times. Apart from a few spherical imperfections, the surface is smooth. The image of a DropSens electrode, however, shows a rougher surface as previously measured. For enzyme immobilisation, as also applied in this project (Chapter 6) a rougher surface provides more sites for the enzyme to attach to.

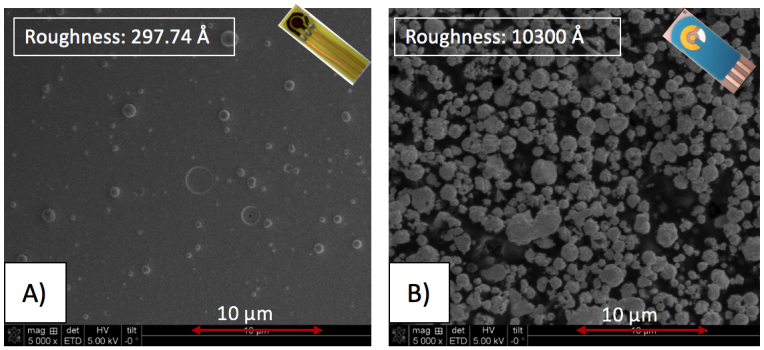

Figure 5.28: *SEM images of the PMMA working electrode (uncleaned) (A)) and a DropSens working electrode (B)) and their respective surface roughness.*

Since rougher surfaces offer both a larger electrochemical area and more sites for enzyme immobilisation, it was therefore tested to roughen the surface prior to the application of the metal layer. For this purpose, the raw PMMA squares were subjected to lapping, where one surface of the PMMA square is rubbed against a rotating disc covered in a lapping slurry, which then abrades the surface. Initial results for the lapping of PMMA squares are listed in Table 5.11. An images of the lapped PMMA sheet are shown in Figure 5.29 A)and is compared to unlapped PMMA sheet in Figure 5.29 B). The PMMA sheets were all lapped in the same session for the same duration. However, the received rough-

ness differs significantly from each other, which suggests that improvement of the lapping process is necessary especially with regards to the attachment of the PMMA sheet to the attachment fixture and the position of the PMMA on the glass wafer.

Table 5.11: *Surface roughness of lapped PMMA sheets in comparison to the working PMMA electrode and the DropSens working electrode and substrate roughness.*

Surface	**PMMA Sheet**			**PMMA electrode**	**DropSens**	
	1	2	3	WE	WE	Substrate
Roughness (Å)	12,859	5,503	6,248	297	10,300	866

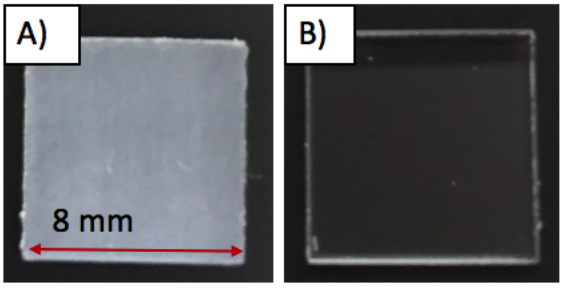

Figure 5.29: *A) Photograph of lapped PMMA square compared to an unmodified PMMA sheet (B)).*

5.7.5 Assembled Sensor

After the fabrication of the adapter as outlined in Section 5.2, this component was tested for compatibility with the DropSens connector. As illustrated in Figure 5.30 the adaptor fits into the connector regarding all dimensions. Also, the copper line connects to the connection inside the connector as planned. Note, there are different connectors available. The connector shown in Figure 5.30 has four contacts to use a electrode including two working electrodes. This connector was utilised to determine the compatibility of the fabricated adapter with the connector.

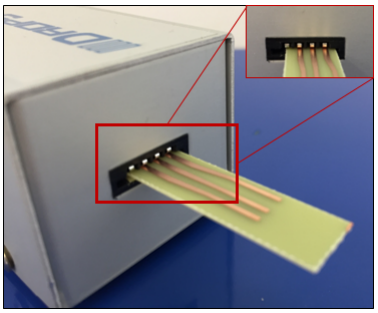

Figure 5.30: *Adapter in DropSens connector.*

The sensor was then assembled as shown in Figure 5.31. The PMMA electrode is attached to the PCB adaptor using double-sided tape. The electrical connection between the working, counter and reference electrode and the respective copper lanes on the PCB were established using conductive silver paste. However, the sensor was not utilised for any electrochemical experiments.

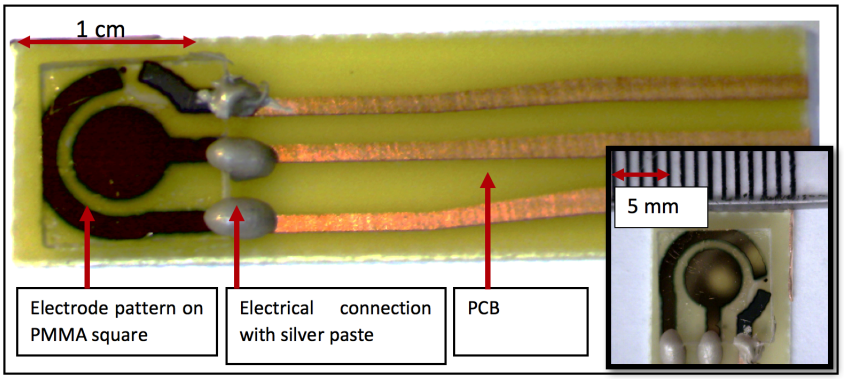

Figure 5.31: *Assembled three-electrode sensor with gold used for the working and counter electrode and silver for the reference electrode.*

5.8 Conclusions

The purchased DropSens electrodes were characterised using the basic electrochemical method cyclic voltammetry. The results showed that the electrode system (electrode and electrolyte used) is reversible and that higher currents were obtained from platinum electrodes, which may be due to the larger geometrical surface area of the platinum electrodes. Furthermore, the electrochemical surface area of the commercial electrodes was determined by applying cyclic voltammetry and solving the Randle Sevcik equation for the

electrochemical surface area. It was found that the electrochemical surface can be as much as twice as large as the geometrical surface, which is attributed to the surface roughness of the electrode surface. The microneedles purchased from MicroPoint were then characterised and tested for modification using the electron beam evaporator. After ensuring that the microneedle arrays are compatible with the electron beam deposition utilising PTFE for masking, a new masking method was developed to avoid the time-consuming masking with which only simple geometries such as stripes can be created. This was achieved by using a mask later-cut from PMMA and a PMMA jig to hold the sample in place. The results show, that the three-electrode pattern was deposited utilising the electron beam evaporator successfully. A dummy sensor was assembled attaching the PMMA sheet onto an adapter fabricated from standard FR4 copper substrate. It was finally shown that the sensor has been developed successfully to fit the geometries of the DropSens connector, which is used to connect sensor electrode to the potentiostat for measurements.

6 Immobilisation

This chapter provides the protocols for the preparation of the electrodes and the following immobilisation of lactate oxidase applying covalent bonding and cross-linking. For these experiments, the commercial DropSens electrodes (gold and platinum) were used. The aim of this chapter is to identify the most effective immobilisation method, which is characterised by the subsequent electrochemical performance utilising electrochemical impedance spectroscopy. All work presented in this chapter and in Chapter 7 has been conducted at the Devision of Infection and Pathway Medicine (DIPM) at the University of Edinburgh under the supervision of Dr. Till Bachmann and Dr. Holger Schulze. The protocols in this chapter were adapted from immobilisation protocols for immobilisation provided by DIPM.

6.1 Electrode Preparation

The electrodes are prepared prior to the functionalisation of the working electrode (WE). Firstly, the reference electrode (RE) is created by applying a 50 mM Iron (III) Chloride Hexahydrate [$FeCl_3$] onto the RE for 20 seconds before it is rinsed with deionised water and dried with argon gas. Subsequently, the whole electrode system is cleaned by the deposition of 0.1 M of sulphuric acid, followed by cyclic voltammetry. The cyclic voltammetry was run for 3 cycles twice to clean the electrodes from dust and roughen the surface. The parameters set in the potentiostat are summarised in Table 6.1. The electrodes are then rinsed with deionised water and dried with argon gas.

Table 6.1: *Parameters for cyclic cleaning for gold and platinum electrodes.*

Parameter	**1^{st} 3 cycles**	**2^{nd} 3 cycles**
Start potential [V]	0.0	0.0
Upper vortex [V]	1.6	1.3
Lower vortex [V]	0.0	0.0
Stop potential [V]	0.0	0.0
Number of scans	3	3
Scan rate [V/s]	0.1	0.1

6.1.1 Cross-linking

This section provides the protocol for the cross-linking process. The reagents and chemicals required for this are summarised in Table 6.2.

Table 6.2: *Chemicals/reagents used for cross-linking and purchase origin.*

Chemical	**Function**	**Company (Country)**
Hydroxyethyl Cellulose (HEC)	Gelling thickening agent to provide a matrix for Lox	Sigma-Aldrich (UK)
Lactate Oxidase (Lox)	Recognition Element	Sorachim (CH)
Bovine serum albumin (BSA)	Improve stability	Sigma-Aldrich (UK)
Glutaraldehyde (GA)	Cross-linking	Sigma-Aldrich (UK)
Phosphate Buffer Saline (PBS)	Buffer to make solutions	Sigma-Aldrich (UK)

This immobilisation process consists of three steps:

1. the preparation of the HEC- Lox solution;
2. the preparation of the BSA solution;
3. the curing of HEC-Lox-BSA composition in Glutaraldehyde vapour.

A 1% hydroxyl cellulose (HEC) solution was prepared by dissolving 1 g of HEC in 100 ml PBS. 100 μl of the HEC solution was then used to dissolve 2 mg Lox which was kept on ice until used. Following that, a 5% BSA solution was prepared by adding 1 μl BSA (50mg/ml) to 9 μl PBS, which was then added

to the HEC/Lox solution. This solution was deposited on the electrode using a pipette, which is then exposed to glutaraldehyde vapour for 30 minutes. This was done by carefully pouring glutaraldehyde into a small beaker under the fume hood, then placing the beaker into a plastic container. The electrodes were placed into the same container next to the beaker, after which its lid was closed. Subsequently, the electrodes were left to dry at room temperature for 1 hour, which finalised the immobilisation process.

6.1.2 Covalent Binding

In this section, the protocol for the covalent bonding process is introduced. The reagents and chemicals required for this are summarised in Table 6.3.

Table 6.3: *Chemicals/reagents used for covalent bonding and purchase origin. Sulfo-LC SDPD =(Sulfosuccinimidyl 6-(3'-(2-pyridyldithio)propionamido)hexanoate), TCEP = Tris(2-carboxyethyl)phosphine hydrochloride.*

Chemical	**Function**	**Company (Country)**
Sulfo-LC SDPD	Bifunctional crosslinker to add thiol group for immobilisation	Sigma-Aldrich (UK)
Lactate Oxidase (Lox)	Recognition Element	Sorachim (CH)
DL-Dithiothreitol (DTT) TCEP	Created free thiol group on bifunctional crosslinker	Sigma-Aldrich (UK)
Saturated Potassium Chloride	To create humid environment	Sigma-Aldrich (UK)
Phosphate buffer saline (PBS)	Buffer to make solutions	Sigma-Aldrich (UK)

This immobilisation process for covalent bonding consists also of three steps:

1. the preparation of the Sulfo-LC SDPD - Lox solution;
2. the preparation of the DTT solution;
3. the incubation of HEC-Lox-BSA composition in at a high humidity environment (approximately 85% relative humidity).

Firstly, a 40 mM Sulfo-LC SDPD solution was prepared by dissolving 4 mg Sulfo-LC SDPD in 189 μl PBS. 20 μl of the 40 mM Sulfo-LC SDPD solution was then used to dissolve 2 mg Lox which was then incubated at room temperature for one hour. Meanwhile, a 150 mM DTT solution is prepared of

which 20 μl is added to the Lox / Sulfo-LC SDPD solution. This DTT/ Lox / Sulfo-LC SDPD solution was incubated for another hour at room temperature before its deposition onto the electrodes, followed by an incubation at high humidity at 4°C for 2 hours. This is achieved by placing the electrode into a box containing saturated potassium chloride (KCl) solution, which is then placed into refrigeration.

6.2 Characterisation: Electrochemical Impedance Spectroscopy

Electrochemical Impedance Spectroscopy (EIS) measurements were conducted in order to determine the success of the immobilisation. In EIS, small sinusoidal potentials (2 - 10 mV) of a frequency range such as 100 kHz - 0.3 Hz are applied to the electrochemical cell. The electrochemical response is measured, the impedance is calculated from that response and plotted for analysis either as a Bode Plot or a Nyquist Plot. The impedance is the sum of the imaginary and the real impedance and represents a complex form of Ohm's law:

$$Z(j\omega) = \frac{U(j\omega)}{I(j\omega)} = Z_{Re}(\omega) + jZ_{Im}(\omega) \tag{6.1}$$

Where Z is the impedance, U the voltage, I the current, Z_{Re} the real impedance, and jZ_{Im} the imaginary impedance. The radial frequency $\omega = 2\pi f$ with f as the frequency. A typical EIS Nyquist plot is shown in Figure 6.1 (left-hand side). It consists of a semi-circle and linear part with the real impedance on the x-axis the imaginary impedance on the y-axis. The Nyquist diagram is plotted from high frequencies to low frequencies as indicated in Figure 6.1 (left-hand side). The three main values that can be acquired from the Nyquist plot are R_s (resistance of the solution), R_{et} (electron transfer resistance) and Z_w (Warburg resistance).

Figure 6.1 (right-hand side) represents the Nyquist plots of a bare electrode (blue graph) and electrode which had undergone an immobilisation process

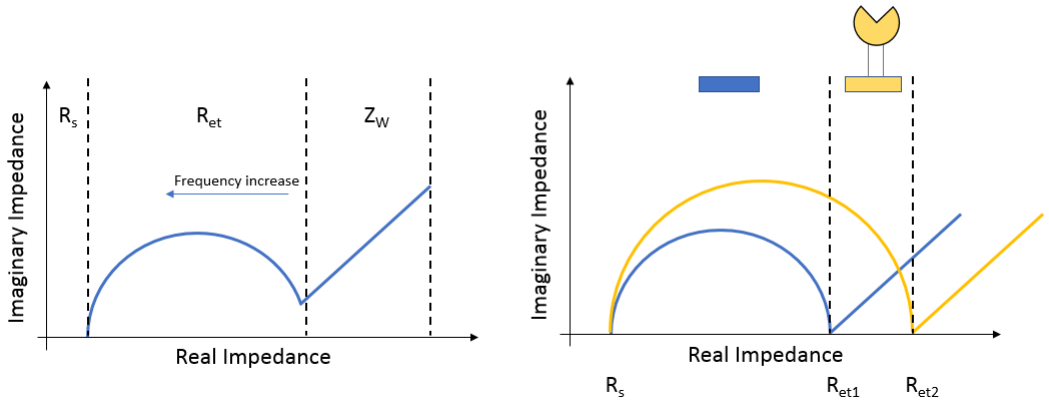

Figure 6.1: *Typical Nyquist plot with an imaginary impedance on the y-axis and the real impedance on the x-axis. The frequency increases from right to left (left-hand side). Visualisation of the difference in Nyquist plots with and without a substance immobilised on the electrode surface (right-hand side).*

(yellow graph). It can be seen that R_s (solution resistance) is the same whereas the electron transfer resistance (R_{et}) increases from R_{et1} to R_{et2}, for the functionalised electrode. Therefore, by determining the R_{et} value the success of the immobilisation process can be accessed [195].

6.3 Results

Results include measurement of blank DropSens electrodes in hydrogen peroxide (H_2O_2), a by-product of the reaction between lactate oxidase and lactate, as explained in Section 4.3.1. Additionally, the results of the amperometric lactate measurements using functionalised electrodes are provided. Comparison of the two immobilisation methods, covalent bonding and cross-linking, is carried out. These measurements are conducted on both gold and platinum electrodes. Electrochemical impedance spectroscopy (EIS) was utilised to determine the success of the immobilisation. The follwing results are shown in the sections below:

1. Cyclic Voltammetry in H_2O_2 and lactate solution.
2. Initial amperometric measurements using functionialised electrodes in lactate solution.

3. Electrochemical impedance spectroscopy (EIS) measurements.

6.3.1 Cyclic Voltammetry

Figure 6.2 shows the result of one CV of a blank Au electrode in 3% H_2O_2 solution. The overpotential is equal to the position of the oxidation peak and is 670 mV (red dotted vertical line). The overpotential is utilised for the amperometric measurements in Section 6.3.2. A potential range of -0.2 - 0.8 V was scanned.

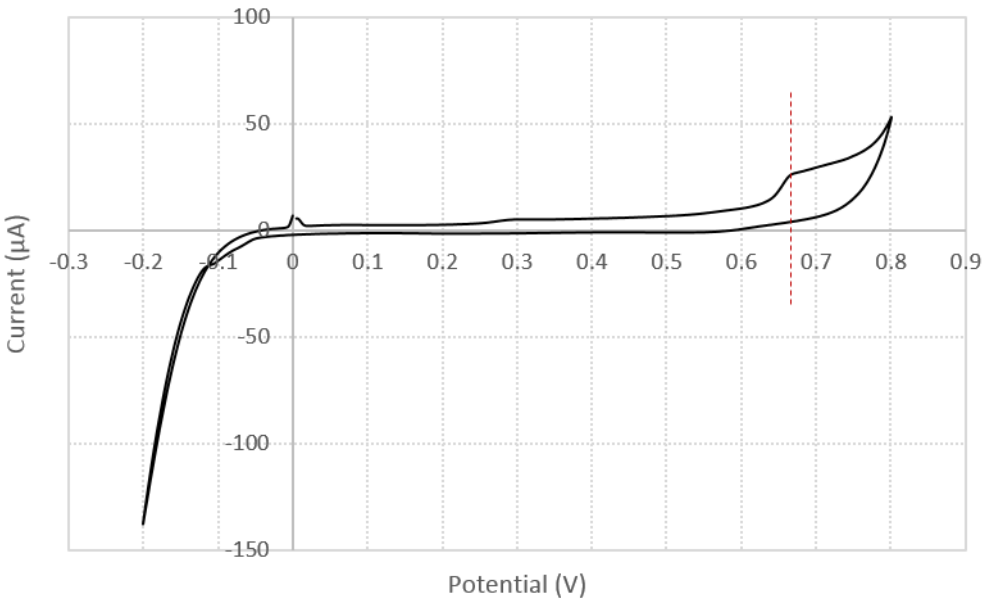

Figure 6.2: *Cyclic voltammogram of a blank gold electrode in 3% hydrogen peroxide.*

Cyclic voltammetry is also performed on a gold electrode that has lactate oxidase cross-linked and covalently bonded onto their working electrode. For the measurement, a 10 mM lactic acid solution was applied to each electrode (the whole three-electrode system is covered). Cyclic voltammetry was performed in the range of -0.2 V to 0.8 V at a scan rate of 0.1 V/s. The results for one measurement for each electrode are presented in Figure 6.3 and Figure 6.4. For the electrode with lactate oxidase cross-linked onto the surface (Figure 6.3) a small oxidation peak was obtained at 670 mV ((red dotted vertical line) as previously measured with the blank electrode in H_2O_2 solution. The fact that the oxidation peak is so small is indicative of either an inactivity of the Lox

or a low concentration of Lox applied to the WE.

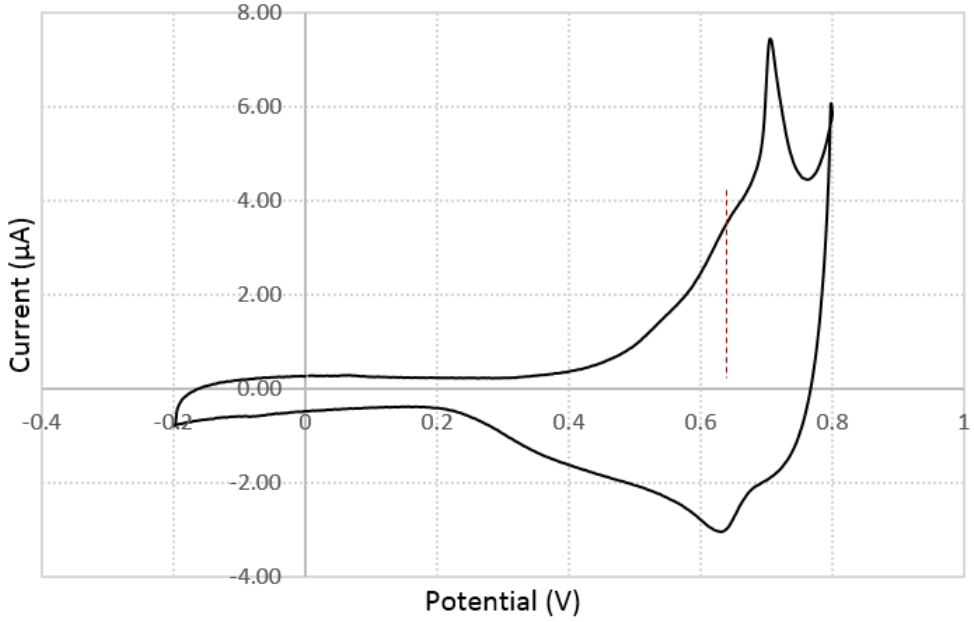

Figure 6.3: *Cyclic voltammogram: Gold electrode with cross-linked lactate oxidase 10 mM lactic acid solution.*

The oxidation peak for the gold electrode with lactate oxidase covalently bonded onto the electrode surface is more distinct as presented in Figure 6.4. CV was performed between -0.2 V and 0.8 V at a scan rate of 0.1 V/s. As expected from the previous measurement (Figure 6.2), the overpotential is at 670 mV. The oxidation is also an indication of lactic acid being oxidised, generating a current of approximately 1.5 μA. The peaks at 0.7 V and 0.8 V are due to the additional evolution of hydrogen and can therefore be ignore for the determination of the overpotential.

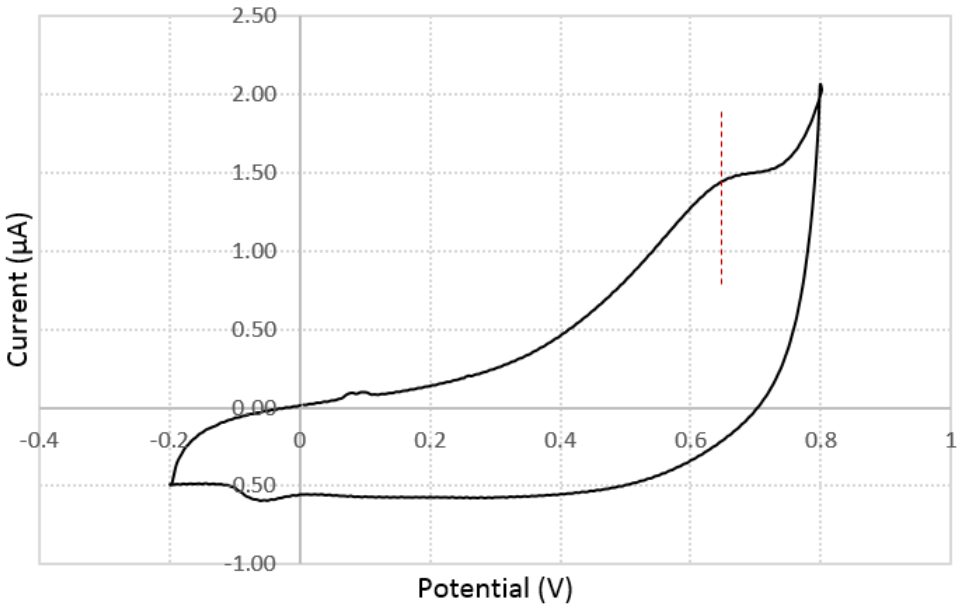

Figure 6.4: *Cyclic Voltammogram: Gold Electrode with Covalently bonded Lactate Oxidase 10 mM lactic acid solution.*

6.3.2 Amperometric Measurements

Following the cyclic voltammetry (Section 6.3), amperometric measurements were conducted using the overpotential of 670 mV obtained from the cyclic voltammograms. Prior to application of the potential, only PBS was deposited. After the equilibrium was reached (for a current of less than 0.05 μA), 10 μl of a 100 mM lactic acid solution was added to the buffer. Each of the following graphs represents the results of one measurement. The resulting currents for the electrode with cross-linked and for covalently bonded lactate oxidase are presented in Figure 6.5 and Figure 6.6 respectively.

The amperometric measurement of the cross-linked lactate oxidase (Figure 6.5) does not show a current response upon the application of lactic acid to the electrode. This correlates with the results received from the cyclic voltammetry measurements presented in Section 6.3. It is most likely that the enzyme lactate oxidase was inactivated during the immobilisation process or that the bovine serum albumin (BSA) is blocking the electrode surface, preventing oxidation. From the amperometric measurement of the electrode with the covalently bonded lactate oxidase (Figure 6.6), a current response of 0.5 μA was

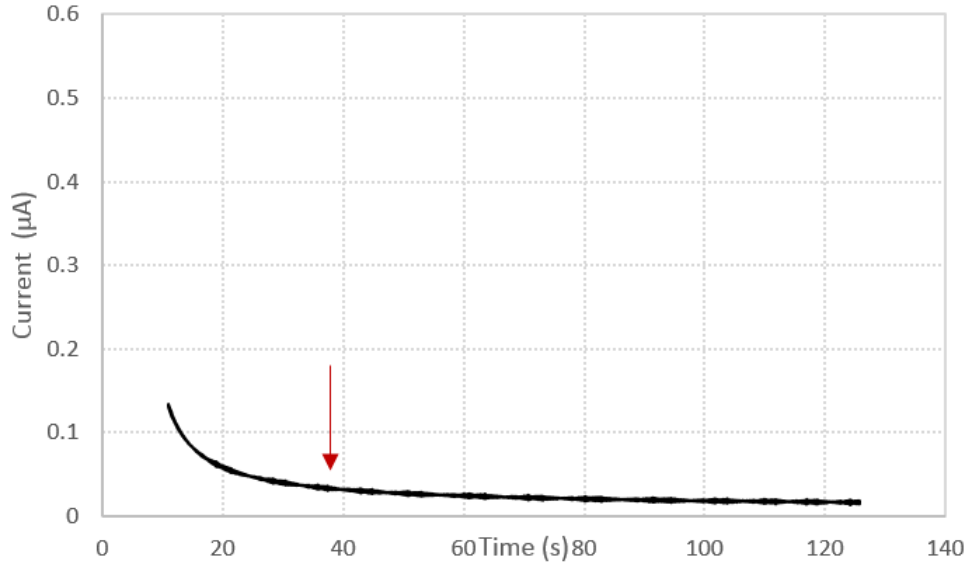

Figure 6.5: *Amperometric measurement: Gold electrode with cross-linked lactate oxidase 100 mM lactic acid solution.*

measured. The red arrow in the graph indicates the application of the lactic acid solution. It can be seen that, upon the application of the lactate acid solution, that the current increases until it reached its peak at about 0.5 μA. The current then decreases over a period of approximately 20 seconds. This is due to the exhaustion of lactic acid which is fully oxidised.

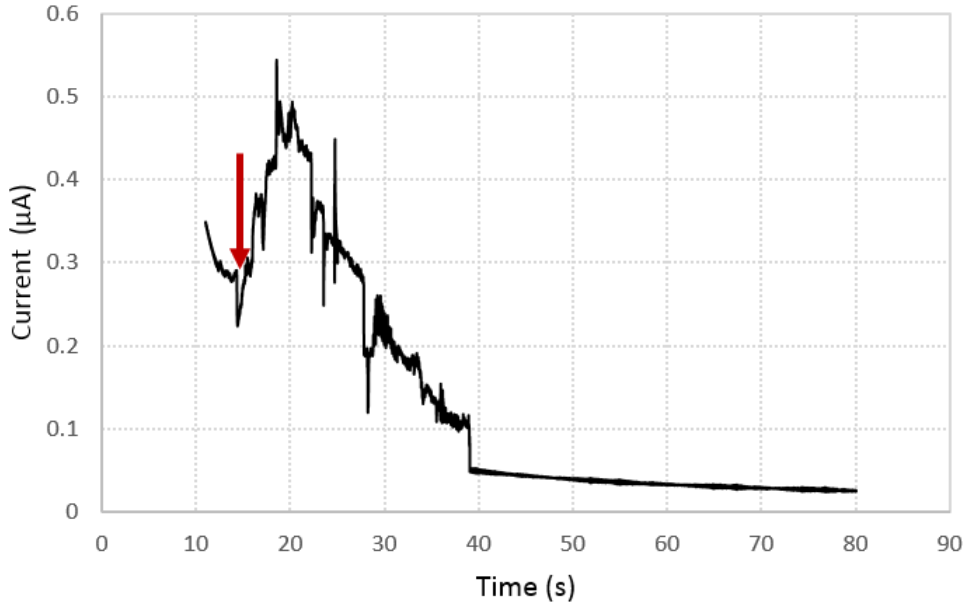

Figure 6.6: *Amperometric Measurement: Gold Electrode with covalently bonded lactate oxidase 100 mM lactic acid after equilibrium was reached.*

As can be seen from the two amperometric measurements above, when a lactate

solution is applied to an electrode with covalently bonded enzymes on the working electrode current response of 0.5 μA was observed. No response with the electrode for which cross-linking was utilised as means of immobilisation was detected. One reason may be that stabilisation reagent bovine serum albumin was blocking the electrode transfer electrodes resulting in no current response. However, it is also possible that the enzymes were deactivated during the immobilisation process. This would lead to the same result and no lactate is metabolised. These initial experiments indicate that covalent bonding may have been more successful than cross-linking for the enzyme lactate oxidase. Further experiments are required to prove repeatability.

6.3.3 EIS Measurements

Electrochemical impedance spectroscopy (EIS) was performed, as introduced in Section 6.2, in order to characterise the immobilisation. The covalent bonding protocol presented in section Section 6.1.2 was applied for the immobilisation of lactate oxidase. Firstly, DL-Dithiothreitol DTT was used as described in the protocol. The solution was incubated on the electrodes overnight. Samples included three platinum (Pt) and three gold (Au) electrodes and one control electrode without the enzyme.

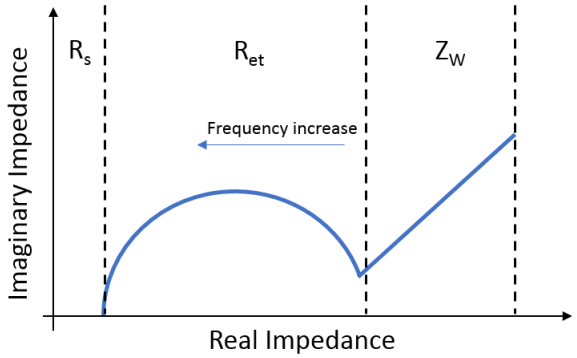

Figure 6.7: *Schematic representation of a EIS Nyquist plot.*

For the measurement, a 10 mM ferro-/ferricyanide solution was applied to the electrodes before the EIS measurements. The electrochemical system was set to a potential of 10 mV and 20 frequencies in the range of 100 kHz to 0.3 Hz were recorded. From the EIS measurements the value R_{et}, which represents the

electron transfer resistance (Figure 6.7), is determined to assess the success of the immobilisation process. The results are shown in Figure 6.8 and Figure 6.9.

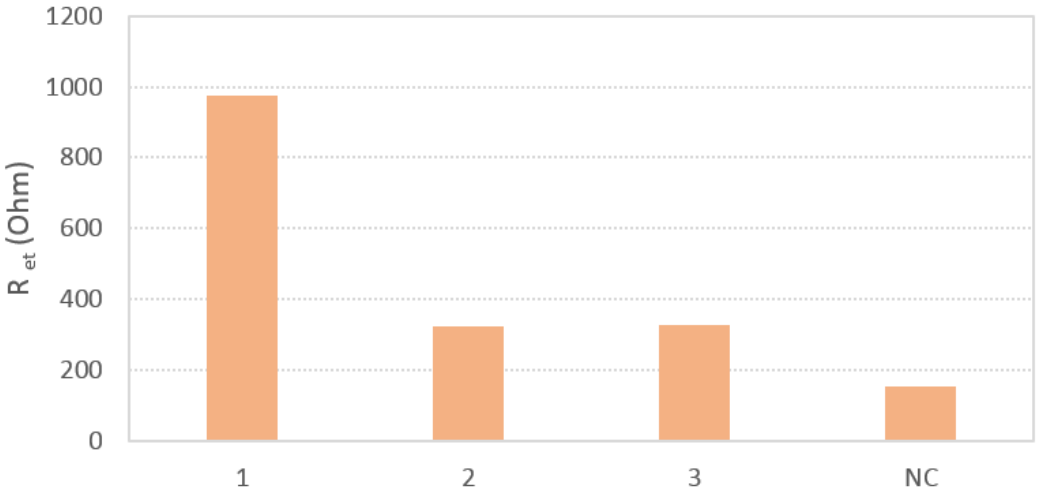

Figure 6.8: *DTT overnight incubation on platinum electrodes. NC = negative control. R_{et} = electron transfer resistance.*

Figure 6.8 shows the results of three (and the negative control (NC)) EIS measurements for the platinum electrodes. The lowest impedance was observed for the control (180 Ohms) as expected.
The other three electrodes exhibit higher impedance (310 - 950 Ohms) due to the immobilisation of the enzyme onto the working electrode. For the three measurements presented the average resistance is 541 Ohms with a standard deviation of 361 Ohms (Table 6.4). These initial results provide a proof of concept that the immobilisation of lactate oxidase on platinum electrodes was successful, despite the high standard deviation.

Figure 6.9 the EIS measurement results of the gold electrodes are presented. Again, the lowest impedance was received for the negative control electrode (11 kOhms). The electrodes that have lactate oxidase immobilised on them show a higher impedance (61 kOhms - 69 kOhms). The resistance measured for electrode 1 is as low as the negative control, which suggests that the immobilisation was unsuccessful due to enzyme deactivation. The average resistance measured for the three electrodes was 63.47 kOhms with a standard deviation of 31.34 kOhms. Despite the high standard deviation these preliminary results show that lactate oxidase was immobilised onto the electrode surface. As the results only show initial proof that the immobilisation was successful but still

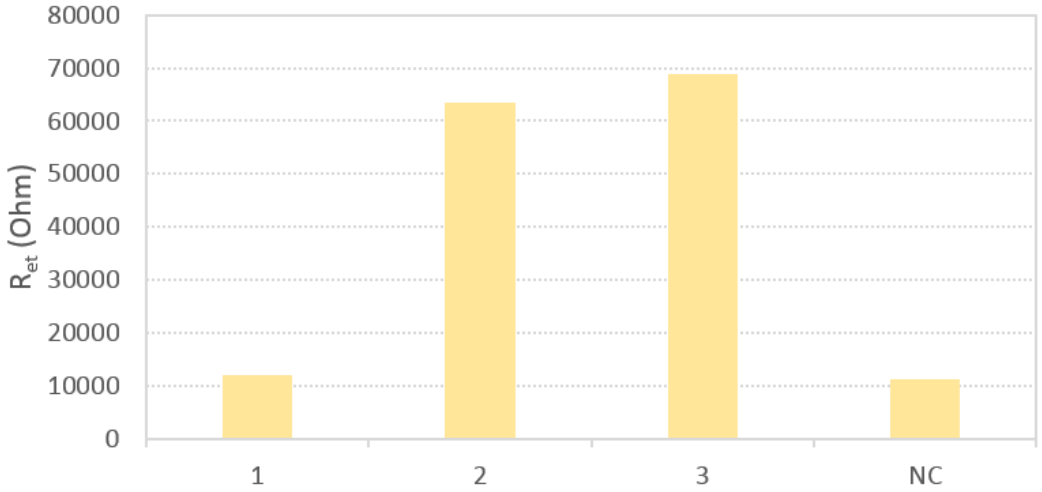

Figure 6.9: *DTT overnight incubation on gold electrodes. NC = negative control. R_{et} = electron transfer resistance.*

show anomalies, further analysis of the immobilisation is required to show that the results are repeatable.

Table 6.4: *Average and Standard deviation of EIS measurements. n=Number of electrodes.*

Electrode	**n**	**Average resistance (kΩ)**	**Standard Dev. (kΩ)**
Platinum	3	0.541	0.361
Gold	3	63.47	3.78 (excl. sample 1)

Table 6.4 provides a comparison of the resistance values obtained from the platinum electrodes and the values measured from the gold electrodes. The impedance value for the gold electrodes is higher by two orders of magnitude, which suggests that the immobilisation is more effective on the gold electrode than on the platinum electrodes. However, it could also mean that the reagents used stick to the gold surface more than to the platinum surface as the EIS measurement does not distinguish between "enzyme on electrode" and "reagents on electrode". Amperometric measurements will confirm the presents of the enzyme and therefore the success of the immobilisation.

Additionally, Tris (2-carboxyethyl) phosphine hydrochloride (TCEP), an alternative reagent to DTT, was tested. The same immobilisation protocol as described in Section 6.1.2 was used, while DTT was exchanged for TCEP. The lactate oxidase solution was incubated for one hour. The measurement

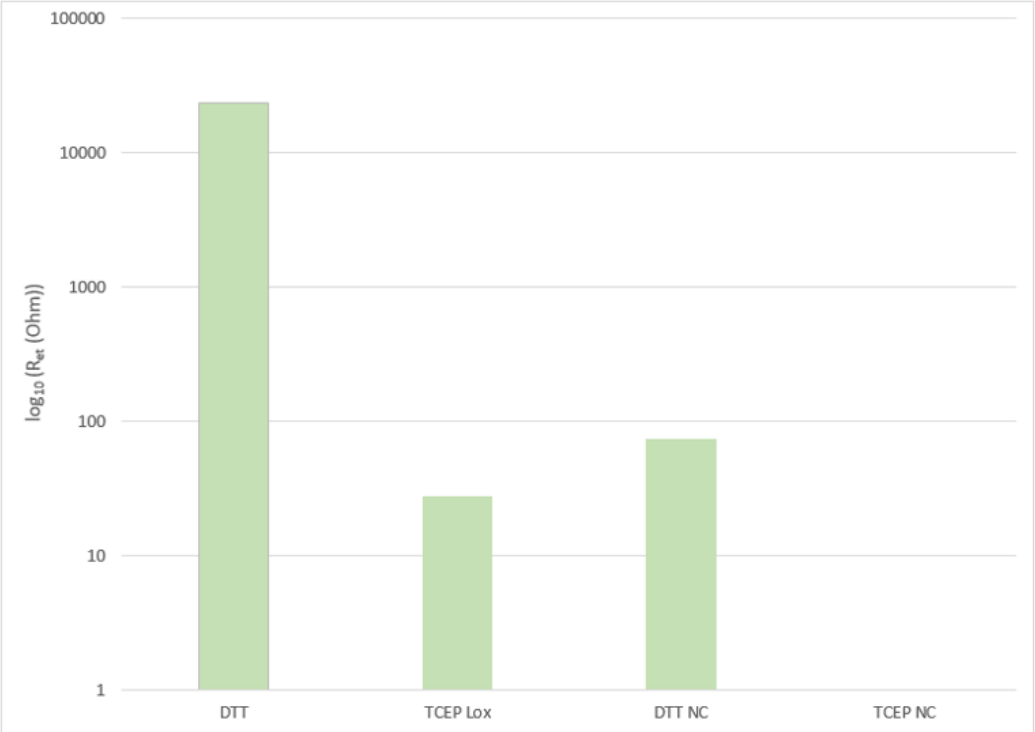

Figure 6.10: *DTT and TCEP after one- hour of incubation on gold electrodes in 1 mM ferro-/ferri cyanide. DTT NC = negative control for DTT, TCEP NC = negative control for TCEP.*

procedure remained as described above. These results are compared to the immobilisation with DTT and are presented in Figure 6.10 and Figure 6.11.

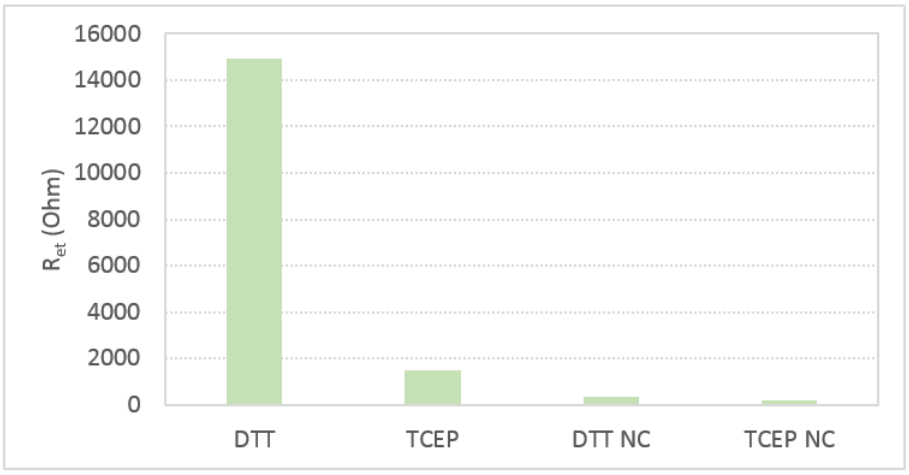

Figure 6.11: *DTT and TCEP after 1 hour of incubation on platinum electrodes 1 mM ferro-/ferri cyanide. DTT NC = negative control for DTT, TCEP NC= negative control for TCEP.*

Each bar represents one measurement. Successful immobilisation was achieved after an hour of incubation using DTT. Figure 6.10 (please note the graph is shown in a logarithmic scale) shows the EIS measurement results of gold

electrodes comparing the immobilisation of DTT with TCEP (each bar representing one measurement on one electrode). The impedance for both negative controls are low which shows that there was no contamination. The immobilisation with DTT exhibits a high impedance of 23.45 kOhms. However, the impedance measured for the electrode on which TCEP was used to immobilise the electrode shows a low impedance of 27.57 Ohms, a three orders of magnitude difference. This result shows that the immobilisation on gold electrodes using TCEP was not successful.

The same measurements were conducted on platinum electrodes (Figure 6.11)(each bar representing one measurement on one electrode). The negative control is low, suggesting no contamination has taken place during the immobilisation process. The immobilisation using DTT as described was also successful on the platinum electrodes. Using TCEP instead of DTT shows a lower impedance value but is distinctively higher than the control (TCEP NC) indicating that the immobilisation worked. Based on these results, DTT was used for all further measurements.

In addition to the above experiments, the incubation time was explored further. Both platinum and gold electrodes were incubated overnight and compared to the data obtained from the one-hour incubation. Figure 6.12 shows the results of the measurements on gold electrodes (each bar representing one measurement on one electrode). The incubation overnight resulted in higher impedance indicating it is more successful. The impedance obtained from the overnight incubation is at least four-fold higher compared to the one-hour incubation.

The same experiment was performed using platinum electrodes. The results of the overnight incubation were compared to the one-hour incubation. The results of the EIS measurements are shown in Figure 6.13. The values are three-fold lower compared to the impedance values obtained from gold electrodes. However, for the platinum electrodes, the electrode that was incubated for only one hour exhibits a much higher impedance value. In addition, the impedance for the overnight control electrode exhibits a high impedance of 7,954 Ohms

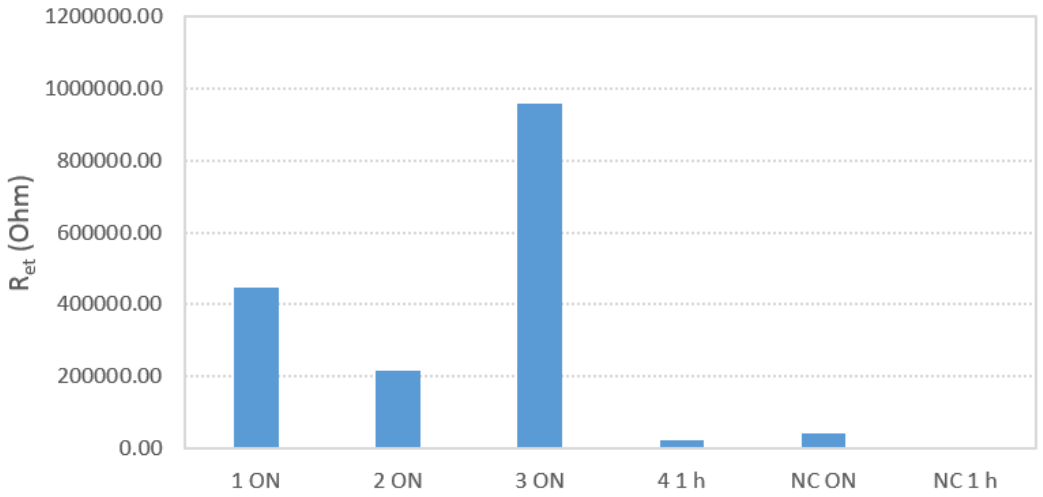

Figure 6.12: *Comparison of overnight (ON) incubation versus one-hour incubation on DropSens gold electrodes. NC = negative control.*

which is higher than some of the positives. This is indicative of a contamination of the control electrode. Due to the lack of repetitions of the measurements more experiments are required to provide representative data.

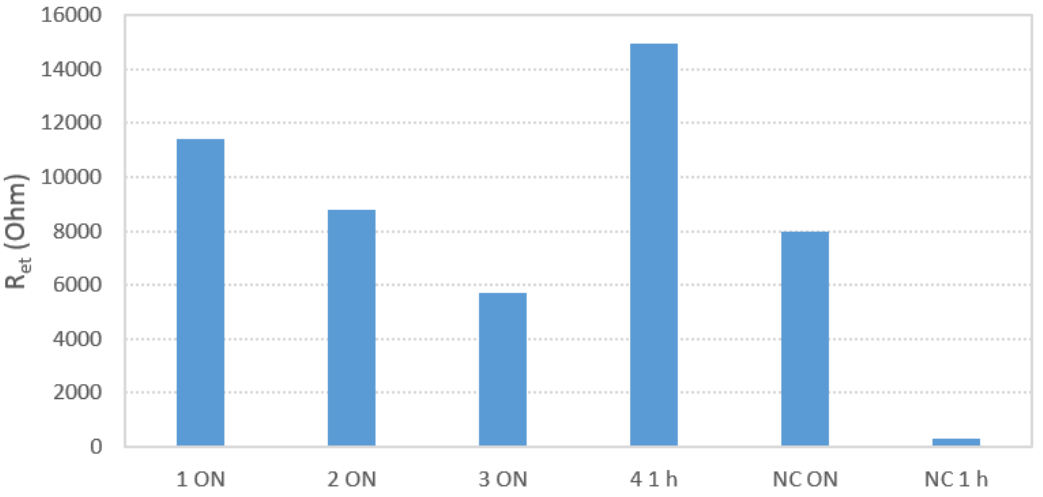

Figure 6.13: *Comparison of overnight (ON) incubation versus one-hour incubation on DropSens platinum electrodes.*

6.4 Conclusions

Initially, cyclic voltammetry was conducted on bare and functionalised DropSens electrodes for the determination of the overpotential. This overpotential was

utilised for initial amperometric measurements, which showed that using covalent bonding lactate oxidase is more successful than cross-linking. Electrochemical impedance spectroscopy was applied to characterise the immobilisation success. An alternative reagent to DTT, TCEP, and the duration of the incubation time were also examined. Better immobilisation was achieved using DTT. On gold, longer incubation times resulted in better immobilisation. The platinum electrodes exhibited better immobilisation results after only one hour. Based on these limited number of tests, the impedance measured from gold electrodes was much higher than on platinum electrodes. However, more experiments are necessary for more concrete conclusions. The amperometric measurements presented in Chapter 7 will provide more information about the immobilisation success by measuring lactate concentration. This will give insight in the enzyme activity on the electrode surface. These were initial experiments. For more representative results, a higher number of repetitions is required.

7 Amperometric Measurements

This chapter provides details about the amperometric measurements of H_2O_2 and lactate and the respective current responses. For all experiments, DropSens gold and platinum electrodes were used. Firstly, H_2O_2 measurements utilising blank gold and platinum electrodes were performed. Next, functionalised electrodes were used for amperometric measurements of a lactate solution, and finally, an additional experiment regarding the storage capabilities of the functionalised electrodes was conducted.

7.1 H_2O_2 Measurements

The H_2O_2 measurements can be divided into three experiments. Firstly, the same concentration of H_2O_2 was applied to gold and platinum electrodes and the resulting current at different potentials was measured. Secondly, two different potentials for platinum and gold respectively were tested. After adding a PBS buffer and the respective potential was applied, a 1.5% H_2O_2 solution is added subsequently. The current response to each addition of H_2O_2 was observed over a duration of two minutes. DropSens electrodes (gold and platinum), as described in Section 5.1, were used for all measurements.

7.1.1 1st H_2O_2 Experiment

This experiment was conducted to observe the influence of the potential to the resulting current when the concentration remains unchanged. Following the preparation of the electrodes (creating the reference electrode and cleaning the whole electrode), as described in Section 6.1, a 1.5% H_2O_2 solution was prepared from a 30% H_2O_2 stock solution by diluting 50 μl of the H_2O_2 stock solution with 950 μl PBS. 60 μl PBS is applied to the electrodes once the

electrodes are connected. The required potential is set and the measurement is started. The different potentials that were tested in this experiment are summarised in Table 7.1. Following the activation of the potentiostat, 30 μl of lactate solution was added to the 60 μl of PBS on the electrode. Each measurement was performed for two minutes.

Table 7.1: *Potentials for gold and platinum electrodes used for H_2O_2 experiments.*

Gold	Platinum
500 mV	170 mV
700 mV	300 mV
	550 mV

7.1.2 2nd H_2O_2 Experiment

This experiment is a continuous measurement of the resulting currents of gold and platinum electrodes. The electrodes were prepared as explained in Section 6.1 and a 1.5 % H_2O_2 solution was prepared. The current of the gold and platinum electrodes were measured at 654 and 415 mV, respectively. These values were determined through cyclic voltammetry (current peak). Before the measurements, 60 μl of PBS was added to the electrode. After the respective potential was applied, 10 μl of the H_2O_2 solution was applied repeatedly after the previous response was observed. The time evolution of the resulting current was recorded for six minutes.

7.1.3 3rd H_2O_2 Experiment

In this experiment, the current responses to different H_2O_2 concentrations were observed. The potential for the gold electrode was set at 420 mV and 153 mV for the platinum electrode. H_2O_2 solutions at different concentrations were achieved by diluting the stock solution using PBS. The concentrations used for this experiment are listed in Table 7.2. Each measurement was conducted separately for three minutes and the electrodes were cleaned by rinsing them with PBS and dried with argon gas.

Table 7.2: *Concentrations used for H_2O_2 experiments.*

	Concentration (M)
Lower concentrations	0.01
	0.03
	0.04
	0.05
Higher concentrations	0.1
	0.5
	1.0

7.2 Lactate Measurements

Lactate measurements were conducted utilising functionalised gold and platinum electrodes. Lactate oxidase was covalently attached to the electrode surfaces as explained in Section 6.1.2. The following experiments were conducted. The protocols for the immobilisation and incubation steps were provided by the Division of Pathway Medicine.

1. Amperometric measurement of electrodes exposed to 1 hour of incubation of the lactate oxidase solution on the working electrode.
2. Amperometric measurement of electrodes exposed to overnight incubation of the lactate oxidase solution of the working electrode.
3. Amperometric measurements after the electrodes were stored for two days . Incubation was completed before the electrodes were stored.

For all experiments, a potential of 550 mV was applied for platinum and 500 mV was applied for gold electrodes. A 100 mM lactic acid solution was prepared for the measurements. The experiments followed the steps below:

1. Electrode preparation
2. Immobilisation (different incubation times)
3. Preparation of lactic acid solution

4. Setting up of the potentiostat
5. Application of 60 μl of PBS
6. Wait for 2 minutes for the system to reaction equilibrium
7. Application of 20 μl of lactic acid solution
8. Measure for 360 seconds
9. Finish measuring

7.3 Results

7.3.1 1st H_2O_2 Measurements

Amperometric measurements at different potentials were conducted to observe the resulting current responses. Platinum electrodes were measured at 170, 300 and 550 mV and gold electrodes were measured at 500 and 700 mV. The measurements were performed for 120 seconds in 3% H_2O_2 solution. The results of these measurements are shown in Figure 7.1. Each graph represents one measurement.

The lowest current response was obtained from the negative control (NC) as expected, followed by the current responses received from the gold electrodes at 500 mV (green) and 700 mV (dark blue). The current responses obtained from the platinum electrodes at the potentials 170 mV (blue), 330 mV (orange) and 550 mV (grey) are higher by one order of magnitude. The visible spikes, in particular, those for the current response of the platinum electrodes, are created by bursting bubbles on top of the H_2O_2 drop placed on the electrode. Overall, it can be seen that greater currents were obtained using the platinum electrodes.

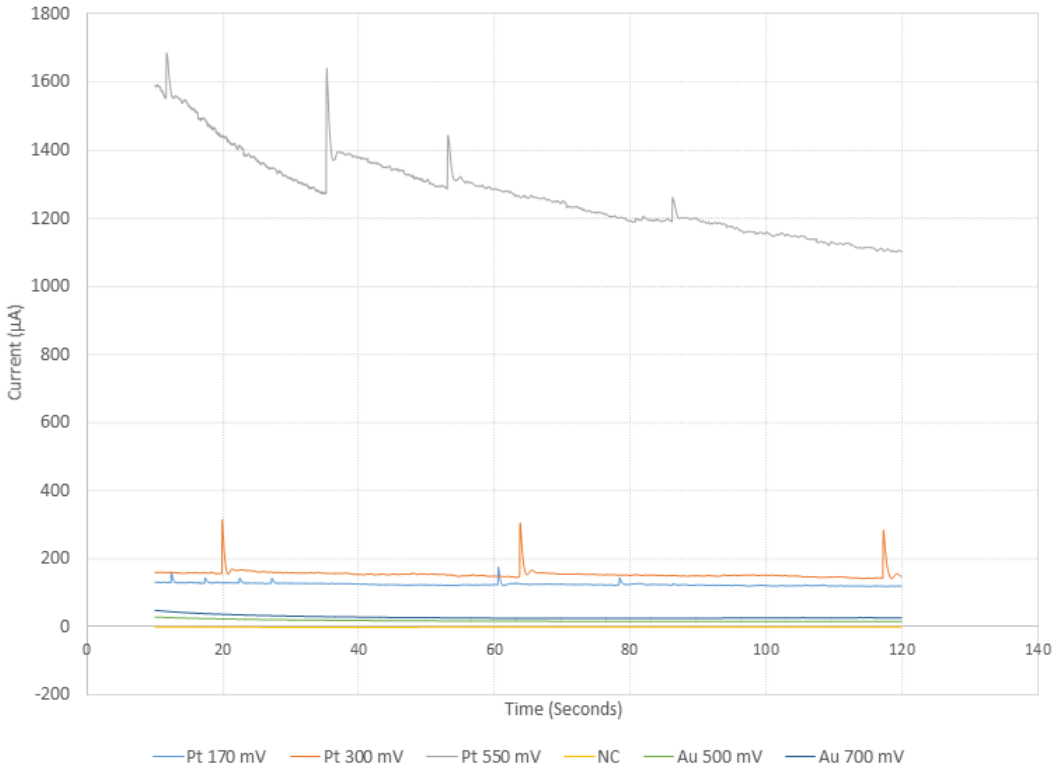

Figure 7.1: *Amperometric results of platinum and gold electrodes in H_2O_2 at different potentials.*

7.3.2 2nd H_2O_2 Measurements

Following that experiment, platinum and gold electrodes were exposed to different H_2O_2 concentrations. The experiment was set up as followed. The prepared (gold or platinum) electrode was connected to the potentiostat and a phosphate buffer saline (PBS) was applied to the electrode. After setting the potential to either 415 or 654 mV, depending on the nature of the metal deposited, the amperometric measurement commenced for a duration of 360 seconds. An additional 10 μl 3% H_2O_2 was added to observe the effect of changing concentrations. The current responses for these measurements are presented in Figure 7.2. Each graph represents one continuous measurement. The green and orange graph represent the current received from the gold electrodes at 415 mV and 654 mV respectively. The current response of the platinum electrodes at the same potentials are represented by the red and blue graph respectively.

The time of H_2O_2 applications occurred always right before the increase in

current for each electrode. Comparing the current responses of the gold and platinum electrodes at the same potentials, it is again clear that the higher currents were obtained from the platinum electrode with greater responses, suggesting that platinum would be an ideal metal for an electrochemical lactate sensor.

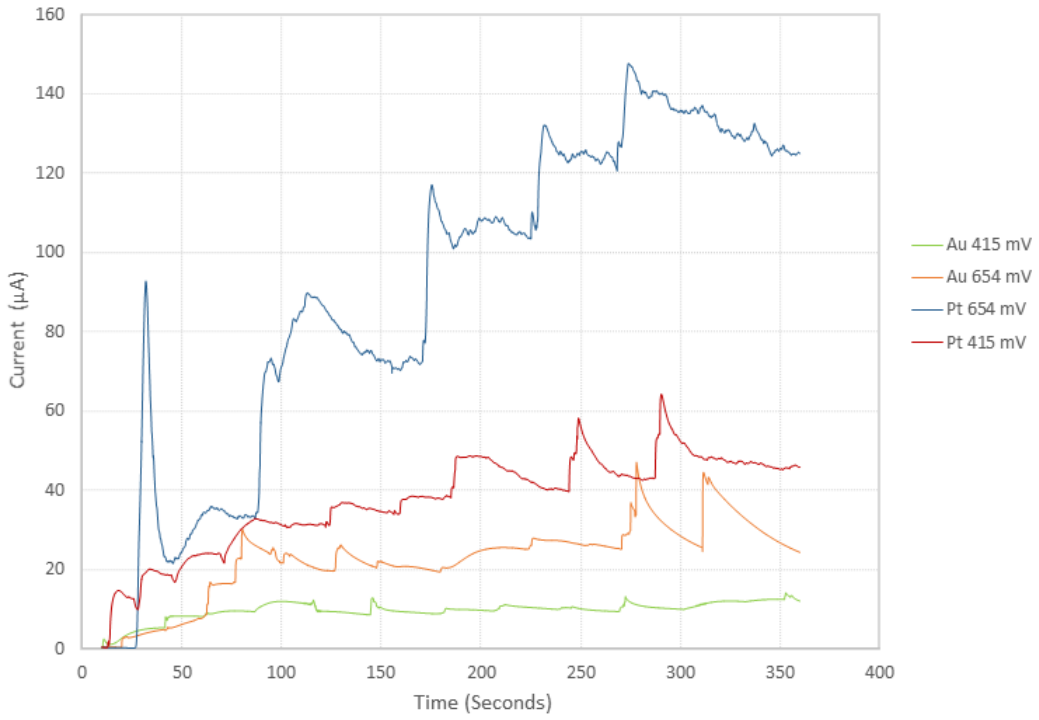

Figure 7.2: *Results of amperometric Measurements of H_2O_2 on gold and Platinum electrodes at 415 mV and 654 mV.*

Additional measurements were conducted in which a 10 % H_2O_2 solution was added to a previously applied PBS solution every 20-30 seconds. The point of application is indicated by red arrows in Figure 7.3 and Figure 7.4. The blue graph represents the negative control and the green graph shows the current response of the platinum and gold electrodes at H_2O_2 application, respectively.

For both responses, there is an increase in current with each application of H_2O_2. The current received from the platinum electrode is again higher than the current received from the gold electrode. Both responses have a sharp increase in current followed by a decrease, representing the oxidation of H_2O_2. The difference between consecutive responses is observed to lessen with each application. This is due to the H_2O_2 concentration on the electrode approach-

ing the concentration of the solution that is applied.

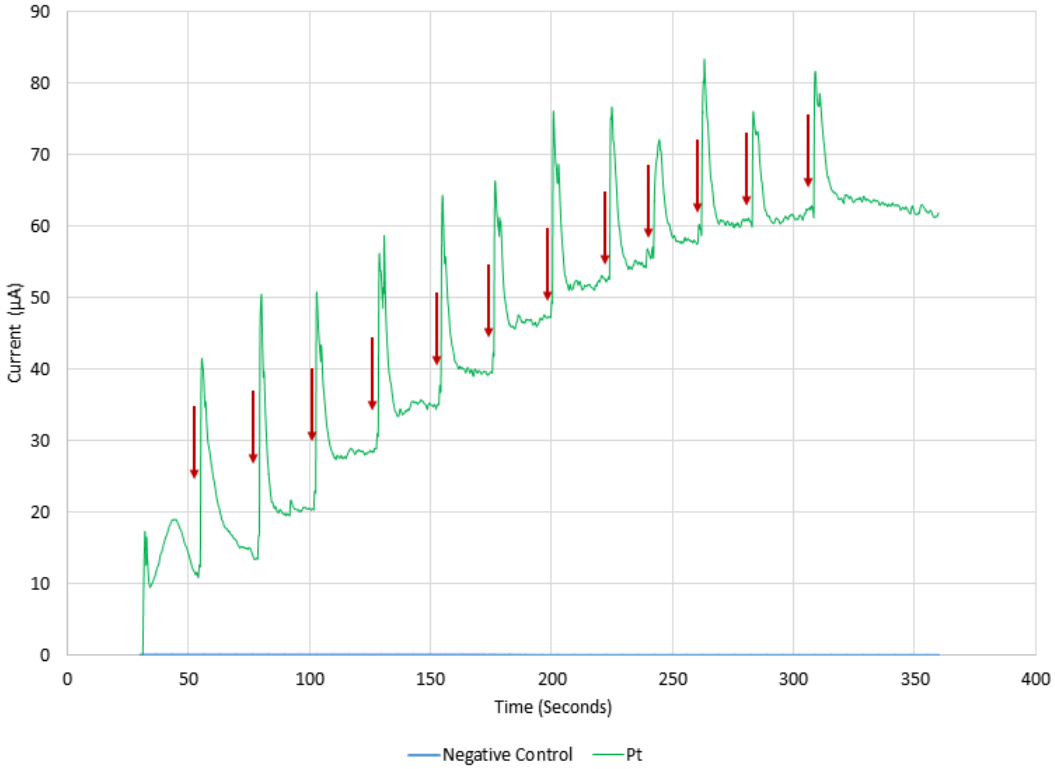

Figure 7.3: *Results of continuous amperometric measurements of platinum electrodes upon subsequent application of H_2O_2. The red arrows indications the time of the application of lactate.*

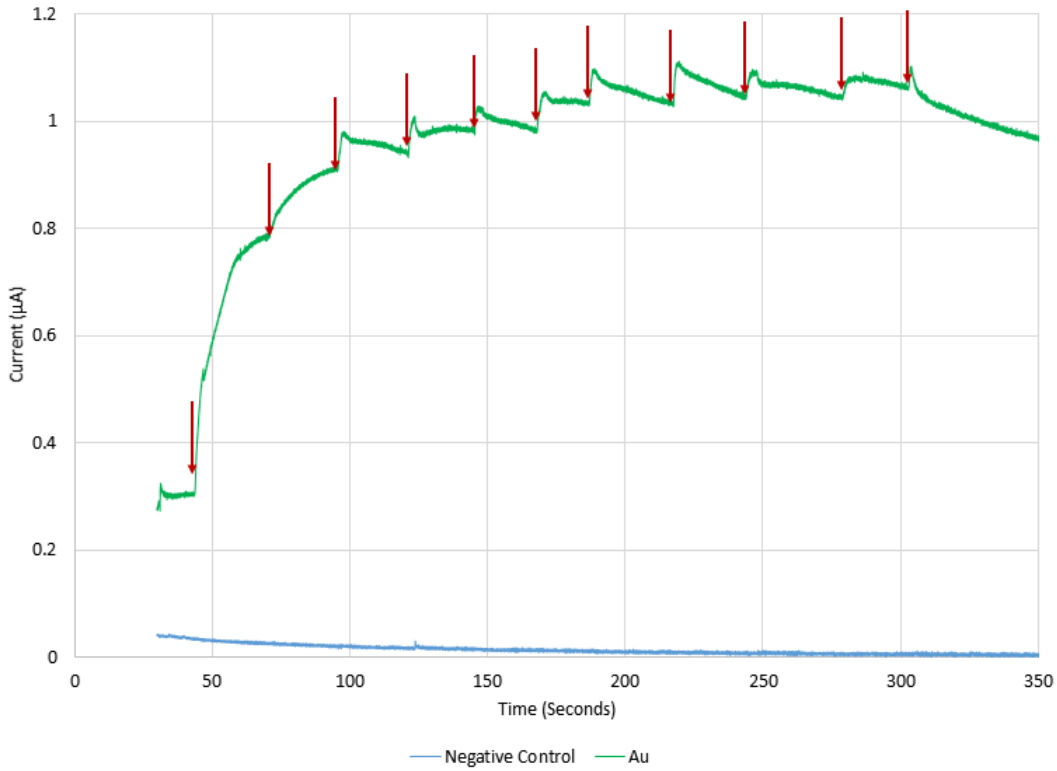

Figure 7.4: *Results of continuous amperometric measurements of gold electrodes upon subsequent application of H_2O_2. The red arrows indications the time of the application of lactate.*

7.3.3 3rd H_2O_2 Measurements

Following continuous measurements of the application of consistent concentrations of H_2O_2 to the electrodes, Figure 7.5 illustrates the result of discontinuous measurement of differing concentrations of H_2O_2. Each graph represents one measurement. These measurements were conducted separately and the electrodes were rinsed with PBS and dried with argon gas in between each measurement. The duration of each measurement was 180 seconds. The results shown in Figure 7.5 are based on gold electrodes. As expected, the lowest concentration results in the lowest current response. When the electrochemical cell is switched on very high currents (in comparison to the following measured currents) are observed, due to the formation of the double layer. Therefore, the first 80 seconds are not represented in the graph for resolution purposes.

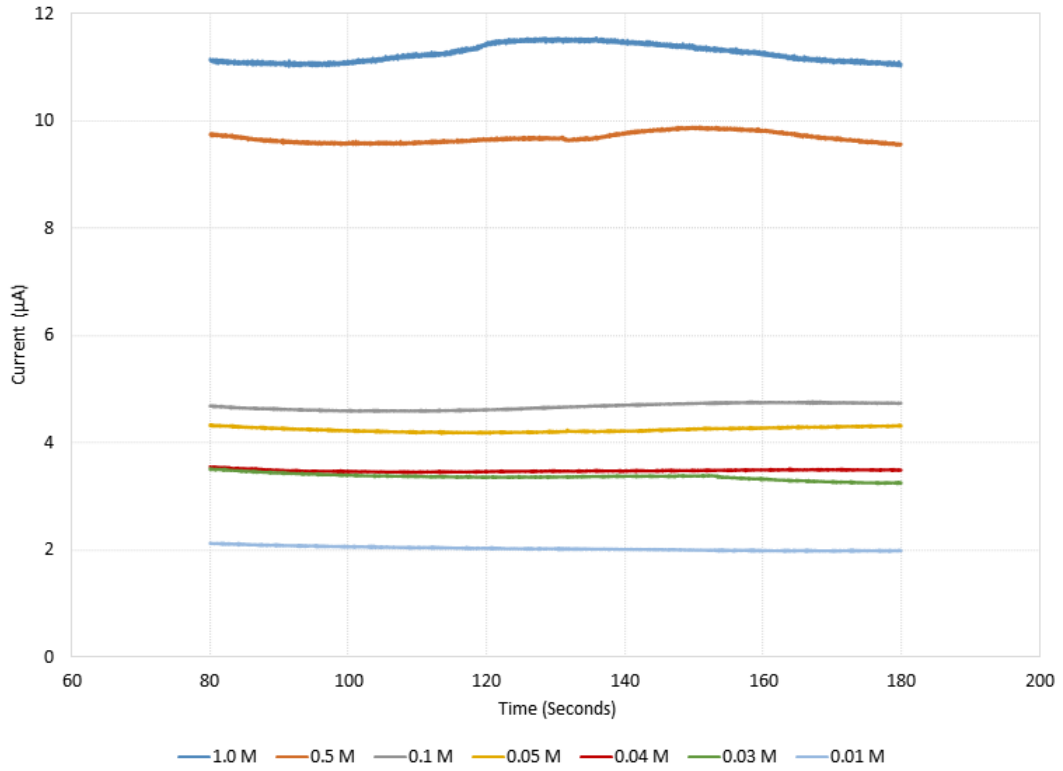

Figure 7.5: *Amperometric measurement of different H_2O_2 concentrations on gold electrodes.*

From these measurements, calibration curves were generated. A calibration curve represents the current received with regard to the concentration applied to the electrode. It shows whether the there is a linear correlation between the applied concentration and the current received. With this information, the concentration of a solution can be determined from the current value in the sensor. Figure 7.6 shows the calibration curve including all concentrations with the respective current. The correlation was found to be $R_2 = 0.90$. Separate calibration curves, shown in Figure 7.7 and Figure 7.8, for the lower (0.01 - 0.05M) and higher (0.1 - 1.0 M) concentration ranges, respectively, were also created. The correlation was still in the same range with $R_2 = 0.92$ and $R_2 = 0.88$, respectively. However, the higher correlation for the lower concentration may indicate a better sensitivity for lower concentrations. More measurements are required for more representative results.

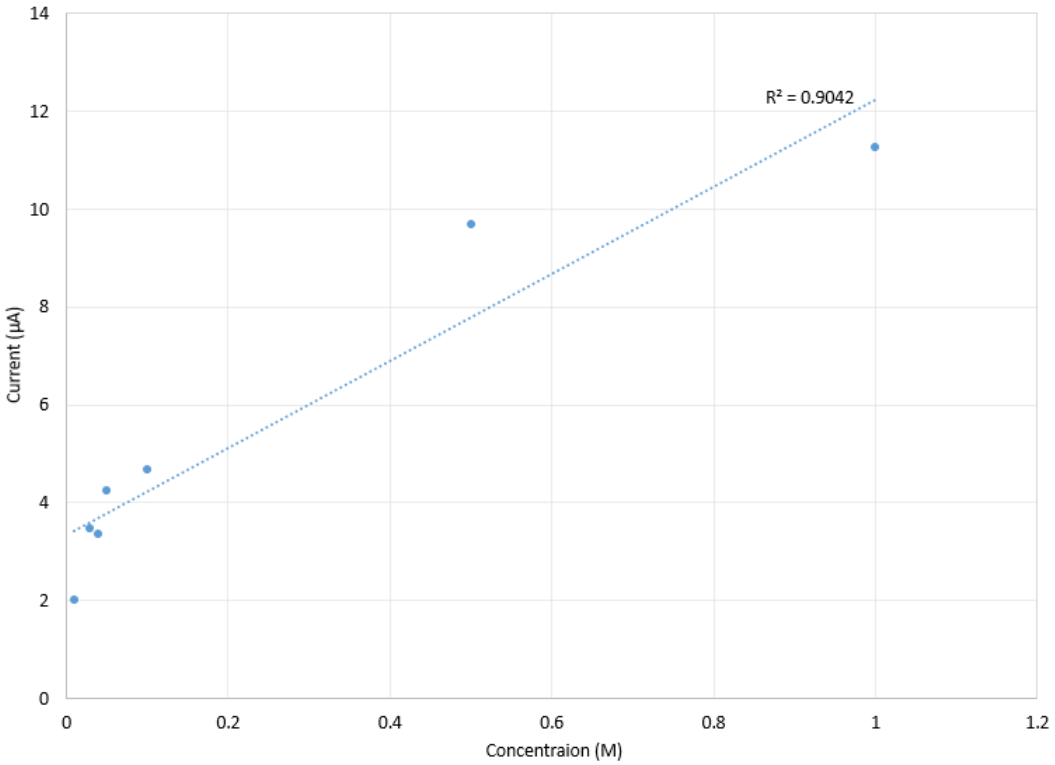

Figure 7.6: *Calibration curve of gold electrode H_2O_2. All measured concentrations.*

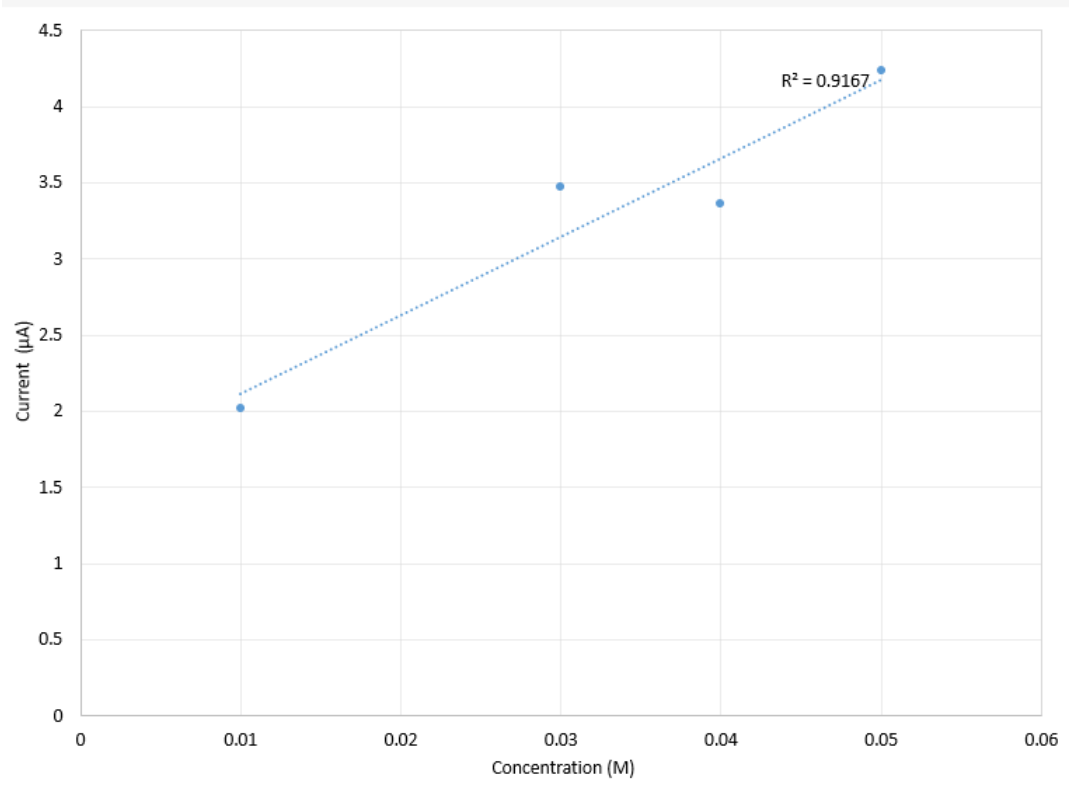

Figure 7.7: *Calibration curve of gold electrode H_2O_2. (Lower concentrations).*

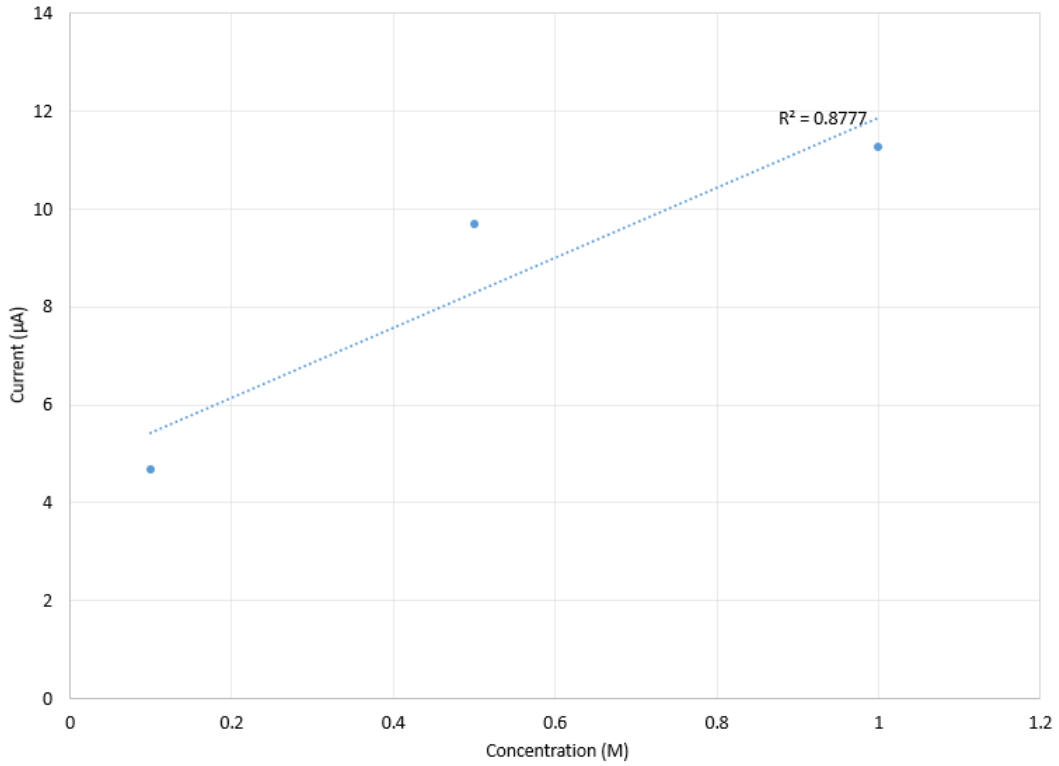

Figure 7.8: *Calibration curve of gold electrode H_2O_2. (Higher concentrations).*

The same measurement was conducted using platinum electrodes with results presented in Figure 7.9. Each graph represents one measurement. In general, a higher current was obtained in these measurements. The lowest current was measured from the lowest concentration and the highest from the highest concentration. Currents obtained from the following concentrations, 0.01. 0.03, 0.04, 0.05, 0.1, 0.5 M and 1.0 M allowing thereby the setup of a calibration curves. As an initial calibration curve (Figure 7.10) containing the respective current values to all concentrations, clearly shows that there are two linear regions, two separate calibration curves were plotted, one for the lower concentration (0.01. 0.03, 0.04 and 0.05 M) (Figure 7.11) and one for the higher concentrations (0.1, 0.5 M and 1.0 M) (Figure 7.12). Then the data plotted in the separate graphs shows a correlation of $R_2 = 0.998$ and $R_2 = 0.96$. The reason for the different linear regions needs to be determined in additional experiments, by increasing the concentration steps and the number of measurement.

Overall, greater signals and better signal correlation were obtained from plat-

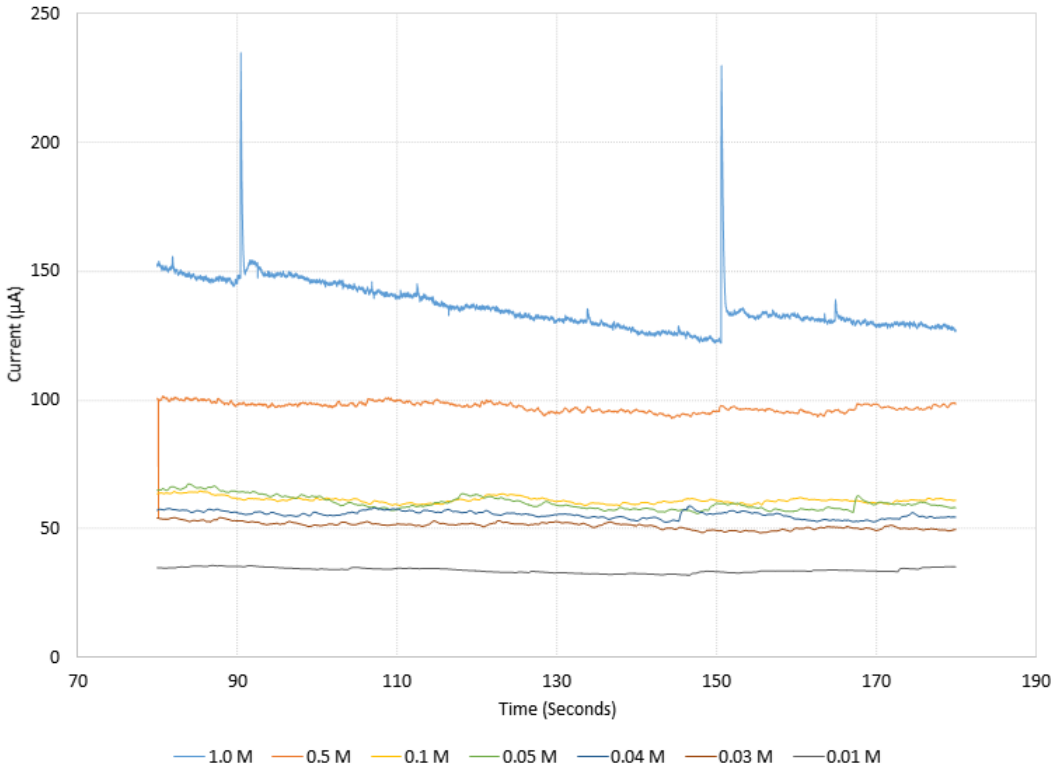

Figure 7.9: *Current response of platinum electrode at different H_2O_2 concentrations.*

inum electrodes Further improvement of the correlation could be achieved by measuring the volumes with smaller pipettes to achieve more accurate determination of the concentrations.

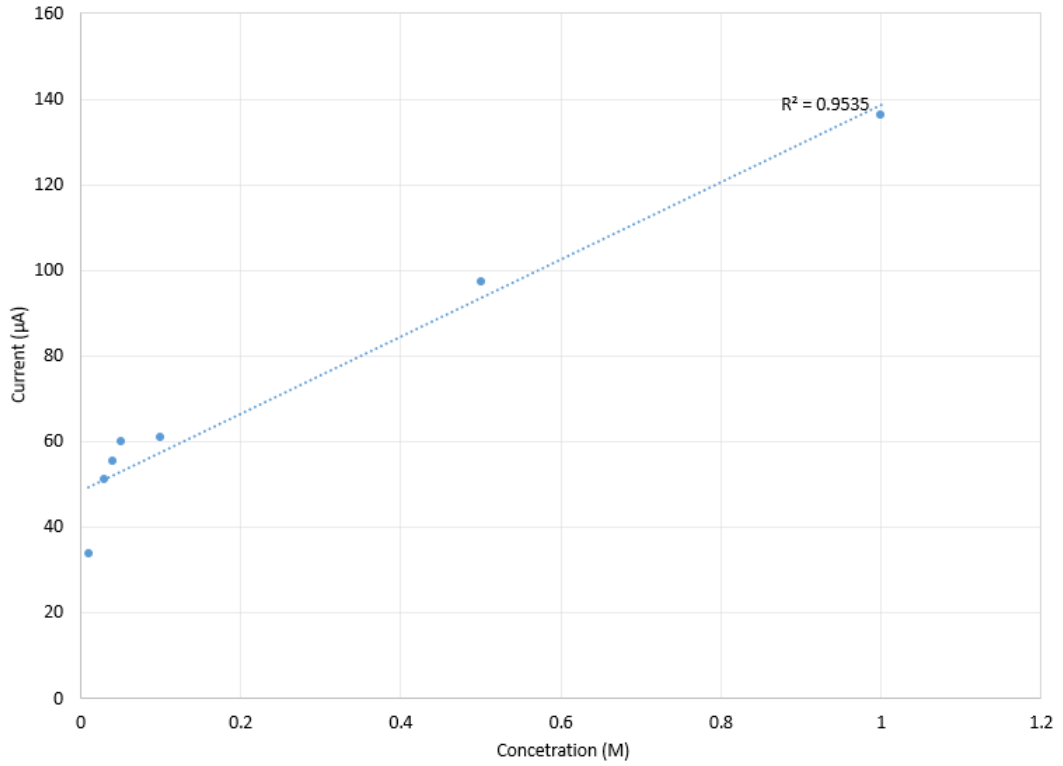

Figure 7.10: *Calibration curve of a platinum electrode in H_2O_2 for all measured concentrations.*

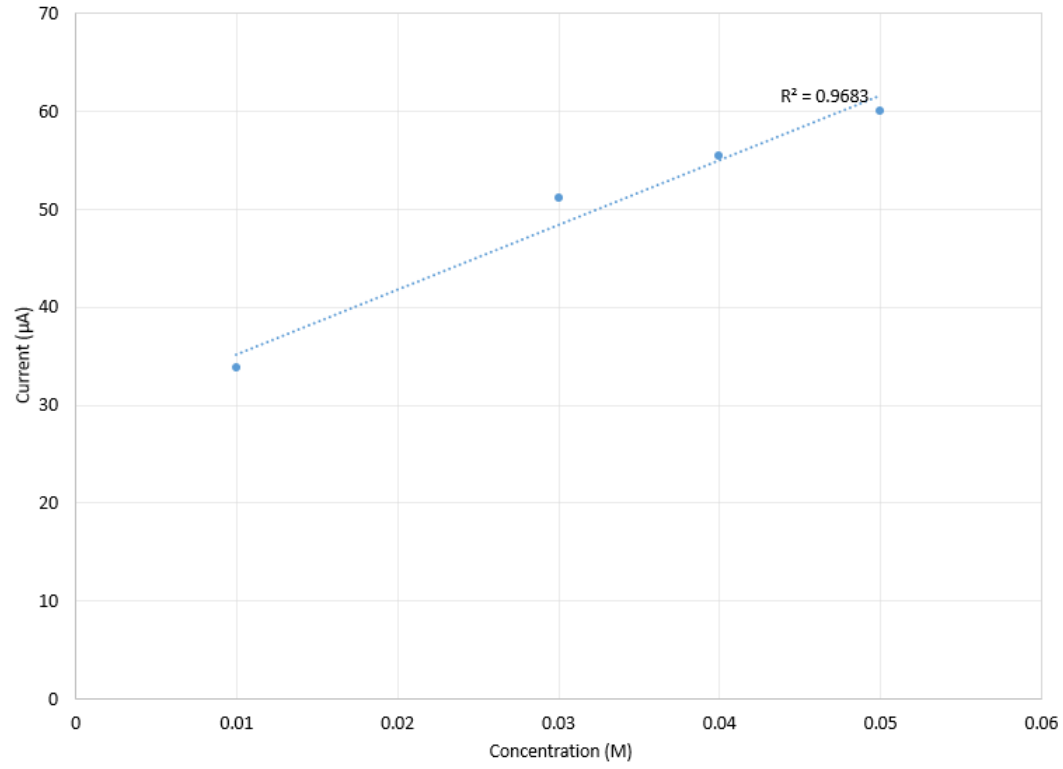

Figure 7.11: *Calibration curve of a platinum electrode in H_2O_2 (lower concentrations).*

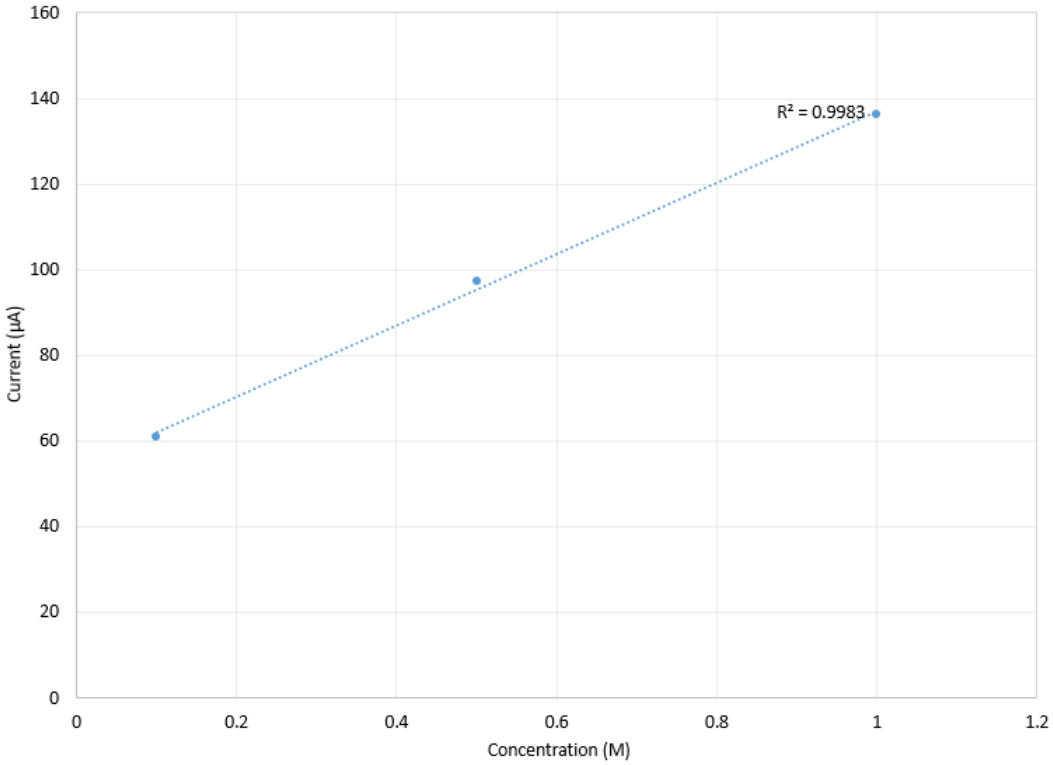

Figure 7.12: *Calibration curve of a platinum electrode in H_2O_2 (higher concentrations).*

7.3.4 Lactate Measurements

In this section, the results of amperometric lactate measurements are presented. These results include amperometric responses of platinum and gold electrode where the incubation time of the immobilisation was one hour or overnight. Furthermore, the strength of the functionalised gold and platinum electrodes was tested after two days of storing them at 4°C.

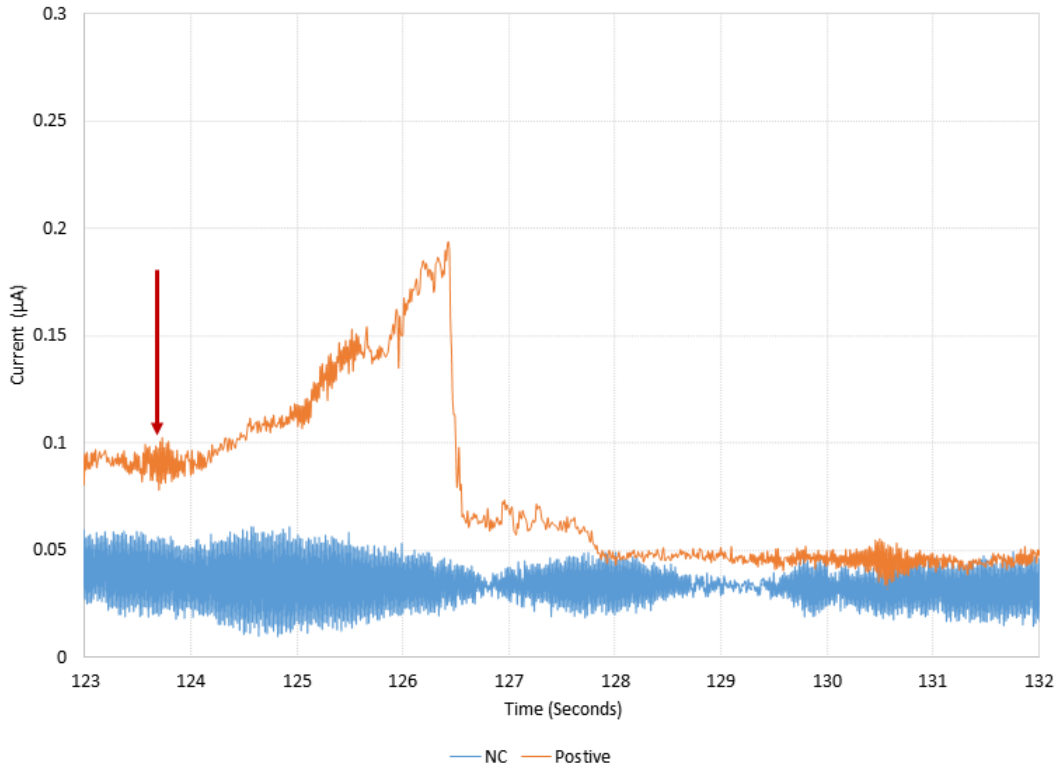

Figure 7.13: *Amperometric measurements of lactate with immobilised lactate oxidase on a gold electrode. The red arrow indications the time of the application of lactate.*

Figure 7.13 shows the amperometric response of one functionalised (one hour incubation time) gold electrode compared to the negative control which was an electrode, "functionalised" with the same solution except for the lactate oxidase. The lactic acid solution was added to both electrodes at the same time. It can be seen from the graph that the current increases (124 - 126.5 seconds) with the application of a lactate solution (red arrow). It decreases again after the lactate has been consumed by the lactate oxidase immobilised on the electrode surface. The noise present in the current response was observed only with gold electrodes and is also present in the negative control. This baseline

noise can be subtracted from the main signal in the future to obtain a clearer response. It may also be possible to reduce the noise applying noise filters in the potentiostat.

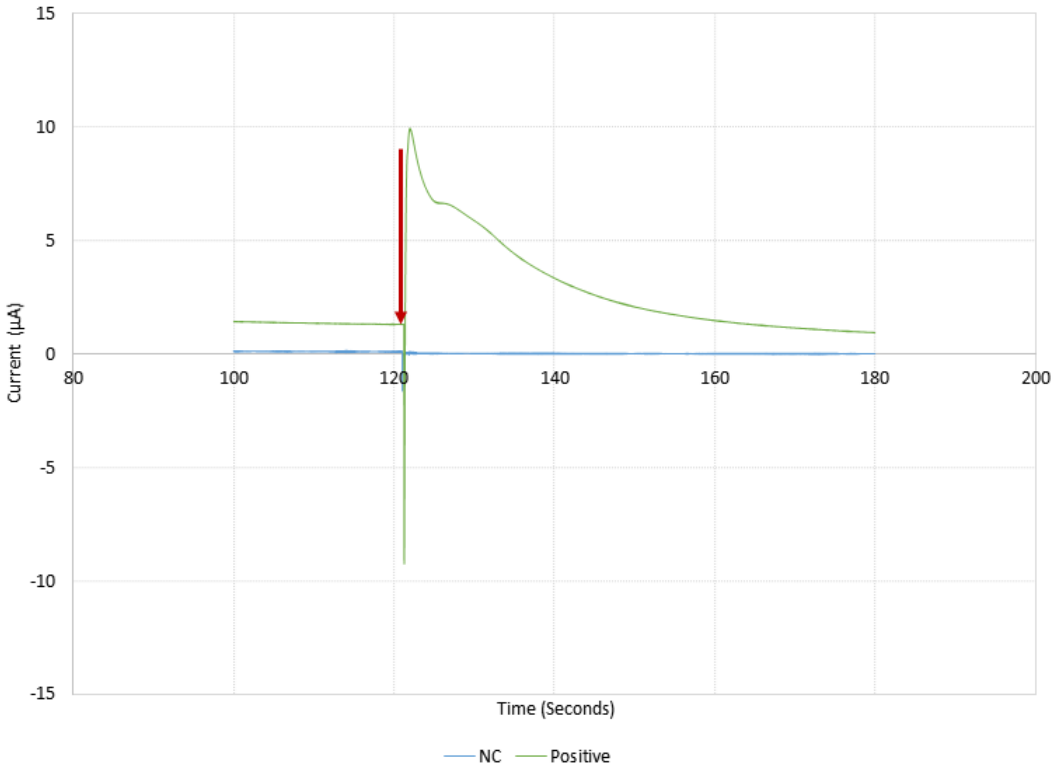

Figure 7.14: *Amperometric measurements of lactate with immobilised lactate oxidase on a platinum electrode. The red arrow indications the time of the application of lactate.*

The same measurement was performed utilising platinum electrodes. The current response is at a much larger value, 10 μA, compared to the current response on the gold electrodes (0.2 μA). Also visible in Figure 7.14 is that, upon the application of the lactate solution (red arrow), currents decreases gradually until no lactate remains to be oxidised, which allows the current return to its original value.

In order to determine the impact of lactate oxidase solution incubation duration, two gold and three platinum electrodes were prepared and the lactate oxidase solution was incubated on the electrode overnight. For these measurements new electrodes were used. For the measurement, the potential was set to 500 mV for the gold electrodes and to 550 mV for the platinum electrodes, which were obtained from the most recent CV. The resulting currents received

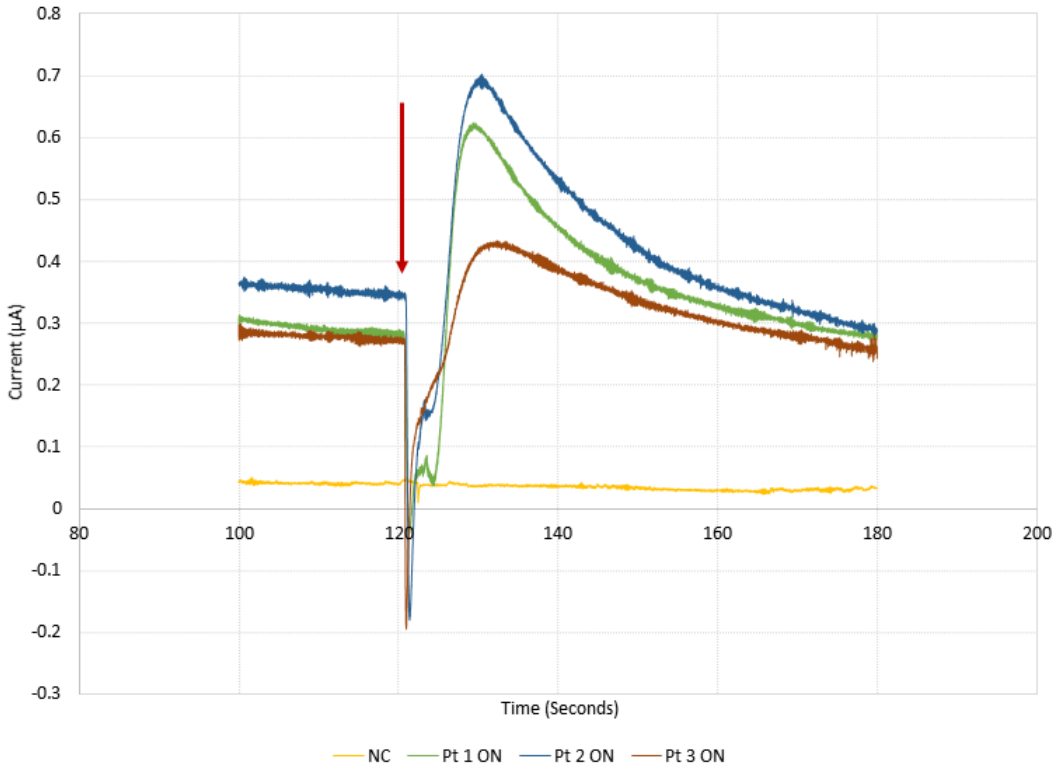

Figure 7.15: *Results of amperometric measurements of lactate using platinum electrodes with immobilised lactate oxidase (overnight (ON) incubation time). The red arrow indications the time of the application of lactate.*

from the platinum electrodes (each graph represents one measurement with one electrode) are shown in Figure 7.15. The yellow graph represents the negative control, whereas the other graphs (red, green and blue) represent the current response of the platinum electrodes exposed to an overnight incubation of the lactate oxidase solution. The peak currents are between 0.43 - 0.7 μA. The currents increase instantly upon the lactate application (100 mM) onto the electrode and decrease gradually afterwards. The current is distinct from the negative control. The immobilisation with overnight incubation was successful on platinum electrodes.

These results were compared to the current response obtained from platinum electrodes that have been exposed to one hour of incubation time. The comparison of the two results is presented in Figure 7.16. The current obtained from the electrodes with one-hour incubation time is much higher (10 μA) than the current received from the electrodes incubated overnight (0.7 μA). Therefore, it can be said, that the one-hour incubation time is not only quicker

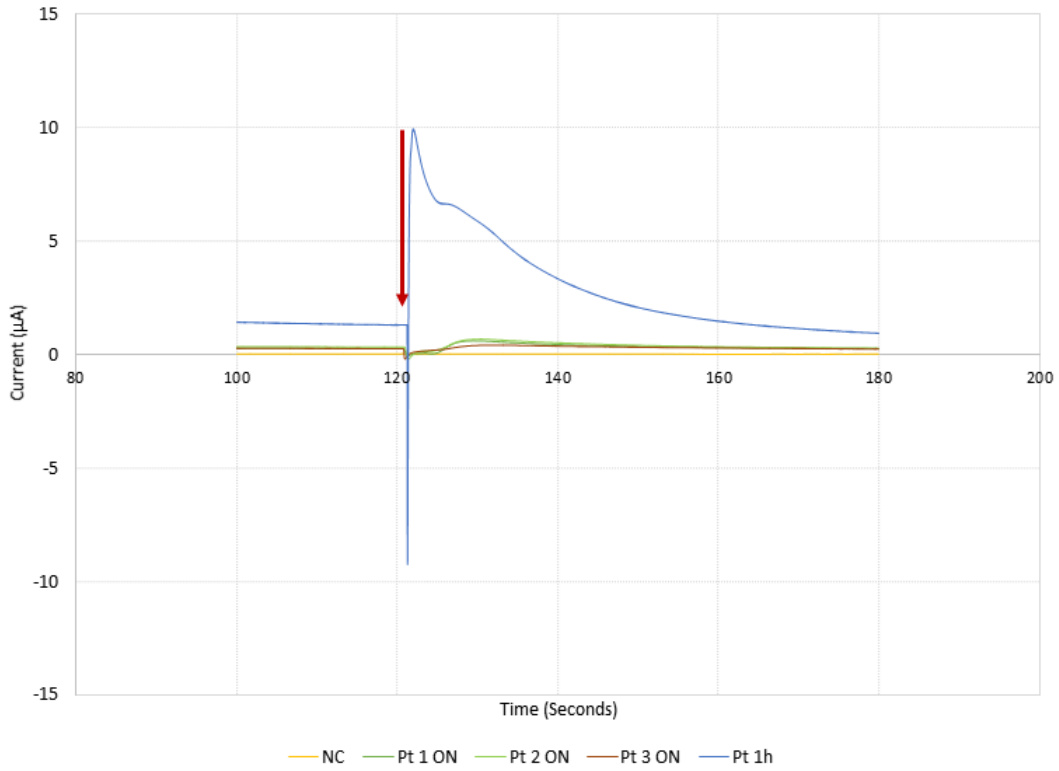

Figure 7.16: *Overnight incubation time (green, red, bright green) compared to one hour incubation time (blue) on platinum electrodes. The red arrow indications the time of the application of lactate.*

but also more successful compared to the current response from the overnight incubation time.

The same measurements were conducted with the new gold electrodes. The gold electrodes were prepared and exposed to an overnight incubation of the lactate oxidase solution. For the measurement, a 100 mM lactate solution was applied to the electrode and the current response after a potential of 500 mV was applied.

The resulting currents are presented in Figure 7.17. The yellow graph represents the negative control and the other two (grey and orange) are the current response of the electrodes exposed to an overnight incubation. No typical amperometric response was observed from the measurement of the gold electrodes. In addition, the negative control is higher than the positives which are indicative of contamination of the negative control electrode. Furthermore, upon the application of the lactate solution, the response is more negative than the baseline. The negative control also exhibits a sudden decrease in current after

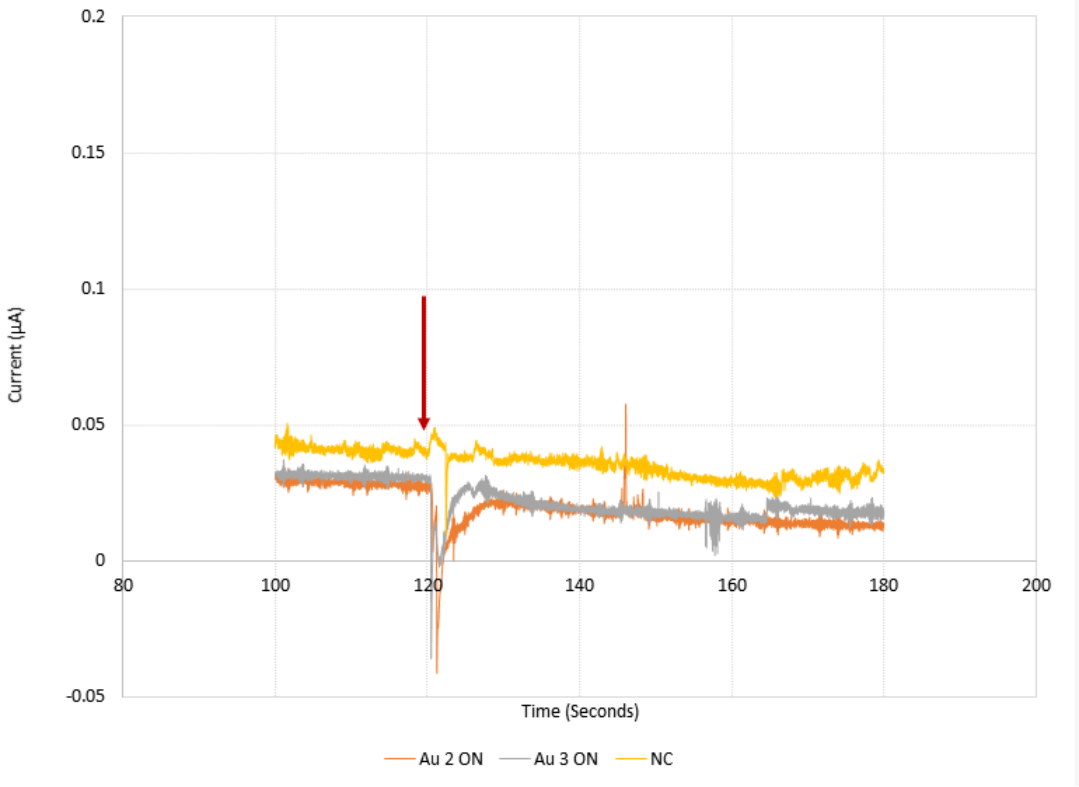

Figure 7.17: *Results of amperometric measurements of lactate using gold electrodes with immobilised lactate oxidase (One hour incubation time). The red arrow indications the time of the application of lactate.*

the application of the lactate solution. The overall currents obtained from all the measurements are between 0.025 and 0.05 μA; low compared to the current (0.2 μA) received from the lactate measurements presented in Figure 7.13.

These results lead to the conclusion that the immobilization of lactate oxidase onto gold electrodes overnight was not successful, which says that the high impedance obtained from the EIS measurements in Section 6.3.3 was due to the reagents accumulating on the surface of the working electrode.

The electrodes that were exposed to a one-hour incubation time were stored in PBS for two days after the measurements. The current response to lactate was measured again after the two days. The results for gold and platinum electrodes are shown in Figure 7.18 and Figure 7.19 respectively. In general, as also observed in the other measurement, platinum exhibits a higher current overall (10 μA) compared to gold (0.2 μA). Both electrodes, however, show a much smaller or no signal upon lactate application after two days of storage. Further improvements for the storage capabilities are required to develop a

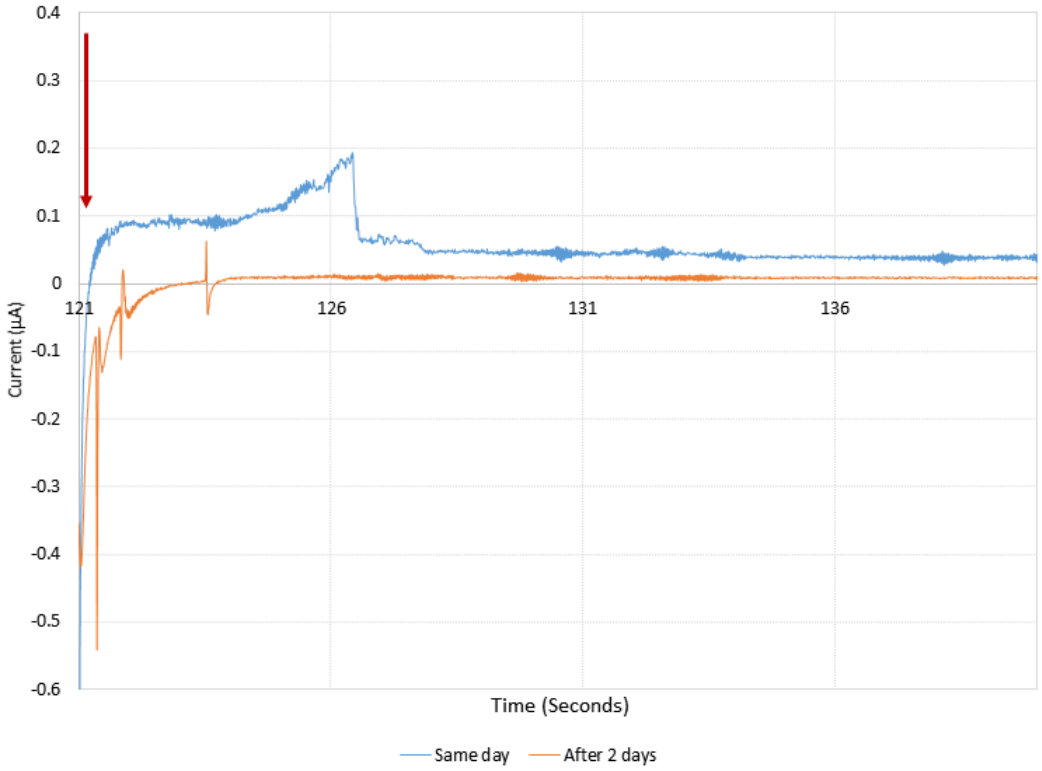

Figure 7.18: *Amperometric measurements of gold electrodes after 1 hour incubation and then after 2 days in PBS. The red arrow indications the time of the application of lactate.*

usable lactate sensor. This could be achieved by adding a layer of nafion as introduced in Section 4.3.1.

From these measurements, it can be concluded that no enzyme activity was found on the gold electrode after two days, but a current response was received from the platinum electrode after two days although it was lower than the current response measured on the same day of immobilisation. This is shown in Figure 7.19.

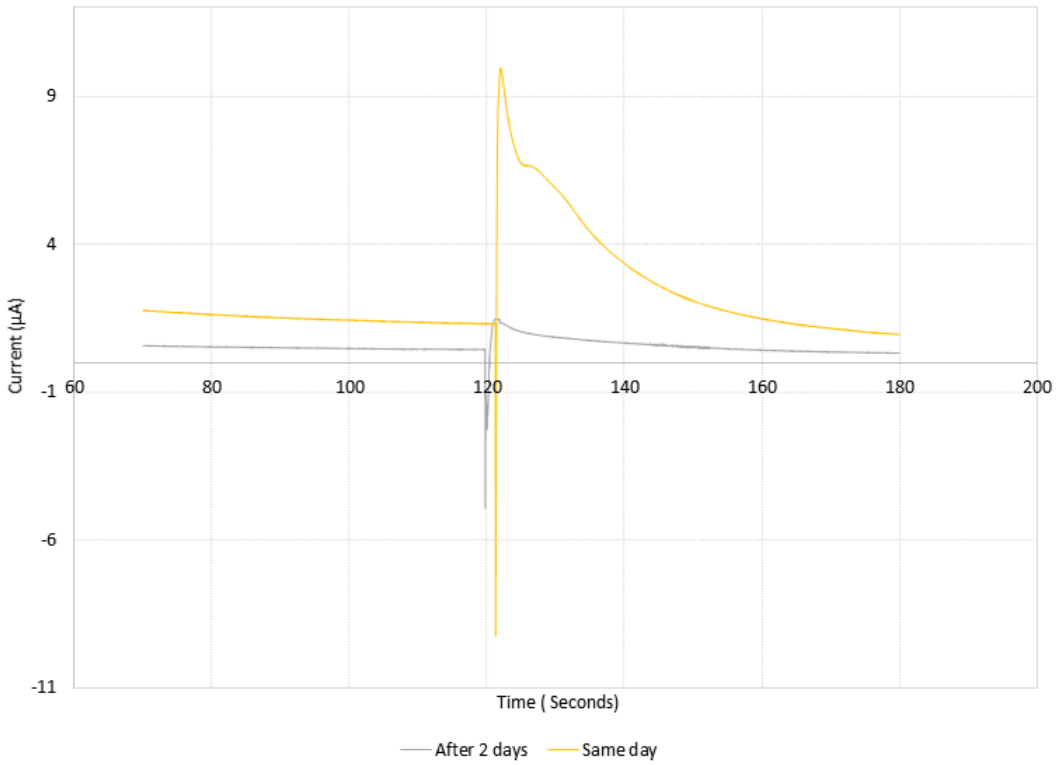

Figure 7.19: *Amperometric measurements with platinum electrodes after 1 hour incubation and then after 2 days in PBS. The red arrow indications the time of the application of lactate.*

7.4 Conclusions

In conclusion, higher currents were obtained from platinum electrodes during H_2O_2 and lactate measurements. One hour of incubation provided better amperometric results for both electrodes.

The amperometric response of the gold electrode exposed to an overnight incubation was indicative of inactive enzymes. After storing the electrodes in PBS for two days the current response from the platinum electrode was lower than the current received on the same day. However, this current was still higher than the current obtained from the measurements of the gold electrode on the same day of immobilisation.

Based on the results of the initial measurements, platinum is most likely to be more successful for the development of lactate sensor for foetal monitoring during birth.

8 Conclusions and future work

In this chapter, the findings of the previous chapters are summarised and overall conclusions are drawn. Additionally, future work is suggested to develop a new foetal monitoring device.

8.1 Conclusions

Although foetal monitoring has improved, there is a common agreement between professionals that more research work into new monitoring techniques needs to be done, as current methods are laborious, prone to errors and invasive [62, 63, 64]. The results and conclusions of this research are based on the aims and objectives laid out in section Section 1.3.

Firstly, the most appropriate measurand had to be identified and selected for further development of a novel foetal monitoring system. Lactate showed the most potential as a potential alternative measurand for intrapartum foetal monitoring, due to its ability to distinguish between different types of acidosis. In current clinical settings it is being measured alongside the pH value when performing foetal scalp blood sampling. It is however not used for decision-making yet.

Additionally, the different biosensor characteristics, such as sampling, recognition, immobilisation and transduction were reviewed for the ideal fit for a intrapartum foetal lactate sensor. Clinical specifications were provided by Dr. Fiona Denison, and Dr. Sarah Stock, expert clinicians dealing regularly with complex labours. Based on these specifications and after having reviewed the medical rationale for monitoring baby's blood during labour, a technical liter-

ature review was carried out in Chapter 4 on biosensing with a focus on lactate sensing.

For sampling, biofluid microneedles were identified to serve as a basis for the new sensor device due to its minimally invasive nature. The transduction method of amperometry was found to be the most common and was useful for this application since more than 90% of the publications reviewed for lactate sensing were based on amperometric measurements. Furthermore, lactate oxidase was identified as a recognition element because it does not require a co-enzyme as lactate dehydrogenase does. The means of immobilising the enzyme were explored and covalent bonding and crosslinking were found to hold the greatest potential because both provide a strong bond with the electrode surface to prevent leaching of the enzyme. The literature demonstrated that gold and platinum electrodes delivered reliable and sensitive results for lactate sensing, with many examples of these materials being successfully applied.
Based on the results of the technical literature review the new prototype sensor was designed, manufactured and tested based on the following three steps:

1. Electrode Fabrication
2. Immobilisation
3. Amperometric Measurements

For the electrode fabrication described in Section 5.4, commercial electrodes from the company DropSens were purchased to perform basic electrochemical measurements. The electrochemical surface area was found to be almost twice as large as the geometrical surface area. Microneedles were also purchased from MicroPoint and their compatibility with the electron beam evaporation process was proven. Using an improved masking method a three-electrode system was deposited onto a dummy substrate made from PMMA utilising the electron beam evaporator. A prototype sensor was successfully assembled using an adapter fabricated from standard FR4 copper printed circuit board.

The fourth aim of this project was the characterisation of the immobilisation protocols on different electrode surfaces. Two immobilisation methods, covalent bonding and crosslinking, were tested in Chapter 6. Initial measurements using cyclic voltammetry and amperometry showed that covalent bonding seems to hold greater potential for lactate oxidase immobilisation, as a greater current signal was obtained. With the focus on covalent bonding, the crosslinking reagents DTT and TCEP, which were adapted from standard immobilisation protocols, were compared and the results show that the immobilisation was successful with DTT but not with TCEP. Different incubation times of the enzyme solution on the electrode surface were tested and characterised using electrochemical impedance spectroscopy with the result that the one-hour incubation time provided larger impedance values.
Subsequent amperometric measurements also investigated different incubation times on the enzyme solution of the electrodes surface were explored and it was found that a one hour incubation time is sufficient. Furthermore, it was found, when testing electrode after storing them for two days, that the enzyme activity decreases over time. In addition, two different electrode materials, gold, and platinum, were compared throughout the above experiments.

Platinum electrodes provided a better a greater amperometric response and the immobilisation was more often successful. Based on the results obtained from this experiment, platinum is most likely to provide a good basis for the electrochemical lactate sensor.

The fifth aim, which was to characterise the performance of the resulting system, was achieved partially. Overall, several key steps have been taken towards the development of a lactate sensor for foetal monitoring, demonstrating that using platinum electrodes and covalent bonding based immobilisation using DTT give promising results with amperometric lactate measurements. Furthermore, a proof-of-principle of the manufacturing steps of the proposed system has been shown, demonstrating the possibility to utilise microneedles in this application. However, further, development is required to integrate these two advances.

This work provides background research and reviews in the field of lactate sensing and intrapartum foetal monitoring in order to improve current foetal monitoring during birth, which is laborious, invasive and prone to errors. By further developing the work carried out in this project as laid out in the following section, it may be possible to continuously monitor babies during birth. This may provide clearer and real-time data for a safer delivery of the baby.

8.2 Future Work

As this work presented preliminary results and proof of concept towards to the development of lactate sensor for foetal monitoring during birth, further work is required to establish a new sensor fulfilling the clinical requirements. There are three main courses for further work:

1. Development of immobilisation protocol
2. Fabrication of a microneedle electrode
3. Microneedle array fabrication.

Firstly, the covalent bonding immobilisation protocol requires further optimisation and characterisation utilising commercial platinum electrodes. Following that, calibration curves can be obtained in the required lactate concentration range (2 - 14 mM). The optimised immobilisation results on the commercial electrodes can be further characterised determining their sensitivity, selectivity, detection limit and response time. During the course of these experiments, the repeatability of the results can be shown. Additionally, measurements over a longer duration, such as 12 hours, have to be taken to ensure stable lactate detection over the length of labour. Finally, the functionalised commercial electrodes should be tested regarding their storage stability, storing them for a longer period and testing the enzyme activity regularly.
Secondly, the electrode fabrication can be optimised further and the repeatability should be ensured. This should be done first on the PMMA sheets. It

might be sensible to explore other metal deposition methods such as sputtering which exhibits less heat generation during the deposition process. The sensor fabricated on the PMMA sheet can be characterised electrochemically as described above. Once optimised, the fabrication protocol can be transferred to the microneedle array which then again should be electrochemically characterised. Amperometric measurements conducted utilising the commercial electrodes should be conducted on the fabricated microneedle electrodes for comparison.

Once a working lactate sensor has been developed successfully the measurements should be conducted using blood. Additionally, methods for preventing potential leaching should be explored. Possible materials such as nafion have been mentioned in the literature review [126]. In addition to the development of the lactate sensor utilising commercial microneedle arrays, possibilities for the fabrication of microneedle arrays can be explored. Common fabrication methods are laser micromachining [104], UV photolithography [105], micromolding [106], drawing lithography in combination with electroplating [116].

In conclusion, the literature review has shown that electrochemical *in vivo* lactate sensing has been achieved. Further improvement of the immobilisation process will most likely lead to a successful development of a lactate sensor based on commercial electrodes.

However, it remains to be proven, whether combining the electrochemical lactate sensor with microneedle arrays provide the ideal solution for foetal monitoring during birth.

References

[1] Bruno Carbonne, Kelly Pons, and Emeline Maisonneuve. Foetal scalp blood sampling during labour for pH and lactate measurements. *Best practice & research. Clinical obstetrics & gynaecology*, 30:62–67, jul 2015.

[2] D. M. F Gibb and S Arulkumaran. *Fetal Monitoring in practice*. Butterworth-Heinemann/Elsevier, Edinburgh, 3 edition, 2007.

[3] Robert V Ridenour, Ravi P Gada, Brian C Brost, and Brad S Karon. Comparison and validation of point of care lactate meters as a replacement for fetal pH measurement. *Clinical biochemistry*, 41(18): 1461–5, dec 2008.

[4] D Tuffnell, WL Haw, and K Wilkinson. How long does a fetal scalp blood sample take? *BJOG: An International Journal of Obstetrics and Gynaecology*, 113(3):332–334, mar 2006.

[5] Alexander Losch, Christian Kainz, Petra Kohlberger, Georg Heinze, Lukas Hefler, Johann Lahodny, and Clemens Tempfer. Influence on fetal blood pH when adding amniotic fluid: An in vitro model. *BJOG: An International Journal of Obstetrics and Gynaecology*, 110(5): 453–456, 2003.

[6] Ayesha M F Heinis, Marc E Spaanderman, Jacqueline M T Klein Gunnewiek, and Fred K Lotgering. Scalp blood lactate for intra-partum assessment of fetal metabolic acidosis. *Acta obstetricia et gynecologica Scandinavica*, 90(10):1107–14, oct 2011.

[7] Banica Florinel-Bariel. *Chemical Sensors and Biosensors*. John Wiley & Sons, Ltd, 2012.

[8] Matthew A. Cooper. *Label-free Biosensors,Techniques and applications*. Cambridge University Press, 2009.

[9] Kourosh Kalantar-zadeh. *Sensors An Introductory Course*. Springer, 2013.

[10] David A Armbruster and Terry Pry. Limit of blank, limit of detection and limit of quantitation. *The Clinical biochemist. Reviews*, 29(Suppl 1):S49–52, aug 2008.

[11] Christopher M. A. Brett and Ana Maria Oliveira Brett. *Electrochemistry Principles, Methods and Applications*. Oxford University Press, Oxford, UK, 1993.

[12] Www.porous-35.com. Electrochemical Cells and Potentiostats. URL `http://www.porous-35.com/electrochemistry-semiconductors-10.html`. Date accessed: 2017-04-15.

[13] Ki Sung Sohn, Seok Jae Oh, Eui Jin Kim, Jeong Min Gim, Nam Soo Kim, Yeong Seuk Kim, and Jong Won Kim. A unified potentiostat for electrochemical glucose sensors. *Transactions on Electrical and Electronic Materials*, 14(5):273–277, 2013.

[14] Arnaldo C. Pereira, Marina R. Aguiar, Alexandre Kisner, and Et Al. Novel lactate and pH biosensor for skin and sweat analysis based on single walled carbon nanotubes. *Sensors and Actuators B: Chemical*, 131(1):308–313, jan 2007.

[15] Hazhir Teymourian, Abdollah Salimi, and Rahman Hallaj. Low potential detection of NADH based on Fe_3O_4 nanoparticles/multiwalled carbon nanotubes composite: fabrication of integrated dehydrogenase-based lactate biosensor. *Biosensors & bioelectronics*, 33(1):60–8, mar 2012.

[16] Fouad Ghamouss, Sophie Ledru, Nadine Ruillé, Françoise Lantier, and Mohammed Boujtita. Bulk-modified modified screen-printing carbon electrodes with both lactate oxidase (LOD) and horseradish peroxide (HRP) for the determination of L-lactate in flow injection analysis mode. *Analytica chimica acta*, 570(2):158–64, jun 2006.

[17] Youngsam Yoon, Gil S Lee, Koangki Yoo, and Jeong-Bong Lee. Fabrication of a microneedle/CNT hierarchical micro/nano surface electrochemical sensor and its in-vitro glucose sensing characterization. *Sensors (Basel, Switzerland)*, 13(12):16672–81, jan 2013.

[18] Univeristy of Cambridge. Potential Step Voltammetry, . URL `http://www.ceb.cam.ac.uk/research/groups/rg-eme/teaching-notes/potential-step-voltammetry`. Date accessed: 2017-04-08.

[19] Derek Pletcher. *A First Course in Electrode Processes*. Royal Society of Chemistry, 2 edition, 2009.

[20] University of Cambridge. Linear Sweep and Cyclic Voltametry: The Principles, . URL `http://www.ceb.cam.ac.uk/research/groups/rg-eme/teaching-notes/linear-sweep-and-cyclic-voltametry-the-principles`. Date accessed: 2017-04-17.

[21] Sankha dip Das. Cyclic Voltammetry. URL `http://urrjaa.blogspot.co.uk/2013/08/cyclic-voltammetry-urrjaa-p0110-2013.html`. Date accessed: 2017-04-17.

[22] Vasiliki Fragkou, Yi Ge, Greg Steiner, Dom Freeman, Norbert Bartetzko, and Anthony P F Turner. Determination of the real surface area of a screen-printed electrode by chronocoulometry. *International Journal of Electrochemical Science*, 7(7):6214–6220, 2012.

[23] Naiara Hernández-Ibáñez, Leticia García-Cruz, Vicente Montiel, Christopher W Foster, Craig E Banks, and Jesús Iniesta. Electrochemical lactate biosensor based upon chitosan/carbon nanotubes modified screen-printed graphite electrodes for the

determination of lactate in embryonic cell cultures. *Biosensors & bioelectronics*, 77:1168–74, mar 2016. URL `http://www.sciencedirect.com/science/article/pii/S0956566315305558`.

[24] S. Suman, Rahul Singhal, Amit L. Sharma, B.D. Malthotra, and C.S. Pundir. Development of a lactate biosensor based on conducting copolymer bound lactate oxidase. *Sensors and Actuators B: Chemical*, 107(2):768–772, jun 2005.

[25] F. Palmisano, R. Rizzi, D. Centonze, and P.G. Zambonin. Simultaneous monitoring of glucose and lactate by an interference and cross-talk free dual electrode amperometric biosensor based on electropolymerized thin films. *Biosensors and Bioelectronics*, 15(9-10):531–539, nov 2000.

[26] John E. Baur. *Diffusion Coefficients*, volume 2334. Elsevier B.V., 1987.

[27] Diogo Ayres-de Campos and Sabaratnam Arulkumaran. FIGO consensus guidelines on intrapartum fetal monitoring: Physiology of fetal oxygenation and the main goals of intrapartum fetal monitoring. 2015.

[28] B Marsh and A Walker. *Oxford Handbook of Midwifery (Oxford handbook series)*. New York: Oxford University Press, USA, 2 edition, 2011.

[29] M Holzmann, S Cnattingius, and L Nordström. Lactate production as a response to intrapartum hypoxia in the growth-restricted fetus. *BJOG : an international journal of obstetrics and gynaecology*, 119(10): 1265–9, sep 2012.

[30] Mitchell Fry. *Essential Biochemistry for Medicine*. John Wiley & Sons, Ltd, 1 edition, 2010.

[31] David Hames and Nigel Hooper. *Biochemistry*. Taylor & Francis Group, Abingdon, 3 edition, 2005.

[32] Nature Education. Comparing basic eukaryotic and prokaryotic differences, 2010. URL `http://www.nature.com/scitable/topicpage/what-is-a-cell-14023083`. Date accessed: 2016-09-01.

[33] S Arulkumaran, L Impey, K Hayes, and S Collins. *Oxford Handbook of Obstetrics and Gynaecology*. New York: Oxford University Press, New York, 2 edition, 2008.

[34] L Bennet, L Booth, and A J Gunn. Potential biomarkers for hypoxic-ischemic encephalopathy. *Seminars in fetal & neonatal medicine*, 15(5):253–60, oct 2010.

[35] National Institute for Health and Care Excellence. Intrapartum care: Care of healthy women and their babies during childbirth., 2014.

[36] Dorothee Grieshaber, Robert MacKenzie, Janos Vörös, and Erik Reimhult. Electrochemical Biosensors - Sensor Principles and Architectures. *Sensors*, 8(3):1400–1458, mar 2008.

[37] M Rei, D Ayres-de Campos, and J Bernardes. Neurological damage arising from intrapartum hypoxia/acidosis. *Best practice & research. Clinical obstetrics & gynaecology*, 30:79–86, jun 2015.

[38] Diogo Ayres-de Campos, Catherine Y. Spong, and Edwin Chandraharan. FIGO consensus guidelines on intrapartum fetal monitoring: Cardiotocography. *International Journal of Gynecology & Obstetrics*, 131(1):13–24, oct 2015.

[39] Office for National Statistics. Birth characteristics. URL `https://www.ons.gov.uk/peoplepopulationandcommunity/birthsdeathsandmarriages/livebirths/datasets/birthcharacteristicsinenglandandwales`. Date accessed: 2017-10-18.

[40] Office for National Statistics. Live births, neonatal and post neonatal deaths by selected causes mentioned on death certificate, England and Wales, 2001 to 2015, 2017. URL `https://www.ons.gov.uk/peoplepopulationandcommunity/birthsdeathsandmarriages/deaths/adhocs/006955livebirthsneonatalandpostneonataldeathsbyselectedcausesmentionedondeathcertificateenglandand\wales20%5C01to2015`. Date accessed: 2017-10-18.

[41] Medical Dictionary. auscultation. URL `https://medical-dictionary.thefreedictionary.com/auscultation`. Date accessed: 2017-11-12.

[42] Howard Herrell. History of Fetal Monitoring. URL `http://www.ob-efm.com/efm-basics/history/`. Date accessed: 2017-08-02.

[43] Obs Gynae & Midwifery News. Fetal Scalp Blood Sampling History, Present And Future, 2007. URL `http://www.ogpnews.com/2007/09/fetal-scalp-blood-sampling-history-present-and-future/363`. Date accessed: 2017-08-02.

[44] Ana Pinas and Edwin Chandraharan. Continuous cardiotocography during labour: Analysis, classification and management. *Best Practice & Research Clinical Obstetrics & Gynaecology*, 30:33–47, jun 2015.

[45] T Kawakita, UM Reddy, HJ Landy, SN Iqbal, C-C Huang, and KL Grantz. Neonatal complications associated with use of fetal scalp electrode: a retrospective study. *BJOG: An International Journal of Obstetrics & Gynaecology*, 123(11):1797–1803, 2016.

[46] Naohiro Kanayama and Masatsugu Niwayama. Examiner's finger-mounted fetal tissue oximetry. *Journal of biomedical optics*, 19 (6):067008, 2014.

[47] M J Nijland, U Shankar, V Iyer, and M G Ross. Assessment of fetal scalp oxygen saturation determination in the sheep by transmission

pulse oximetry. *American journal of obstetrics and gynecology*, 183(6): 1549–53, dec 2000.

[48] Andreas Nonnenmacher, Hartmut Hopp, and Joachim Dudenhausen. Predictive value of pulse oximetry for the development of fetal acidosis. *J. Perinat. Med*, 38:83–86, 2010.

[49] Christine E East, Lisa Begg, Paul B Colditz, and Rosalind Lau. Fetal pulse oximetry for fetal assessment in labour. *The Cochrane database of systematic reviews*, 10:CD004075, jan 2014.

[50] Isis Amer-Wahlin and Anneke Kwee. Combined cardiotocographic and ST event analysis: A review. *Best practice & research. Clinical obstetrics & gynaecology*, 30:48–61, jun 2015.

[51] Tamara L. Turnbull, Ben Willem J. Mol, Geoff Matthews, Chris Wilkinson, Edwin Chandraharan, and Sabrina Kuah. Does ST analysis have a place in electronic fetal monitoring? *The Journal of Maternal-Fetal & Neonatal Medicine*, 30(5):520–524, mar 2017.

[52] Gianluca Straface, Giovanni Scambia, and Vincenzo Zanardo. Does ST analysis of fetal ECG reduce cesarean section rate for fetal distress? *The Journal of Maternal-Fetal & Neonatal Medicine*, 30(15):1799–1802, aug 2017.

[53] Michelle EMH Westerhuis, Karel GM Moons, Erik van Beek, Saskia M Bijvoet, Addy P Drogtrop, Herman P van Geijn, Jan MM van Lith, Ben WJ Mol, Jan G Nijhuis, S Guid Oei, Martina M Porath, Robbert JP Rijnders, Nico WE Schuitemaker, Ingeborg van der Tweel, Gerard HA Visser, Christine Willekes, and Anneke Kwee. A randomised clinical trial on cardiotocography plus fetal blood sampling versus cardiotocography plus ST-analysis of the fetal electrocardiogram (STAN®) for intrapartum monitoring. *BMC Pregnancy and Childbirth*, 7(1):13, jul 2007.

[54] M. A. Belfort, G. R. Saade, E. Thom, S.C. Blackwell, U. M. Reddy, J. M Thorp, T. T. N. Tita, R. S. Miller, A.M. Peaseman, D. S. McKenna, E. K. S. Chien, D. J. Rouse, R. S. Gibbs, Y. Y. El-Sayed, Y. Sorokin, S. N. Caritis, and J. P. VanDorsten. A Randomized Trial of Intrapartum Fetal ECG ST-Segment Analysis. *N Engl J Med*, 7373 (13):632–41, 2015.

[55] Neoventa. goldtrace. URL `http://www.neoventa.com/products/goldtrace/`. Date accessed: 2017-09-12.

[56] Mom.girlstalkinsmack. Scalp electrode. URL `http://mom.girlstalkinsmack.com/health/labor-and-birth---1st-stage-of-labor-(part-4)---monitoring-during-labor.aspx`. Date accessed: 2016-09-01.

[57] Susan Bewley, Tracey Cooper, Sarah Fishburn, Helen Ford, Kevin Ives, Mike Lane, Nuala Lucas, Bryony Strachan, Derek Tuffnell, Kylie

Watson, and Catherine Williams. Intrapartum Care Care of healthy women and their babies during childbirth Clinical. Technical report, National Collaborating Centre for Women's and Children's Health, 2014.

[58] K. Ojala, M. Vääräsmäki, K. Mäkikallio, M. Valkama, and A. Tekay. A comparison of intrapartum automated fetal electrocardiography and conventional cardiotocography - A randomised controlled study. *BJOG: An International Journal of Obstetrics and Gynaecology*, 113 (4):419–423, 2006.

[59] Rocketmedical. Rocket FBS Fetal Blood Sampling Kit with Sampling Wand, . URL `http://sales.rocketmedical.com/rocket-fbs-fetal-blood-sampling-kit-amnilume-and-sampling-wand-3-x-long-hep-tubes-angled`. Date accessed: 2016-09-01.

[60] Rocketmedical. Seven Key Steps to improving sample quality. Technical report, . URL `http://sales.rocketmedical.com/media/attachment/file/r/o/rocket_fbs_seven_key_steps.pdf`. Date accessed: 2016-10-15.

[61] D Mowbray, Lennart Nordström, WN Ofunne, and S Akhtar. Is it Time for UK Obstetricians to Accept Fetal Scalp Lactate as an Alternative to Scalp pH? *Royal College of Obstetricuans and Gynaecologists*, (47):1–6, 2015.

[62] G S Sykes, P M Molloy, P Johnson, G M Stirrat, and a C Turnbull. Fetal distress and the condition of newborn infants. *British medical journal (Clinical research ed.)*, 287(October):943–945, 1983.

[63] Amita A Mahendru and Christoph C Lees. Is intrapartum fetal blood sampling a gold standard diagnostic tool for fetal distress? *European journal of obstetrics, gynecology, and reproductive biology*, 156(2):137–9, jun 2011.

[64] Yvonne M O'Brien and Deirdre J Murphy. The reliability of foetal blood sampling as a test of foetal acidosis in labour. *European journal of obstetrics, gynecology, and reproductive biology*, 167(2):142–5, apr 2013.

[65] Maria Bitsori. 2. The development of renal function. In *Essentials in Pediatric Urology*, volume 37, pages 9–20. Essentials in Pediatric Urology, 2012.

[66] Jan S Jørgensen and Tom Weber. Fetal scalp blood sampling in labor–a review. *Acta obstetricia et gynecologica Scandinavica*, 93(6): 548–55, jun 2014.

[67] Per Olofsson. Determination of base excess in umbilical cord blood at birth: accessory or excess? *American Journal of Obstetrics & Gynecology*, 2015.

[68] Per Olofsson. Current status of intrapartum fetal monitoring: cardiotocography versus cardiotocography + ST analysis of the fetal ECG. *European Journal of Obstetrics & Gynecology and Reproductive Biology*, 110:S113–S118, sep 2003.

[69] James A. Low, Brian G. Lindsay, and E.Jane Derrick. Threshold of metabolic acidosis associated with newborn complications. *American Journal of Obstetrics and Gynecology*, 177(6):1391–1394, 1997.

[70] Ayesha M F Heinis, Jacqueline Dinnissen, Marc E A Spaanderman, Fred K Lotgering, and Jacqueline M T Klein Gunnewiek. Comparison of two point-of-care testing (POCT) devices for fetal lactate during labor. *Clinical chemistry and laboratory medicine*, 50(1):89–93, jan 2012.

[71] Kerstin Kruger, B. Hallberg, M. Blennow, M. Kublickas, and M. Westgren. Predictive value of fetal scalp blood lactate concentration and pH as markers of neurologic disability. *American Journal of Obstetrics and Gynecology*, 181(5):1072–1078, nov 1999.

[72] Lena Liljeström, Anna-Karin Wikström, Ulf Hanson, Helena Akerud, and Maria Jonsson. Evaluation of the discrepancy between pH and lactate in combined fetal scalp blood sampling. *Acta obstetricia et gynecologica Scandinavica*, 90(10):1088–93, oct 2011.

[73] Christine E East, Stefan C Kane, Mary-Ann Davey, C Omar Kamlin, and Shaun P Brennecke. Protocol for a randomised controlled trial of fetal scalp blood lactate measurement to reduce caesarean sections during labour: the Flamingo trial [ACTRN12611000172909]. *BMC pregnancy and childbirth*, 15(1):285, jan 2015.

[74] Malin Holzmann and Lennart Nordström. Follow-up national survey (Sweden) of routines for intrapartum fetal surveillance. *Acta Obstetricia et Gynecologica*, 89:712–714, 2010.

[75] Christina Rørbye, Anette Perslev, and Carsten Nickelsen. Lactate versus pH levels in fetal scalp blood during labor - using the Lactate Scout System. *The journal of maternal-fetal & neonatal medicine : the official journal of the European Association of Perinatal Medicine, the Federation of Asia and Oceania Perinatal Societies, the International Society of Perinatal Obstetricians*, pages 1–5, jun 2015.

[76] E Wiberg-Itzel, C Lipponer, M Norman, A Herbst, D Prebensen, A Hansson, A-L Bryngelsson, M Christoffersson, M Sennström, U-B Wennerholm, and L Nordström. Determination of pH or lactate in fetal scalp blood in management of intrapartum fetal distress: randomised controlled multicentre trial. *BMJ (Clinical research ed.)*, 336(7656): 1284–7, jun 2008.

[77] Adolf Faller and Michael Schuenke. *Der Koerper des Menschen Einfuehrung in Bau und Funktion des Menschen.* Georg Thieme Verlag, Stuttgart, 15 edition, 2008.

[78] Jim Waterhouse, Marina Sawdon, and Emrys Kirkman. Capillary dynamics and the interstitial fluid–lymphatic system. *Anaesthesia & Intensive Care Medicine*, 17(2):106–111, feb 2016.

[79] Jaep De Boer, Hillie Plijter-groendijk, Klaas R Visser, Gerrit A Mook, and Jakob Korf. Continuous monitoring of lactate during exercise in humans using subcutaneous and transcutaneous microdialysis. *Eur J Appl Physiol*, pages 281–286, 1994.

[80] P A Jansson, A L Krogstad, and P Lönnroth. Microdialysis measurements in skin: evidence for significant lactate release in healthy humans. *The American journal of physiology*, 271(1 Pt 1):E138–42, 1996.

[81] M Ellmer, L Schaupp, Z Trajanoski, G Jobst, I Moser, G Urban, F Skrabal, and P Wach. Continuous measurement of subcutaneous lactate concentration during exercise by combining open-flow microperfusion and thin-film lactate sensors. *Biosensors and Bioelectronics*, 13(9):1007–1013, oct 1998.

[82] Petros Kopterides, Maria Theodorakopoulou, Ioannis Ilias, Nikitas Nikitas, Frantzeska Frantzeskaki, Dimitra Argyro Vassiliadi, Apostolos Armaganidis, and Ioanna Dimopoulou. Interrelationship between blood and tissue lactate in a general intensive care unit: A subcutaneous adipose tissue microdialysis study on 162 critically ill patients. *Journal of Critical Care*, 27(6):742.e9–742.e18, 2012.

[83] Zhaohui Li and Zhanfeng Cui. Application of microdialysis in tissue engineering monitoring. *Progress in Natural Science*, 18(5):503–511, 2008.

[84] T S Shippenberg and A C Thompson. Overview of microdialysis. *Current protocols in neuroscience / editorial board, Jacqueline N. Crawley ... [et al.]*, Chapter 7:Unit7.1, may 2001.

[85] P.S. Petrou, I. Moser, and G. Jobst. Microdevice with integrated dialysis probe and biosensor array for continuous multi-analyte monitoring. *Biosensors and Bioelectronics*, 18(5-6):613–619, may 2003.

[86] T Vering, S Adam, H Drewer, C Dumschat, R Steinkuhl, A Schulze, E G Siegel, and M Knoll. Wearable microdialysis system for continuous in vivo monitoring of glucose. *The Analyst*, 123(7):1605–9, 1998.

[87] D.G. Pijanowska, A.J. Sprenkels, H. van der Linden, W. Olthuis, P. Bergveld, and A. van den Berg. A flow-through potentiometric sensor for an integrated microdialysis system. *Sensors and Actuators B: Chemical*, 103(1-2):350–355, sep 2004.

[88] CMA Microdialysis AB. Products for microdialysis research. URL `http://www.harvardapparatus.com/media/harvard/pdf/2016_CMA_Catalog.pdf`. Date accessed: 2017-09-18.

[89] Ryoji Kurita, Katsuyoshi Hayashi, Xu Fan, Katsunobu Yamamoto, Takeshi Kato, and Osamu Niwa. Microfluidic device integrated with

pre-reactor and dual enzyme-modified microelectrodes for monitoring in vivo glucose and lactate. *Sensors and Actuators B: Chemical*, 87(2): 296–303, dec 2002.

[90] Jannik Kruse Nielsen, Christian Born Djurhuus, Claus Højbjerg Gravholt, Andreas Christiansen Carus, Jacob Granild-Jensen, Hans Ørskov, and Jens Sandahl Christiansen. Continuous glucose monitoring in interstitial subcutaneous adipose tissue and skeletal muscle reflects excursions in cerebral cortex. *Diabetes*, 54(6):1635–1639, 2005.

[91] R F Donnelly, Raj Singh, Ryan F Donnelly, Thakur Raghu, and A David Woolfson. Microneedle-based drug delivery systems: Microfabrication, drug delivery, and safety. *Drug Delivery*, 17(4): 187–207, 2010.

[92] Han J G E Gardeniers, Regina Luttge, Erwin J W Berenschot, Meint J. De Boer, Shuki Y. Yeshurun, Meir Hefetz, Ronny Van't Oever, and Albert Van Den Berg. Silicon micromachined hollow microneedles for transdermal liquid transport. *Journal of Microelectromechanical Systems*, 12(6):855–862, 2003.

[93] Harvinder S. Gill and Mark R. Prausnitz. Coated microneedles for transdermal delivery. *Journal of Controlled Release*, 117(2):227–237, 2007.

[94] Jeong W. Lee, Jung-Hwan Park, and Mark R. Prausnitz. Dissolving microneedles for transdermal drug delivery. *Biomaterials*, 29(13): 2113–2124, 2008.

[95] Jung-Hwan Park, Mark G. Allen, and Mark R. Prausnitz. Biodegradable polymer microneedles: Fabrication, mechanics and transdermal drug delivery. *Journal of Controlled Release*, 104(1):51–66, 2005.

[96] Yeu-Chun Kim, Jung-Hwan Park, and Mark R. Prausnitz. Microneedles for drug and vaccine delivery. *Advanced Drug Delivery Reviews*, 64(14):1547–1568, 2012.

[97] Ai Ling Teo, Christopher Shearwood, Kian Chye Ng, Jia Lu, and Shabbir Moochhala. Transdermal microneedles for drug delivery applications. *Materials Science and Engineering: B*, 132(1):151–154, 2006.

[98] Z Ali, Eb Türeyen, Y Karpat, and M Çakmakcı. Fabrication of Polymer Micro Needles for Transdermal Drug Delivery System Using DLP Based Projection Stereo-lithography. *Procedia CIRP*, 42:87–90, 2016.

[99] Jaspreet Singh Kochhar, Wei Jiang Goh, Sui Yung Chan, and Lifeng Kang. A simple method of microneedle array fabrication for transdermal drug delivery. *Drug Devand Ind Pharm*, 39(2):1–11, 2012.

[100] Yuya Nishinaka, Rina Jun, Gunawan Setia Prihandana, and Et Al. Fabrication of Polymer Microneedle Electrodes Coated with

Nanoporous Parylene. *Japanese Journal of Applied Physics*, 52(6S): 06GL10, jun 2013.

[101] K B Vinayakumar, G M Hegde, M M Nayak, N S Dinesh, and K Rajanna. Fabrication and characterization of gold coated hollow silicon microneedle array for drug delivery. *Microelectronic Engineering*, 128:12–18, 2014.

[102] Joseph Wang, Maria Pedrero, Henning Sakslund, Ole Hammerich, and Jose Pingarron. Electrochemical activation of screen-printed carbon strips. *The Analyst*, 121(3):345, jan 1996.

[103] Po Chun Wang, Seung Joon Paik, Seong Hyok Kim, and Mark G. Allen. Hypodermic-needle-like hollow polymer microneedle array: Fabrication and characterization. *Journal of Microelectromechanical Systems*, 23(4):991–998, 2014.

[104] Po Chun Wang, Seung Joon Paik, Shuodan Chen, Swaminathan Rajaraman, Seong Hyok Kim, and Mark G. Allen. Fabrication and characterization of polymer hollow microneedle array using UV lithography into micromolds. *Journal of Microelectromechanical Systems*, 22(5):1041–1053, 2013.

[105] Zhuoqing Yang, Yi Zhang, Toshihiro Itoh, and Ryutaro Maeda. New Fabrication Method of Three-Electrode System on Cylindrical Capillary Surface as a Flexible Implantable Microneedle. *Surface Review and Letters*, 20(3&4), aug 2013.

[106] Jun Zhu, Qi Shen, Ying Cao, Xiang Chen, and Xiaolin Zhao. The fabrication and property of a novel coated out-of-plane microneedle arrays. *Microsystem Technologies*, 22:143–149, 2016.

[107] Angela Longo, Lucanos Marsilio Strambini, Letizia Ventrelli, Giuseppe Barillaro, and Università Pisa. Silicon Microneedles for Transdermal Applications by Electrochemical Micromachining Technology. *IEEE*, pages 7–9, 2014.

[108] M. Suzuki, T. Sawa, T. Takahashi, and S. Aoyagi. Ultrafine three-dimensional (3D) laser lithographic fabrication of microneedle and its application to painless insertion and blood sampling inspired by mosquito. *IEEE International Conference on Intelligent Robots and Systems*, 2015-Decem:2748–2753, 2015.

[109] Natalia Vasylieva, Stéphane Marinesco, Daniel Barbier, and Andrei Sabac. Silicon/SU8 multi-electrode micro-needle for in vivo neurochemical monitoring. *Biosensors and Bioelectronics*, 72:148–155, 2015.

[110] Joshua Ray Windmiller, Nandi Zhou, Min-Chieh Chuang, Gabriela Valdés-Ramírez, Padmanabhan Santhosh, Philip R Miller, Roger Narayan, and Joseph Wang. Microneedle array-based carbon paste amperometric sensors and biosensors. *The Analyst*, 136(9):1846–51, 2011.

[111] Sunaina Indermun, Regina Luttge, Yahya E Choonara, Pradeep Kumar, Lisa C Du Toit, Girish Modi, and Viness Pillay. Current advances in the fabrication of microneedles for transdermal delivery. *Journal of Controlled Release*, 185:130–138, 2014.

[112] Sean P Sullivan, Dimitrios G Koutsonanos, Maria Del Pilar Martin, Jeong Woo Lee, Vladimir Zarnitsyn, Seong-O Choi, Niren Murthy, Richard W Compans, Ioanna Skountzou, and Mark R Prausnitz. Dissolving polymer microneedle patches for influenza vaccination. *Nature medicine*, 16(8):915–920, 2010.

[113] Harvinder S Gill, Donald D Denson, Brett A Burris, and Mark R Prausnitz. Effect of microneedle design on pain in human subjects. *Clin J Pain*, 24(7):585–594, 2008.

[114] Suzanne M. Bal, Julia Caussin, Stan Pavel, and Joke A. Bouwstra. In vivo assessment of safety of microneedle arrays in human skin. *European Journal of Pharmaceutical Sciences*, 35(3):193–202, 2008.

[115] Shawn P Davis, Benjamin J Landis, Zachary H Adams, Mark G Allen, and Mark R Prausnitz. Insertion of microneedles into skin: measurement and prediction of insertion force and needle fracture force. *Journal of Biomechanics*, 37(8):1155–1163, 2004.

[116] Cheng Guo Li, Chang Yeol Lee, Kwang Lee, and Hyungil Jung. An optimized hollow microneedle for minimally invasive blood extraction. *Biomedical Microdevices*, 15(1):17–25, feb 2013.

[117] Koen van der Maaden, Wim Jiskoot, and Joke Bouwstra. Microneedle technologies for (trans)dermal drug and vaccine delivery. *Journal of Controlled Release*, 161(2):645–655, 2012.

[118] Liam P. Andrus, Rachel Unruh, Natalie A. Wisniewski, and Michael J. McShane. Characterization of lactate sensors based on lactate oxidase and palladium benzoporphyrin immobilized in hydrogels. *Biosensors*, 5 (3):398–416, 2015.

[119] Sawsen Azzouzi, Lucian Rotariu, Ana M Benito, Wolfgang K Maser, Mounir Ben Ali, and Camelia Bala. A novel amperometric biosensor based on gold nanoparticles anchored on reduced graphene oxide for sensitive detection of l-lactate tumor biomarker. *Biosensors & bioelectronics*, 69:280–6, jul 2015.

[120] Liza Rassaei, Wouter Olthuis, Seiya Tsujimura, Ernst J R Sudhölter, and Albert van den Berg. Lactate biosensors: current status and outlook. *Analytical and bioanalytical chemistry*, 406(1):123–37, jan 2014.

[121] Dorothea Pfeiffer, Barbara Möller, Norbert Klimes, Jan Szeponik, and Sylvio Fischer. Amperometric lactate oxidase catheter for real-time lactate monitoring based on thin film technology. *Biosensors and Bioelectronics*, 12(6):539–550, jan 1997.

[122] Lyudmyla V Shkotova, Nataliia Y Piechniakova, Oleksandr L Kukla, and Sergei V Dzyadevych. Thin-film amperometric multibiosensor for simultaneous determination of lactate and glucose in wine. *Food chemistry*, 197(Pt A):972–8, apr 2016.

[123] Kavita Rathee, Vikas Dhull, Rekha Dhull, and Sandeep Singh. Biosensors based on electrochemical lactate detection: A comprehensive review. *Biochemistry and Biophysics Reports*, 5:35–54, 2016.

[124] Pedro J Lamas-Ardisana, Oscar A Loaiza, Larraitz Añorga, Elena Jubete, Maryam Borghei, Virginia Ruiz, Estibalitz Ochoteco, Germán Cabañero, and Hans J Grande. Disposable amperometric biosensor based on lactate oxidase immobilised on platinum nanoparticle-decorated carbon nanofiber and poly(diallyldimethylammonium chloride) films. *Biosensors & bioelectronics*, 56:345–51, jun 2014.

[125] Roger C H Kwan, Phoebe Y T Hon, Karen K W Mak, and Reinhard Renneberg. Amperometric determination of lactate with novel trienzyme/poly(carbamoyl) sulfonate hydrogel-based sensor. *Biosensors & bioelectronics*, 19(12):1745–52, jul 2004.

[126] Takeshi Shimomura, Touru Sumiya, Masatoshi Ono, Tetsuji Ito, and Taka-aki Hanaoka. Amperometric L-lactate biosensor based on screen-printed carbon electrode containing cobalt phthalocyanine, coated with lactate oxidase-mesoporous silica conjugate layer. *Analytica chimica acta*, 714:114–20, feb 2012.

[127] Qingling Yang, Plamen Atanasov, and Ebtisam Wilkins. Needle-type lactate biosensor. This paper was presented at the Fifth World Congress on Biosensors, Berlin, Germany, 3–5 June 1998.1. *Biosensors and Bioelectronics*, 14(2):203–210, feb 1999.

[128] Xin Wei, Maogen Zhang, and Waldemar Gorski. Coupling the lactate oxidase to electrodes by ionotropic gelation of biopolymer. *Analytical Chemistry*, 75(9):2060–2064, 2003.

[129] Siwei Ma, Xiaohui Zhang, Qingliang Liao, Hanshuo Liu, Yunhua Huang, Yu Song, Yanguang Zhao, and Yue Zhang. Enzymatic lactic acid sensing by In-doped ZnO nanowires functionalized AlGaAs/GaAs high electron mobility transistor. *Sensors and Actuators B: Chemical*, 212:41–46, jun 2015.

[130] Jacob M. Goran, Jennifer L. Lyon, and Keith J. Stevenson. Amperometric detection of l-lactate using nitrogen-doped carbon nanotubes modified with lactate oxidase. *Analytical Chemistry*, 83(21): 8123–8129, 2011.

[131] Keith B Male, Sabahudin Hrapovic, and John H T Luong. Electrochemically-assisted deposition of oxidases on platinum nanoparticle/multi-walled carbon nanotube-modified electrodes. *The Analyst*, 132(12):1254–1261, 2007.

[132] Jiadong Huang, Jing Li, Yu Yang, Xinsheng Wang, Baoyan Wu, Jun-ichi Anzai, Tetsuo Osa, and Qiang Chen. Development of an amperometric l-lactate biosensor based on l-lactate oxidase immobilized through silica sol–gel film on multi-walled carbon nanotubes/platinum nanoparticle modified glassy carbon electrode. *Materials Science and Engineering: C*, 28(7):1070–1075, aug 2008.

[133] Chia I. Li, Yi Hua Lin, Cheng Ling Shih, Jeng Pyng Tsaur, and Lai Kwan Chau. Sol-gel encapsulation of lactate dehydrogenase for optical sensing of L-lactate. *Biosensors and Bioelectronics*, 17(4): 323–330, 2002.

[134] M M Rahman, Muhammad J A Shiddiky, Md Aminur Rahman, and Yoon-Bo Shim. A lactate biosensor based on lactate dehydrogenase/nictotinamide adenine dinucleotide (oxidized form) immobilized on a conducting polymer/multiwall carbon nanotube composite film. *Analytical biochemistry*, 384(1):159–65, jan 2009.

[135] Pablo Fanjul-Bolado, David Hernández-Santos, Pedro José Lamas-Ardisana, Alberto Martín-Pernía, and Agustín Costa-García. Electrochemical characterization of screen-printed and conventional carbon paste electrodes. *Electrochimica Acta*, 53(10):3635–3642, apr 2008.

[136] Xia Cai, Jilin Yan, Haihong Chu, Meisheng Wu, and Yifeng Tu. An exercise degree monitoring biosensor based on electrochemiluminescent detection of lactate in sweat. *Sensors and Actuators B: Chemical*, 143 (2):655–659, jan 2010.

[137] Xiaojing Liu and Weihong Tan. Development of an Optical Fiber Lactate Sensor. *Mikrochimica Acta*, 131:129–135, 1999.

[138] Xin Ting Zheng, Hong Bin Yang, and Chang Ming Li. Optical detection of single cell lactate release for cancer metabolic analysis. *Analytical Chemistry*, 82(12):5082–5087, 2010.

[139] Fisher Science. Material Safety Data Sheet Luminol, 1997. URL `https://fscimage.fishersci.com/msds/30356.htm`. Date accessed:2017-08-28.

[140] M Albareda-Sirvent and A.L Hart. Preliminary estimates of lactic and malic acid in wine using electrodes printed from inks containing sol–gel precursors. *Sensors and Actuators B: Chemical*, 87(1):73–81, nov 2002.

[141] Sandra Perez and Esteve Fabregas. Amperometric bienzymatic biosensor for l-lactate analysis in wine and beer samples. *The Analyst*, 137(16):3854, 2012.

[142] Marcelo Ricardo Romero, Facundo Ahumada, Fernando Garay, and Ana M Baruzzi. Amperometric biosensor for direct blood lactate detection. *Analytical chemistry*, 82(13):5568–72, jul 2010.

[143] Kyoko Hibi, Kengo Hatanaka, Mai Takase, Huifeng Ren, and Hideaki

Endo. Wireless biosensor system for Real-Time L-lactic acid monitoring in fish. *Sensors (Switzerland)*, 12(5):6269–6281, 2012.

[144] Ryoji Kurita, Norikuni Yabumoto, and Osamu Niwa. Miniaturized one-chip electrochemical sensing device integrated with a dialysis membrane and double thin-layer flow channels for measuring blood samples. *Biosensors and Bioelectronics*, 21(8):1649–1653, 2006.

[145] Oscar A Loaiza, Pedro J Lamas-Ardisana, Larraitz Añorga, Elena Jubete, Virginia Ruiz, Maryam Borghei, Germán Cabañero, and Hans J Grande. Graphitized carbon nanofiber-Pt nanoparticle hybrids as sensitive tool for preparation of screen printing biosensors. Detection of lactate in wines and ciders. *Bioelectrochemistry (Amsterdam, Netherlands)*, 101:58–65, feb 2015.

[146] J Haccoun, B Piro, L D Tran, L A Dang, and M C Pham. Reagentless amperometric detection of l-lactate on an enzyme-modified conducting copolymer poly(5-hydroxy-1,4-naphthoquinone-co-5-hydroxy-3-thioacetic acid-1,4-naphthoquinone). *Biosensors & bioelectronics*, 19(10):1325–9, may 2004.

[147] Eugenia I. Yashina, Anastasiya V. Borisova, Elena E. Karyakina, Olga I. Shchegolikhina, Mikhail Yu Vagin, Dmitry A. Sakharov, Alexandr G. Tonevitsky, and Arkady A. Karyakin. Sol-Gel immobilization of lactate oxidase from organic solvent: Toward the advanced lactate biosensor. *Analytical Chemistry*, 82(5):1601–1604, 2010.

[148] Zimei Rong, Eugenia Leitao, Jonathan Popplewell, Burçak Alp, and Pankaj Vadgama. Needle enzyme electrode for lactate measurement in vivo. *IEEE Sensors Journal*, 8(1):113–120, 2008.

[149] Claire Forsyth, Siddharth V Patwardhan, S V Patwardhan, and · C Forsyth. A Comparison with Traditional Methods. In Paul Zelisko, editor, *Bio-Inspired Silicon-Based Materials*, chapter 4. Springer Science+Business Media, 5 edition, 2014.

[150] Ulf Hanefeld, Lucia Gardossi, and Edmond Magner. Understanding enzyme immobilisation. *Chem.Soc.Rev.*, 38:453–468, 2008.

[151] Teofil Jesionowski, Zdarta Jakub, and Barbara Krajewska. Enzyme immobilization by adsorption: a review. *Adsorption*, 20:801–821, 2014.

[152] Marcelo Ricardo Romero, Fernando Garay, and Ana M. Baruzzi. Design and optimization of a lactate amperometric biosensor based on lactate oxidase cross-linked with polymeric matrixes. *Sensors and Actuators B: Chemical*, 131(2):590–595, may 2008.

[153] T Park. Sol-gel based amperometric biosensor incorporating an osmium redox polymer as mediator for detection of lactate. *Talanta*, 44 (6):973–978, jun 1997.

[154] Danfeng Jiang, Zhenyu Chu, Jingmeng Peng, and Wanqin Jin. Screen-printed biosensor chips with Prussian blue nanocubes for the detection of physiological analytes. *Sensors and Actuators B: Chemical*, 228:679–687, jan 2016.

[155] Naimish P. Sardesai, Mallikarjunarao Ganesana, Anahita Karimi, James C. Leiter, and Silvana Andreescu. Platinum-doped ceria based biosensor for in vitro and in vivo monitoring of lactate during hypoxia. *Analytical Chemistry*, 87(5):2996–3003, 2015.

[156] Gerhard Jobst, Isabella Moser, Mehdi Varahram, Peter Svasek, Elmar Aschauer, Zlatko Trajanoski, Paul Wach, Peter Kotanko, Falko Skrabal, and Gerald Urban. Thin-Film Microbiosensors for Glucose–Lactate Monitoring. *Analytical Chemistry*, 68(18):3173–3179, jan 1996.

[157] Akiyo Tanaka. Toxicity of indium arsenide, gallium arsenide, and aluminium gallium arsenide. *Toxicology and Applied Pharmacology*, 198 (3):405–411, 2004.

[158] Nur Royhaila Mohamad, Nur Haziqah Che Marzuki, Nor Aziah Buang, Fahrul Huyop, and Roswanira Abdul Wahab. An overview of technologies for immobilisation of enzymes and surface analysis techniques for immobilised enzymes. *Biotechnology & Biotechnological Equipment*, 29(2), 2015.

[159] Ulf Hanefeld, Linqiu Cao, and Edmond Magner. Enzyme immobilisation: fundamentals and application. *Chemical Society Reviews*, 42(15):6211, 2013.

[160] Xiaoqiang Cui, Chang Ming Li, Jianfeng Zang, and Shucong Yu. Highly sensitive lactate biosensor by engineering chitosan/PVI-Os/CNT/LOD network nanocomposite. *Biosensors & bioelectronics*, 22(12):3288–92, jun 2007.

[161] Yanguang Zhao, Xiaofei Fang, Yousong Gu, Xiaoqin Yan, Zhuo Kang, Xin Zheng, Pei Lin, Leichao Zhao, and Yue Zhang. Gold nanoparticles coated zinc oxide nanorods as the matrix for enhanced L-lactate sensing. *Colloids and surfaces. B, Biointerfaces*, 126:476–80, feb 2015.

[162] J. Perdomo, H. Hinkers, C. Sundermeier, W. Seifert, O. MartÄśÌĄnez Morell, and M. Knoll. Miniaturized real-time monitoring system for l-lactate and glucose using microfabricated multi-enzyme sensors. *Biosensors and Bioelectronics*, 15(9-10):515–522, nov 2000.

[163] Thanh Thuy Nguyen-Boisse, Joelle Saulnier, Nicole Jaffrezic-Renault, and Florence Lagarde. Highly sensitive conductometric biosensors for total lactate, d- and l-lactate determination in dairy products. *Sensors and Actuators B: Chemical*, 179:232–239, 2013.

[164] Anthony Guiseppi-Elie, Sean Brahim, Gymama Slaughter, and Kevin R. Ward. Design of a subcutaneous implantable biochip for monitoring of glucose and lactate. *IEEE Sensors Journal*, 5(3): 345–355, 2005.

[165] Zafar Hussain Ibupoto, Syed Muhammad Usman Ali Shah, Kimleang Khun, and Magnus Willander. Electrochemical L-lactic acid sensor based on immobilized ZnO nanorods with lactate oxidase. *Sensors*, 12 (3):2456–2466, 2012.

[166] Behzad Haghighi and Somayyeh Bozorgzadeh. Fabrication of a highly sensitive electrochemiluminescence lactate biosensor using ZnO nanoparticles decorated multiwalled carbon nanotubes. *Talanta*, 85(4): 2189–2193, 2011.

[167] C Marquette. Electrochemiluminescent biosensors array for the concomitant detection of choline, glucose, glutamate, lactate, lysine and urate. *Biosensors and Bioelectronics*, 19(5):433–439, dec 2003.

[168] Min Hsien Wu, Junbo Wang, Taha Taha, Zhanfeng Cui, Jill P G Urban, and Zheng Cui. Study of on-line monitoring of lactate based on optical fibre sensor and in-channel mixing mechanism. *Biomedical Microdevices*, 9(2):167–174, 2007.

[169] Tsuyoshi Minami, Tsubasa Sato, Tsukuru Minamiki, Kenjiro Fukuda, Daisuke Kumaki, and Shizuo Tokito. A novel OFET-based biosensor for the selective and sensitive detection of lactate levels. *Biosensors & bioelectronics*, 74:45–8, dec 2015.

[170] M Briones, E Casero, M D Petit-Domínguez, M A Ruiz, A M Parra-Alfambra, F Pariente, E Lorenzo, and L Vázquez. Diamond nanoparticles based biosensors for efficient glucose and lactate determination. *Biosensors & bioelectronics*, 68:521–8, jun 2015.

[171] Pavel Ripka and Alois Tipek, editors. *Mondern Sensors Handbook*. iste, 2007.

[172] Mark R Prausnitz. Microneedles for transdermal drug delivery. *Advanced Drug Delivery Reviews*, 56(5):581–587, 2004.

[173] Anna Lukowiak and Wieslaw Strek. Sensing abilities of materials prepared by sol–gel technology. *J Sol-Gel Sci Technol*, 50:201–2015, 2009.

[174] Sandra Pérez, Samuel Sánchez, and Esteve Fàbregas. Enzymatic Strategies to Construct L-Lactate Biosensors Based on Polysulfone/Carbon Nanotubes Membranes. *Electroanalysis*, 24(4): 967–974, 2012.

[175] Jiadong Huang, Zhao Song, Jing Li, Yu Yang, Haibin Shi, Baoyan Wu, Jun-ichi Anzai, Tetsuo Osa, and Qiang Chen. A highly-sensitive l-lactate biosensor based on sol-gel film combined with multi-walled carbon nanotubes (MWCNTs) modified electrode. *Materials Science and Engineering: C*, 27(1):29–34, jan 2007.

[176] DropSens. Screen-printed gold electrodes. URL `http://www.dropsens.com/en/screen_printed_electrodes_pag.html#unmodified_spes`. Date accessed: 2017-11-15.

[177] Dropsens. Screen-printed platinum electrodes. URL http://www.dropsens.com/en/screen_printed_electrodes_pag.html#unmodified_spes. Date accessed: 2017-11-15.

[178] DropSens. Screen-printed Carbon Electrodes. URL http://www.dropsens.com/en/pdfs_productos/new_brochures/110-c110.pdf. Date accessed: 2017-11-15.

[179] Jung-Hwan Park, Mark G Allen, and Mark R Prausnitz. Polymer Microneedles for Controlled-Release Drug Delivery. *Pharmaceutical Research*, 23(5), 2006.

[180] Ying Liu, Yuliang Zhao, Baoyun Sun, and Chunying Chen. Understanding the Toxicity of Carbon Nanotubes. *Accounts of Chemical Research*, 46(3):702–713, mar 2013.

[181] Jun Yan, Valber A. Pedrosa, Aleksandr L. Simonian, and Alexander Revzin. Immobilizing enzymes onto electrode arrays by hydrogel photolithography to fabricate multi-analyte electrochemical biosensors. *ACS Applied Materials and Interfaces*, 2(3):748–755, 2010.

[182] T.B. Goriushkina, A.P. Soldatkin, and S.V. Dzyadevych. Application of Amperometric Enzyme Biosensors for Wine and Must Analysis. *Procedia Chemistry*, 1(1):277–280, sep 2009.

[183] A Poscia, D Messeri, D Moscone, F Ricci, and F Valgimigli. A novel continuous subcutaneous lactate monitoring system. *Biosensors & bioelectronics*, 20(11):2244–50, may 2005.

[184] R.J. Gfrerer, G.A. Brunner, Z. Trajanoski, L. Schaupp, G. Sendlhofer, F. Skrabal, G. Jobst, I. Moser, G. Urban, T.R. Pieber, and P. Wach. Novel system for real-time ex vivo lactate monitoring in human whole blood. *Biosensors and Bioelectronics*, 13(12):1271–1278, dec 1998.

[185] European Patent Office. Espacenet Patent search. URL https://worldwide.espacenet.com/advancedSearch?locale=en_EP. Date accessed: 2016-05-05.

[186] Paul D'Hond and Mathijs Ten Berg. Device for determining foetal reserves during childbirth, 2002.

[187] Bahar Reghabi, Rebecca Gottlieb, Shah Rajiv, and Bardley Enegren. Implantable multi-parameter sensing system and method, 2005.

[188] Mikael Ryttinger, Johanna Lundstedt, Carina Mallard, and Jan Soederlund. Device for detecting oxygen depletion in foetuses during childbirth, 2009.

[189] Thomas Ivo Franciscus Huberta Cremers. Integrated Electrode for Sampling of Lactate and other Analytes, 2015.

[190] Juang-Tang Huang. Lactate measuring device and method for training adjustment in sports, 2015.

[191] MicroPoint Technologies. MicroPoint Technologies, 2017. URL https://micropoint-tech.com/. Date accessed: 2017-11-13.

[192] Innoture Medical Technology. Innoture Medical Technology, 2017. URL http://www.innoture.co/. Date accessed: 2017-11-13.

[193] Minghui Yang, Yunhui Yang, Yanli Liu, Guoli Shen, and Ruqin Yu. Platinum nanoparticles-doped sol-gel/carbon nanotubes composite electrochemical sensors and biosensors. *Biosensors & bioelectronics*, 21 (7):1125–31, jan 2006.

[194] Australian Microscopy & Microanalysis Research Facility. Troubleshooting: edge effect, charging, sample damage. URL http://www.ammrf.org.au/myscope/sem/practice/principles/troubleshooting.php. Date accessed: 2017-11-13.

[195] Dominika Pihíková, Peter Kasák, and Jan Tkac. Glycoprofiling of cancer biomarkers: Label-free electrochemical lectin-based biosensors. *Open Chemistry*, 13(1), jan 2015.